ENGINEERING High-Performance Manufacturing
https://doi.org/10.2738/ENGHPM.2026.0001

Review

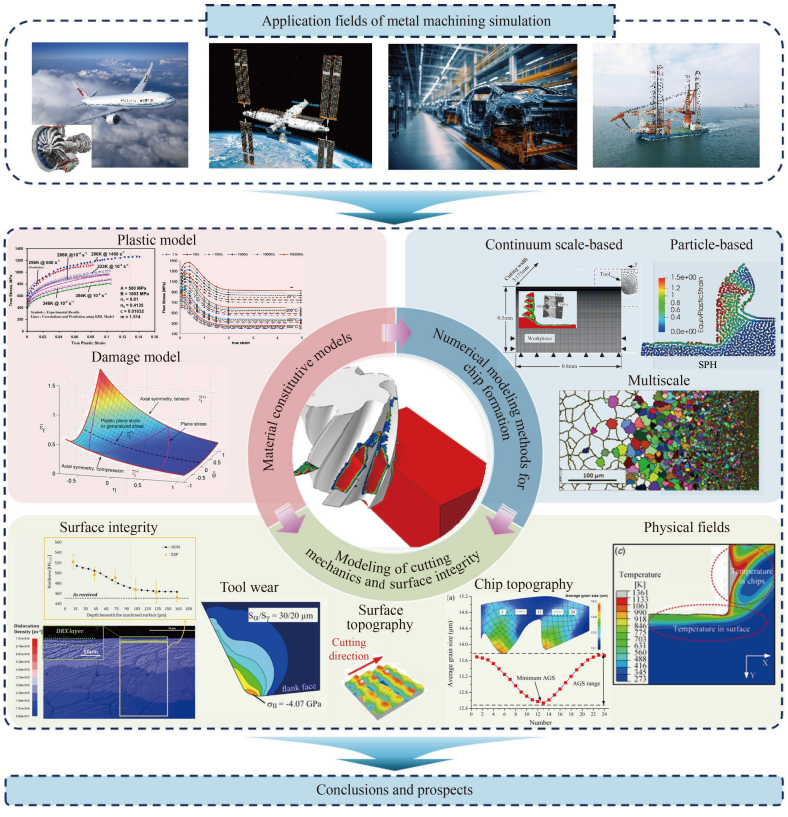
Review on Modeling of Metal Machining: Mechanical Behavior, Microstructure and Surface Integrity

Jiangting Wu[1], Guang Chen (✉)[1,2,3], He Zhang[1], Zhiyi Wang[1], Ling Jin[1], Zhuoyang Wu[1], Bingchen Duan[1], Hongtao Wang[1], Qian Gao[1], Chengzu Ren[1,2,3,4]

1 School of Mechanical Engineering, Tianjin University, Tianjin 300354, China
2 Key Laboratory of Mechanism Theory and Equipment Design (Ministry of Education), Tianjin University, Tianjin 300354, China
3 Key Laboratory of Equipment Design and Manufacturing Technology, Tianjin University, Tianjin 300354, China
4 School of Mechanical Engineering, Tianjin Renai College, Tianjin 301636, China

© The Author(s) 2026. This article is published by Higher Education Press.

GRAPHICAL ABSTRACT



HIGHLIGHTS

- Material plastic constitutive models which characterize work hardening behavior in cutting are reviewed.
- Physics based modeling approaches considering microstructure evolution are reviewed.
- Plastic instability and damage modeling approaches involved in cutting are reviewed.
- Continuum, particle, and multiscale approaches are highlighted with their application scenarios.
- Modeling of cutting mechanics and surface integrity is comprehensively summarized.
- Prospects of multi-scale/multi-physics and performance-driven modeling for machining are outlined.

Received 28 Jun 2026; accepted 29 Sep 2026

E-mail: guangchen@tju.edu.cn (Chen G.).

ABSTRACT Numerical modeling for metal machining has advanced significantly over decades, evolving from early analytical shear slip theory to macro–micro thermomechanical coupled finite element simulations, which now accurately predict machining performances and surface integrity indicators, serving as an essential tool to explore in-process states and intrinsic mechanisms. This review comprehensively summarizes the fundamental theories, key methods, and application progress of machining simulation modeling, focusing on three core aspects: material constitutive modeling, numerical modeling for chip formation, and modeling applications for cutting mechanics and surface integrity. Material constitutive models (plastic and damage/failure types) are the core of simulation accuracy. Plastic models are categorized into phenomenological, physics-based, and semi-physical. Damage/failure models, ranging from empirical stress-state-dependent criteria to energy-based fracture models, are discussed with emphasis on calibration, physical mechanisms, and computational robustness. Chip formation modeling methods are divided into continuum, particle, and multiscale approaches, each with distinct features and applicable scales. Cutting mechanics and surface integrity modeling have advanced to coupled thermomechanical simulations, though challenges like high computational cost and unresolved scientific issues remain. Future research will focus on improving constitutive model accuracy, constructing comprehensive damage model frameworks, developing high-fidelity multiscale chip formation models, and establishing multi-scale/multi-physics models for cutting mechanics. Ultimately, machining simulation is expected to evolve from a post-processing analysis tool into a core element for performance-driven, multi-scale, multi-objective process optimization, enabling predictive, adaptive, and intelligent manufacturing systems.

KEYWORDS Numerical modeling; Machining simulation; Constitutive models; Microstructure evolution; Surface integrity; Multi-scale/multi-physics modeling

1 Introduction

Metal machining stands as a cornerstone of modern manufacturing, underpinning critical industries including aerospace, automotive, medical devices, and precision engineering. With the continuous advancement of manufacturing technologies, the development of the manufacturing industry is gradually shifting toward high-performance manufacturing—that is, from a focus on geometric precision to a priority on ensuring accurate product performance [1]. Guided by scientific principles, interdisciplinary and cross-domain systematic modeling and simulation have become increasingly urgent. These models empower manufacturers to optimize cutting parameters, select optimal tool geometries and materials, mitigate tool wear, and guarantee consistent surface integrity—all while reducing costly trial-and-error experimentation and minimizing material waste [2,3]. Advanced simulation frameworks further enable the prediction of complex thermo-mechanical and microstructural phenomena, bridging lab-scale insights to industrial-scale process design and supporting the transition toward data-driven, sustainable manufacturing [4–6]. In high-value sectors such as aerospace, where components are often fabricated from difficult-to-machine materials like titanium alloys (Ti–6Al–4V) and nickel-based superalloys, reliable modeling is not merely a matter of efficiency but a prerequisite for ensuring structural safety and performance [7,8].

The evolution of metal cutting modeling has exhibited a distinct, stage wise trajectory over more than eight decades, evolving from early analytical frameworks to modern multi-physics and microstructure integrated simulations, as illustrated in Fig. 1. The early research began in the 1940s–1950s with foundational analytical models. Merchant's shear plane model [9] and Palmer and Oxley's slip line field theory [10] laid the groundwork for quantifying cutting forces and deformation mechanics, establishing the first quantitative relationships between process parameters and material response. From the 1990s onward, numerical methods (notably finite element method, FEM) emerged as practical tools, enabling 2D and later 3D simulations of chip formation [6,11] and overcoming the limitations of analytical models in capturing complex, non linear deformation. By the 2010s, the focus expanded to chip formation modeling that accounts for physical factors (e.g., strain rate sensitivity, thermal softening) and microstructure prediction [12,13], alongside advanced damage models [14] that describe failure initiation and propagation under extreme cutting conditions. Since 2015, research has centered on surface integrity characterization by material characterization such as electron backscatter diffraction (EBSD), transmission electron microscopy (TEM), and X-ray diffraction (XRD) and multi-physics modeling [15,16], integrating thermal, mechanical, and metallurgical effects to predict machining induced microstructural evolution and its impact on component performance.

Central to the success of any machining model is the accurate representation of material behavior under the extreme conditions encountered during cutting—strains exceeding 100%–1700%, strain rates up to 10^6 s^{-1}, temperatures ranging from 500 to 1400 °C, and pressures

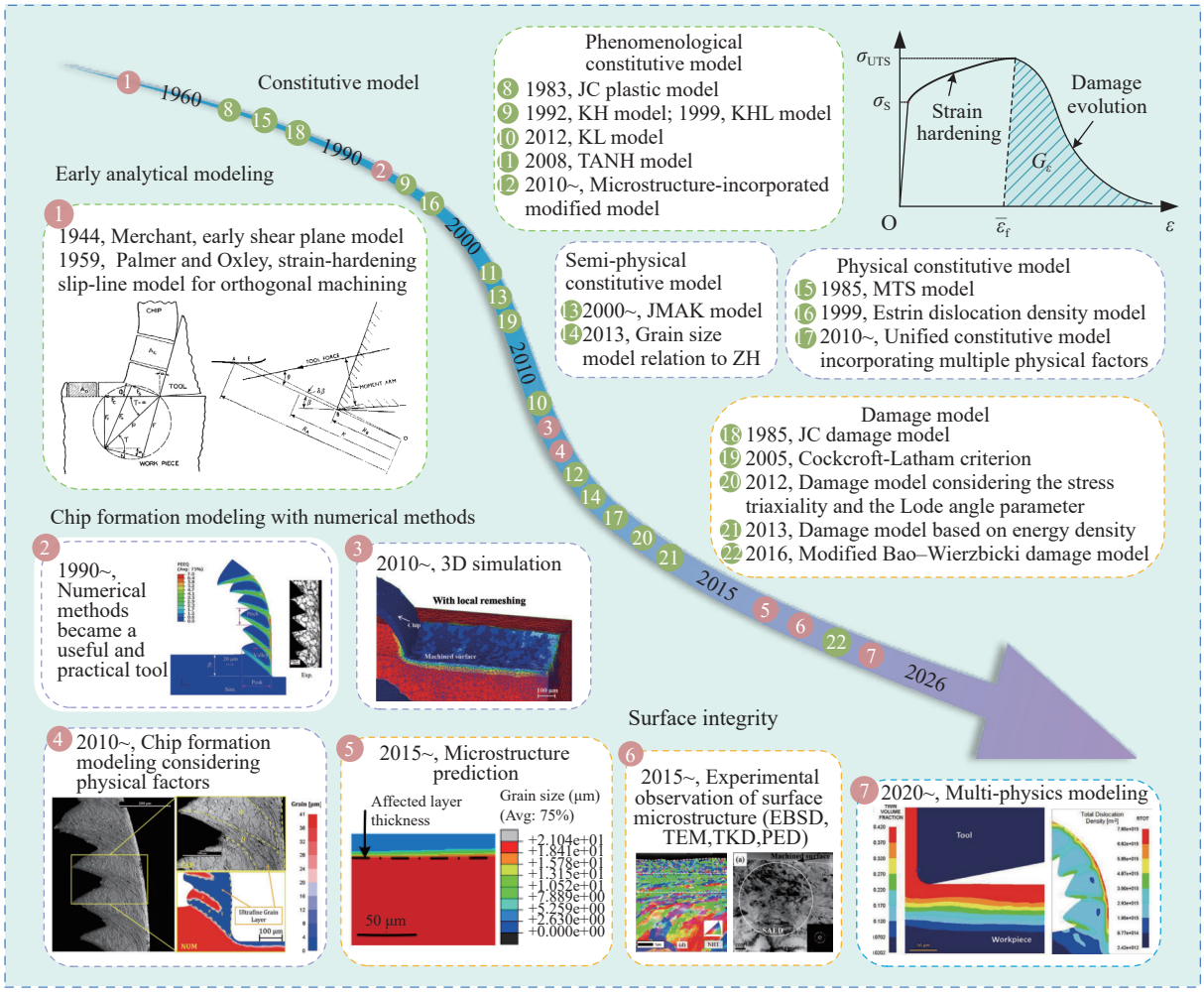


Fig. 1 Progress and timeline of modeling advances in metal cutting simulation: from constitutive/damage models to surface integrity prediction. Reprinted from Ref. [12,29–34].

approaching 2–3 GPa [17]. Constitutive models, which describe the relationship between stress, strain, strain rate, and temperature, are the key components affecting the accuracy of machining simulations. Early formulations, such as Oxley's work hardening model [10], provided a baseline for understanding material flow but often failed to capture the complex, coupled effects of thermal softening, strain hardening, strain rate sensitivity and grain size [18,19]. The Johnson–Cook (JC) model [20], introduced in the 1980s, gained widespread use for its numerical robustness and explicit treatment of these three effects. Yet, its limitations in modeling strain rate temperature coupling and microstructural evolution spurred the development of enhanced phenomenological and semi physical alternatives: the Khan–Huang–Liang (KHL) model [21,22] and Zerilli–Armstrong (ZA) model [23,24], for instance, embed dislocation dynamics and grain size dependencies, yielding more precise predictions for alloys like Ti–6Al–4V and advanced high strength steels [25,26]. In recent decades, the field has advanced toward microstructure sensitive constitutive frameworks, which bridge macroscopic deformation to underlying mechanisms such as dynamic recrystallization (DRX), twinning, and grain refinement—essential for accurately predicting surface integrity in high speed machining scenarios [27–29].

The landscape of machining modeling continues to evolve, driven by the need to address emerging challenges and capitalize on technological advancements. A key trend in recent years is the shift toward multi-scale modeling, which integrates macro-scale process simulations with micro-scale predictions of grain size evolution, phase transformation, and residual stress distribution [35,36]. This shift is motivated by the recognition that microstructural changes induced during machining—such as grain refinement in Ti–6Al–4V [13] and phase transformation in hardened steels [37,38]—directly influence the functional performance of

machined components, including fatigue life, corrosion resistance, and mechanical strength [39,40]. Advanced numerical methods, such as the coupled Eulerian–Lagrangian (CEL) approach [16], smoothed particle hydrodynamics (SPH) [41], and crystal plasticity finite element method (CPFEM) [42,43], have enabled more accurate simulations of these microstructural phenomena by overcoming limitations related to mesh distortion, contact handling, and material anisotropy [2,11]. Additionally, the integration of experimental techniques such as high-speed imaging, EBSD, and digital image correlation (DIC) has facilitated the validation and refinement of these multi-scale models [44,45].

Another notable trend is the increasing focus on sustainable machining practices, such as minimum quantity lubrication (MQL) and cryogenic machining, which require models capable of capturing the effects of alternative cooling strategies on material behavior and process performance [46,47]. Furthermore, the rise of additive manufacturing (AM) has created new opportunities for hybrid manufacturing processes, where machining is used to finish AM components—demanding models that account for the unique microstructures and residual stress states of additively manufactured materials [48,49]. The development of user-friendly, industry-ready modeling tools remains a priority, as the adoption of predictive models by manufacturing facilities depends on their accessibility, computational efficiency, and ability to directly predict process outcomes such as tool life, surface roughness, and part distortion [3,50].

To contextualize the growing academic interest in this field, bibliometric analysis of publications indexed in the Web of Science, retrieved using the keywords “cutting or machining”, “modeling or simulation”, and “finite element”, with 2000 selected for analysis in VOSviewer, reveals a robust upward trend in research output, as shown in Fig. 2. As illustrated in the annual publication trend, the number of relevant studies has been rising steadily since 2005, peaking at over 200 articles in 2025 (data collected from January 2005 to May 2026), reflecting the escalating global investment in understanding and optimizing metal cutting processes. Co-occurrence keyword analysis further highlights the intellectual structure of the field, with core themes centered on simulation, chip formation, finite element and machining, alongside interconnected topics such as constitutive model, microstructure, numerical simulation and surface integrity. This network of research interests underscores the interdisciplinary nature of metal cutting modeling, which integrates mechanics, materials science, computational engineering, and manufacturing science to address the complex, multi-physics challenges of modern machining.

The CIRP keynote paper [3] reviewed the modeling of metal machining processes back in 2013. Several representative reviews [36,51] have addressed finite element modeling on metal cutting or effect of microstructure in metal cutting in recent years. This review provides a comprehensive overview of the modeling of mechanical behavior, microstructure and surface integrity involved in cutting processes, with special emphasis on synthesizing constitutive models encompassing plastic, failure, and damage behaviors, alongside state-of-the-art numerical simulation studies for predicting machined surface integrity. By synthesizing recent research findings and highlighting key challenges and future directions, this work seeks to guide researchers

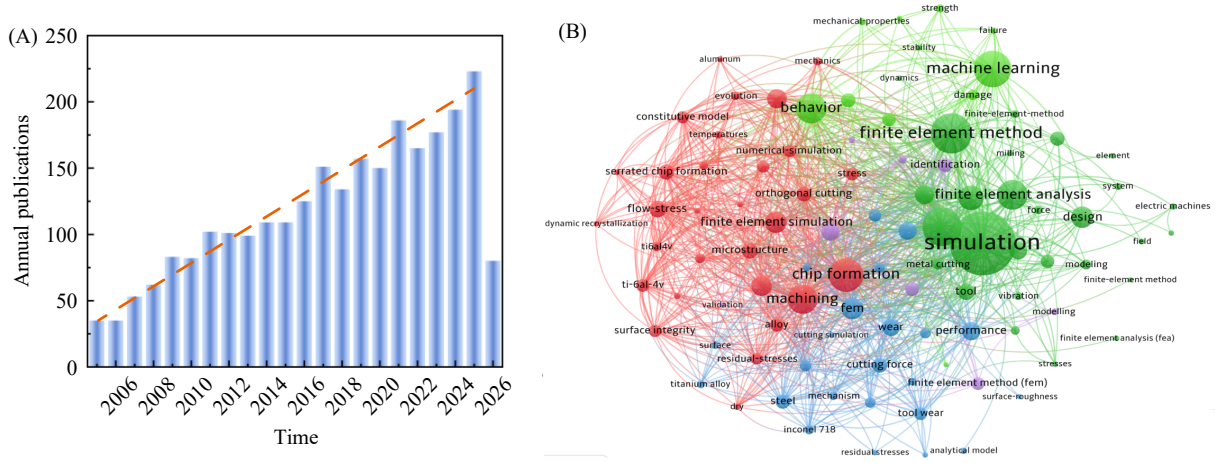


Fig. 2 Temporal evolution of research hotspots in modelling of metal machining (based on Web of Science Core Collection data, search query: “cutting or machining, modeling or simulation, finite element”). (A) Annual publication trends (data collected from January 2005 to May 2026). (B) Keyword co-occurrence network visualized by VOSviewer.

and practitioners in the development and application of machining models that meet the evolving demands of modern manufacturing. The following sections will delve into the details of constitutive model development, multi-scale modeling techniques, modeling of cutting mechanism and surface integrity prediction, and the integration of these elements to address practical machining challenges, as indicated in Fig. 3.

2 Material Constitutive Models

Metal machining process involves the intense plastic deformation of materials under the action of a cutting tool, ultimately leading to the formation of chips and the integrity of the machined surface. Numerical modeling provides an essential approach that can be used to investigate the in-process states and underlying mechanisms of the instantaneous machining process [6,59]. As the machining process involves strong coupling effects of high strain, high strain rate, and high temperature, the key factor affecting the accuracy of metal cutting simulations is the material constitutive model, which must adequately describe the deformation behavior under various loading conditions, including high strain rate, wide temperature range, and high strain encountered during severe plastic deformation in machining [60,61]. It is worth noting that other factors,

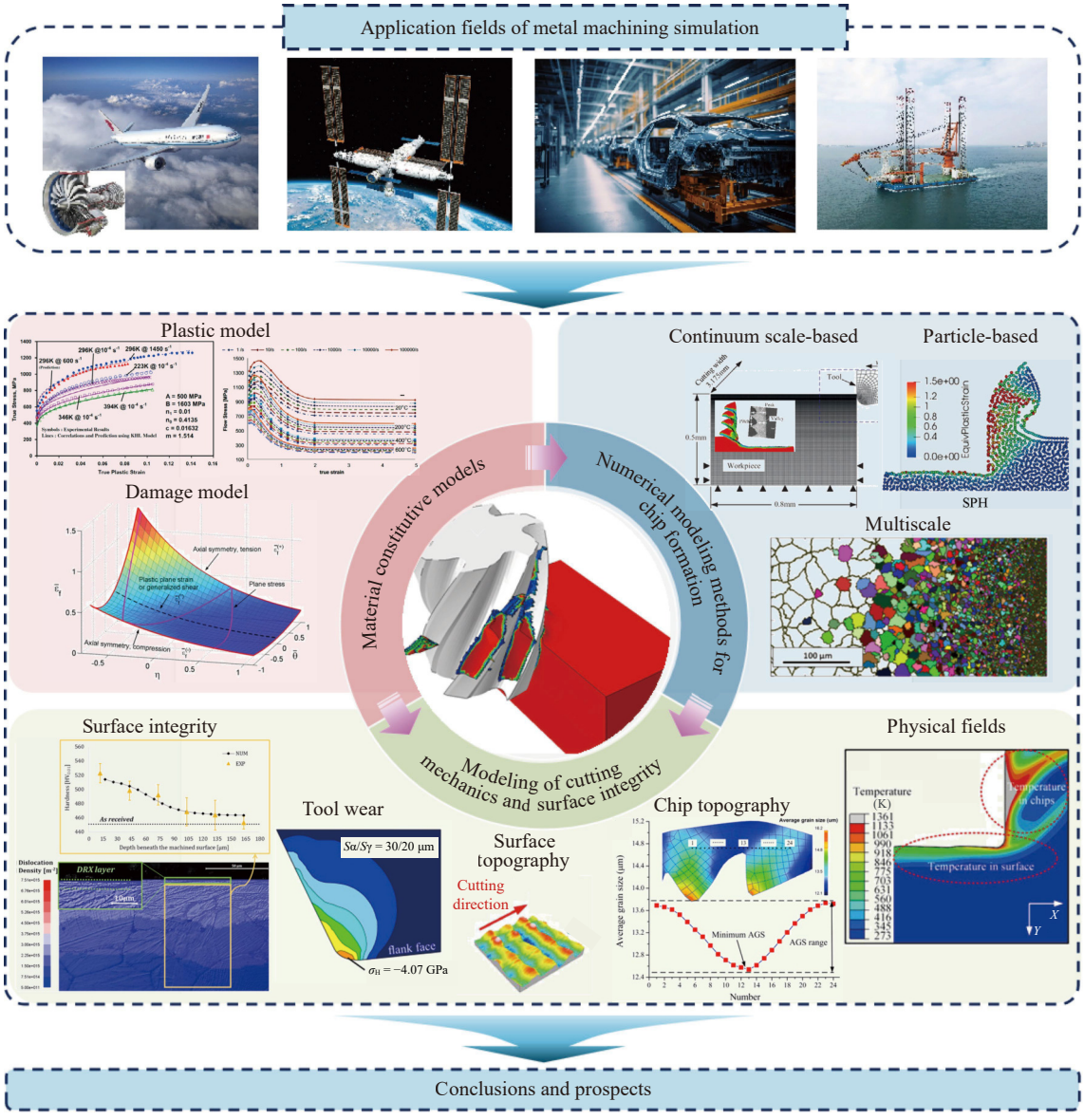


Fig. 3 The overall framework of the review. Reprinted from Ref. [13,16,22,32,52–58].

such as friction at the tool-chip interface and heat partition conditions, also influence simulation accuracy. However, compared to the constitutive model, which fundamentally determines the mechanical behaviors of metals under extreme thermo-mechanical conditions, these factors are generally considered secondary in terms of their overall impact on simulation fidelity. Moreover, friction modeling and heat partition in metal cutting fall outside the primary scope of the present review; readers are referred to dedicated comprehensive reviews on these topics [62,63].

Material constitutive model can be considered as a kind of mathematical or physical relationship which is used to describe the relationship between loading conditions (strain, strain rate, temperature and stress state) and mechanical behaviors or material microstructure dependent physical parameters, e.g. dislocation density, grain size, etc. The rational selection of a constitutive model is based on prior knowledge of the material's deformation behavior [65,66]. Fig. 4 illustrates the stress-strain response and the evolution of mechanical behaviors during deformation including the plastic and damage/failure stages. Metal plastic deformation and failure process can be classified into three typical stages: (1) Stage OA corresponds to the elastic deformation stage, in which stress and strain exhibit a linear relationship and the slope of the linear section is the Young's modulus [67]. (2) Stage AB represents the stable plastic deformation (or strain hardening) stage. Once the stress exceeds the elastic limit σ_y, the plastic flow stress of the material increases with increasing strain owing to the strain-hardening effect. (3) Stage BC is the stage of damage evolution and unstable plastic deformation. Point B is the maximum engineering stress for damage initiation, corresponding to the ultimate tensile strength σ_{UTS}. After damage initiation, the flow stress gradually decreases with further straining. At point C, the material loses its global stiffness and load-bearing capacity, eventually leading to fracture [68]. Note that, the evolution of the stress-strain relationship is directly related to the microstructure evolution during deformation. For instance, the effects of the dislocation strengthening, grain boundary strengthening, and twinning strengthening will contribute to the strain hardening during the plastic deformation [69–71].

2.1 Plastic models

Metal cutting process involves the material stable plastic deformation and the material damage behaviors. The plastic behavior defines the mechanical behavior and microstructure evolution associated with work hardening. An ideal plastic constitutive model should accurately describe the complex coupling of effects such as strain hardening, strain-rate sensitivity, and thermal softening during this process. Plastic constitutive models can be mainly categorized into two types: phenomenological models and physics-based models [19,72]. Phenomenological models normally propose the mathematical expression to characterize the relationship of stress-strain under different loading conditions [20,73,74]. The constants of the constitutive models are fitted by the uniaxial stress–strain curves at different strain rates and temperatures [75–78]. Physical-based models take into account physical parameters such as dislocation density, grain size, phase component and twinning, etc. These kinds of models can be applied to characterize the plastic deformation behaviors and the microstructure evolution during the deformation process [18,29,79–81]. It should be noted that it is very difficult to obtain the constants of the models by materials characterization tests such as EBSD, TEM, XRD. The constants of constitutive models are mostly fitted by the

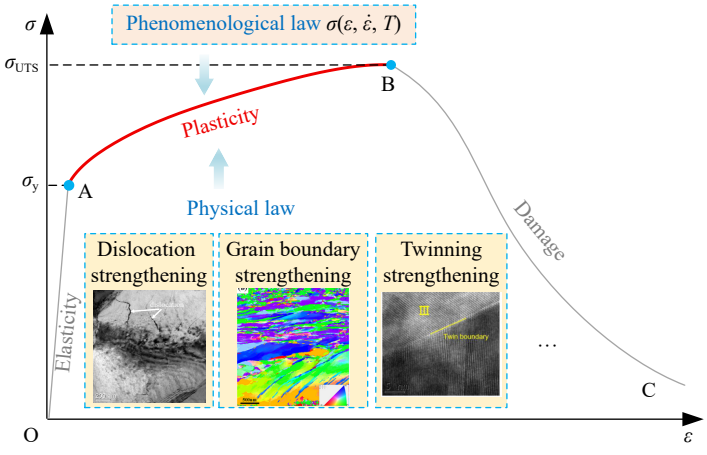


Fig. 4 Schematic of the flow stresses at the stages of elastic, plastic and damage. Reprinted from Ref. [28,64].

stress–strain responses under different loading conditions or by reverse engineering method [72,82]. The following sections will systematically introduce the above-mentioned models, as well as methods for determining, calibrating, and optimizing their parameters.

2.1.1 Phenomenological plastic models

Phenomenological plastic models utilize mathematical functions to describe the relationship between the flow stress and the loading conditions, including the strain, strain rate, temperature and stress state in metal deformation processes [19,83]. The constants of the phenomenological models are fitted by mechanical tests, such as quasi-static compression test and dynamic Split-Hopkinson Pressure Bar (SHPB) technique.

2.1.1.1 Johnson-Cook (JC) model and the JC-modified models

Among numerous phenomenological models, the JC model [20] is the most widely applied model for simulating the high strain rate deformation due to the high precision for metals and its concise form. The JC model describes the influences of strain hardening, strain-rate hardening, and thermal softening on the flow stress, making it suitable for the material deformation behavior under conditions of large deformation and high strain rate [84]. However, the original JC model has difficulty in universally depicting the unique deformation behaviors of different types of metals. It fails to accurately predict typical mechanical responses such as flow softening that occur under high strain conditions, especially without considering the coupling effects of strain, strain rate, and temperature on strain hardening, strain rate hardening and thermal softening [26,85–87]. This limitation restricts its prediction accuracy for different types of materials under complex deformation conditions. To address the above-mentioned issues, many researchers have carried out studies and presented some improved constitutive models by considering the coupled effects of strain, strain rate, and temperature on plastic deformation behaviors under high strain rate conditions, such as temperature dependent strain hardening [75,88], strain rate dependent strain hardening [89], temperature dependent strain rate hardening [87,90] and other approaches that consider the coupled effects or introduce new parameters [91,92]. These typical constitutive models named as "modified JC" models were proposed for different materials, as listed in Table 1.

Several studies have observed weakened strain-hardening behavior in metals under high-temperature conditions, and have sought to improve the accuracy of constitutive models by modifying the original JC model. For instance, Chen et al. [75] investigated the flow behavior of Ti–6Al–4V alloy by incorporating temperature-dependent effects. Their predicted flow stresses showed good agreement with experimental measurements over the full range of strain rates and temperatures. Compared with the JC model, the modified formulation yielded predictions closer to experimental data, owing to the reduced work-hardening rate at high temperatures ($T > 500$ °C), as illustrated in Fig. 5A. Regarding the effect of strain rate on the flow stress, Wang et al. [87] revised the formulation of the strain-rate hardening term. They extended the constant C in the strain-rate hardening term to a coupled function of temperature and strain rate, thereby quantifying the strain-rate softening effect and its temperature dependence for Inconel 718 at high strain rates (5000–11,000 s^{-1}).This modification eliminated the systematic bias exhibited by the original JC model under high-temperature and high-strain-rate conditions, yielding a high-accuracy constitutive model.

With the continuous progress in this field, numerous researchers have developed composite modified JC models that incorporate corrections to at least two terms [85]. Chen et al. [90] investigated the dynamic mechanical behavior of Inconel 690 welding claddings over a wide temperature range (20–800 °C) and high strain rates (5000–12,500 s^{-1}) using SHPB experiments, aiming to meet the accuracy requirements for high-speed cutting simulations. Their proposed model accounts for softening induced by dynamic recovery under large strains, as well as strain rate softening at high strain rates and its coupling effect with temperature. As shown in Fig. 5B, under conditions of high strain rate and high temperature, the flow stress predicted by this modified JC model agrees considerably better with experimental measurements than that of the original model. Yue et al. [85] incorporated the strain–temperature coupling effect and DRX softening, achieving a 4.3% reduction in prediction error for Ti–6Al–4V in milling processes.

In addition to the aforementioned modifications to the strain hardening, strain rate hardening, and thermal softening terms, several studies have further incorporated the influence of complex stress states on material deformation behavior, leading to a more comprehensive extension of the JC model. Such extensions typically involve the introduction of stress triaxiality and Lode angle parameters to enable a more accurate description of mechanical responses and damage evolution [95]. For instance, Hu et al. [94] enhanced the model's adaptability to complex stress states by incorporating these two parameters. Cheng et al. [95], conversely, developed a

Table 1 The JC model and the JC-modified models.

References	Constitutive equation	Description
Johnson and Cook [20]	$\sigma = \left[A + B\varepsilon_p^n\right]\left[1 + C\ln\left(\frac{\dot{\varepsilon}_p}{\dot{\varepsilon}_0}\right)\right]\left[1 - \left(\frac{T - T_0}{T_m - T_0}\right)^m\right]$	Original JC model
Hou et al. [88]	$\sigma = \left[A + B\left(1 + m_1 \ln\frac{T}{T_r}\right)\varepsilon^n\right]\left(1 + C\ln\frac{\dot{\varepsilon}}{\dot{\varepsilon}_0}\right)\left[1 - \left(\frac{T - T_r}{T_m - T_r}\right)^m\right]$	Considering temperature dependent strain hardening effect
Chen et al. [75]	$\sigma = \left[A + B\left(\frac{T_0 - T/2}{T_0}\right)^{n_2}\varepsilon^n\right]\left[1 + C\ln\left(\frac{\dot{\varepsilon}}{\dot{\varepsilon}_0}\right)\right]\left[1 - \left(\frac{T - T_r}{T_m - T_r}\right)^m\right]$	
Wang et al. [87]	$\sigma = (A + B\varepsilon^n)\left[1 + C\ln\left(\frac{\dot{\varepsilon}}{\dot{\varepsilon}_0}\right)\right]\left[1 - \left(\frac{T - T_r}{T_m - T_r}\right)^m\right]$, $C = C_0 - \left(C_1 + C_2\sin\left(\frac{\dot{\varepsilon} - 5000}{3000}\pi\right)\right)\sin\left(\frac{T - 500}{150}\pi\right)$	Considering strain rate softening effect
Chen et al. [90]	$\sigma = \{A + B[1 - \exp(n_1\varepsilon^{n_2})]\}\left[1 + C(\dot{\varepsilon}, T)\ln\left(\frac{\dot{\varepsilon}}{\dot{\varepsilon}_0}\right)\right]\left[1 - \left(\frac{T - T_r}{T_m - T_r}\right)^m\right]$	Considering the stress saturation behavior under large strains and strain rate softening effect
Yue et al. [85]	$\begin{cases}\sigma = (A + BM(T)\varepsilon^n)\left[1 + c\ln\left(\frac{\dot{\varepsilon}}{\dot{\varepsilon}_0}\right)\right]\left[1 - \left(\frac{T - T_0}{T_m - T_0}\right)^m\right], & T < T_C \\ \sigma = (A + BM(T)\varepsilon^n)\left[1 + c\ln\left(\frac{\dot{\varepsilon}}{\dot{\varepsilon}_0}\right)\right]\left[1 - \left(\frac{T - T_0}{T_m - T_0}\right)^m\right]\varphi(T), & T > T_C\end{cases}$, $M(T) = 1 - r\ln\frac{T}{T_0}$, $\varphi(T) = \left(\frac{\overline{\sigma}_b}{\sigma_a}\right)$	Considering the strain-temperature coupling and DRX softening effects
Zeng et al. [93]	$\sigma = (A + B\varepsilon^n)\left[1 + C\ln\left(\frac{\dot{\varepsilon}}{\dot{\varepsilon}_0}\right)\right]\left[1 - \left(\frac{T - T_r}{T_m - T_r}\right)^m\right]$, $C = 0.0028\dot{\varepsilon}^{0.27552}$, $m = C_0 + C_1T^* + C_2T^{*2} + C_3T^{*3} + C_4T^{*4}$	Introducing new coefficients for strain rate hardening and thermal softening
Hu et al. [94]	$\sigma = \left(A + m(\varepsilon_p)^n\right)\left(B + C\cdot\ln\left(E + \frac{\dot{\varepsilon}_p}{\dot{\varepsilon}_0}\right)\right)\left(1 - \left(\frac{T - T_0}{T_m - T_0}\right)^t\right) \times\left(1 - c_\eta(\eta - \eta_0)\right)\left(c_\theta^s + (c_\theta^{ax} - c_\theta^s)\left(\gamma - \frac{\gamma^{a+1}}{a+1}\right)\right)$, $\gamma = 6.464\left(\sec\left(\bar{\theta}\cdot\frac{\pi}{6}\right) - 1\right)$, $c_\theta^{ax} = \begin{cases}c_\theta^t & (\bar{\theta} > 0) \\ c_\theta^c & (\bar{\theta} \leqslant 0)\end{cases}$	Considering stress state, including the stress triaxiality and Lode angle parameter

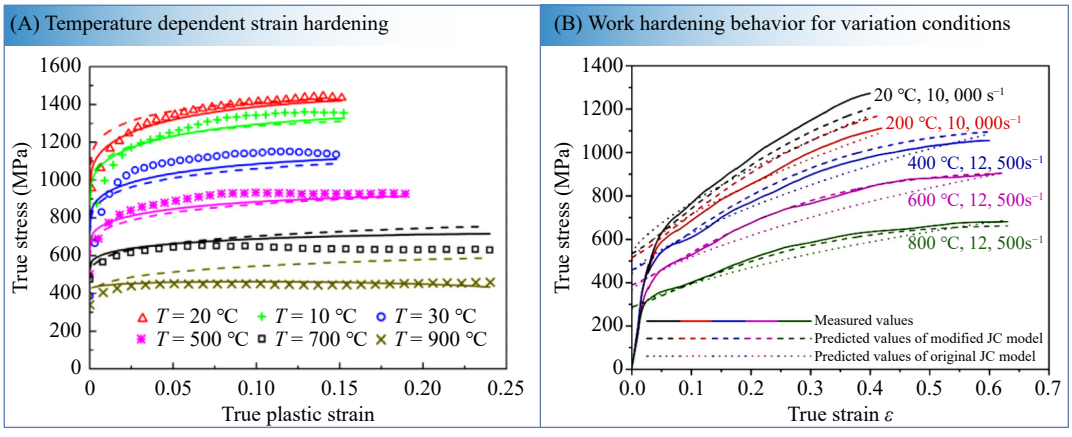


Fig. 5 Comparison of experimental flow stresses and calculated results with JC and modified JC models. (A) The modified model with temperature-dependent strain hardening [75]. (B) The modified model with stress saturation and strain rate softening [90].

unified constitutive framework for the cutting process of Ti–6Al–4V alloy by integrating the effects of stress state and strain rate. A detailed discussion of the stress state is provided in Section 2.2.

2.1.1.2 KHL model and Hyperbolic tangent (TANH) model

From the early 1990s, Khan and Huang et al. [21,22,89]

developed a series of phenomenological models including the KHL model or modified KHL models. Similar to JC model, these types of models use nonlinear formulas to express the relationships among stress, strain, strain rate and temperature, as listed in Table 2. They generally feature a small number of model parameters, which are usually obtained by fitting quasi-static and SHPB dynamic tests under different loading conditions, and deliver high accuracy in stress prediction for different materials, such as titanium alloys, aluminum alloys, steels, nanocrystalline metals [72,96–98].

The KHL model describes the mechanical behavior of body-centered cubic (BCC) metals and nanocrystalline materials. It evolved from the viscoplastic model proposed by Khan and Huang in 1992, commonly referred to as the KH model [21]. By incorporating work-hardening and strain-rate effects, the KH model accurately predicts the flow stress of 1100 aluminum alloy across a wide range of strain rates; however, it does not account for temperature effects. To incorporate the influence of strain, strain rate, and temperature on work hardening and to enhance predictive accuracy under dynamic loading, Khan and Liang [89] developed the classical KHL model. Subsequently, Khan and his collaborators systematically extended the applicability of this model through a series of studies. For DP 800 steel [22], the material exhibited positive strain-rate sensitivity, and model predictions aligned well with experimental results, as shown in Fig. 6A. In a study on Ti–6Al–4V alloy [99] , the KHL model demonstrated superior predictive accuracy over the JC model across a broad range of strain rates and temperatures. To address the limitations of the original KHL model under specific conditions, several modifications have been proposed. To overcome the KHL model's inability to accurately represent the temperature-dependent strain rate sensitivity of Al 2024-T351 in the quasi-static regime, the KL model was developed [73]. By incorporating a temperature threshold term and a strain-rate softening term, this model effectively captures the reduction in work-hardening rate with increasing temperature and strain rate. As illustrated in Fig. 6B, the simulated flow stress curves at 505 K across various strain rates clearly reflect this trend. Chen et al. [75] proposed the KHLM model, which integrates temperature-related effects, thereby improving the predictive capability of the KHL model for the high-temperature work-hardening behavior of Ti–6Al–4V and extending its applicability to elevated temperature conditions.

In addition to modifications based on the KHL framework, other forms of constitutive models have also been proposed to better capture flow softening and thermal effects. In 2008, Calamaz et al. [100] developed a TANH constitutive model, which introduces flow softening at higher strain levels as well as temperature-dependent flow softening, accounting for dynamic recovery and DRX mechanisms. As shown in Fig. 6C, the TANH model naturally captures material instability, distinguishing it from the JC and KHL models. It accurately describes the adiabatic shear effect without requiring preset fracture criteria and improves the prediction of serrated chip formation under low-speed, small-feed conditions. Subsequently, Sima and Özel [58] and Özel et al. [101] systematically extended the original

Table 2 Evolution and modification of KHL and TANH constitutive models.

Model	References	Constitutive equation	Description
KH	Khan and Huang [21]	$\sigma = (\sigma_0 + E_\infty \varepsilon^p - a\mathrm{e}^{-\alpha\varepsilon^p}) \dfrac{1}{\left[1 - \dfrac{\ln(\dot{\varepsilon}^p)}{\ln(D_0^p)}\right]^n}$	Considering strain- and strain rate-dependent work hardening
KHL	Khan and Liang [89]	$\sigma = \left[A + B\left(1 - \dfrac{\ln \dot{\varepsilon}}{\ln D_0}\right)^{n_1} \varepsilon^{n_0}\right]\left(\dfrac{\dot{\varepsilon}}{\dot{\varepsilon}_0}\right)^C \left(\dfrac{T_m - T}{T_m - T_r}\right)^m$	Incorporating thermal softening effects
KL	Khan and Liu [73]	$\sigma_p = \left[A + B\mathrm{e}^{-C_3 \frac{\dot{\varepsilon}}{\dot{\varepsilon}^*}} \left(\dfrac{T_m - T}{T_m - T_r}\right)^{m_3} \varepsilon_p^{n_0}\right]\left[\mathrm{e}^{C_1 \frac{\dot{\varepsilon}}{\dot{\varepsilon}^*}} - C_2(T)\mathrm{e}^{-K_1 \dot{\varepsilon}}\right]\left[\dfrac{T_m - T}{T_m - T_r}\right]^{m_2}$	Introducing temperature threshold and strain rate softening terms
KHLM	Chen et al. [75]	$\sigma = \left[A + B\left(1 - \dfrac{\ln \dot{\varepsilon}}{\ln D_0}\right)^{n_1} \left(\dfrac{T_0 - T/2}{T_0}\right)^{n_2} \varepsilon^{n_0}\right]\left(\dfrac{\dot{\varepsilon}}{\dot{\varepsilon}_0}\right)^C \left(\dfrac{T_m - T}{T_m - T_r}\right)^m$	Coupling strain, strain rate, and temperature effects
Original TANH	Calamaz et al. [100]	$\sigma = \left(A + B\varepsilon^n \left(\dfrac{1}{\exp(\varepsilon^n)}\right)\right)\left(1 + C\ln \dfrac{\dot{\varepsilon}}{\dot{\varepsilon}_0}\right) \times \left(1 - \left(\dfrac{T - T_r}{T_m - T_r}\right)^m\right) \times \left(D + (1 - D)\tanh\left(\dfrac{1}{(\varepsilon + S)^c}\right)\right)$	Incorporating both temperature-dependent flow softening and strain softening terms
Modified TANH	Özel and Sima [58,101]	$\sigma = \left[A + B\varepsilon^n \left(\dfrac{1}{\exp(\varepsilon^\alpha)}\right)\right]\left[1 + C\ln \dfrac{\dot{\varepsilon}}{\dot{\varepsilon}_0}\right]\left[1 - \left(\dfrac{T - T_r}{T_m - T_r}\right)^m\right] \times \left[D + (1 - D)\left[\tanh\left(\dfrac{1}{(\varepsilon + p)^r}\right)\right]^s\right]$	Introducing the control parameter s to more precisely adjust the shape of the hyperbolic tangent function

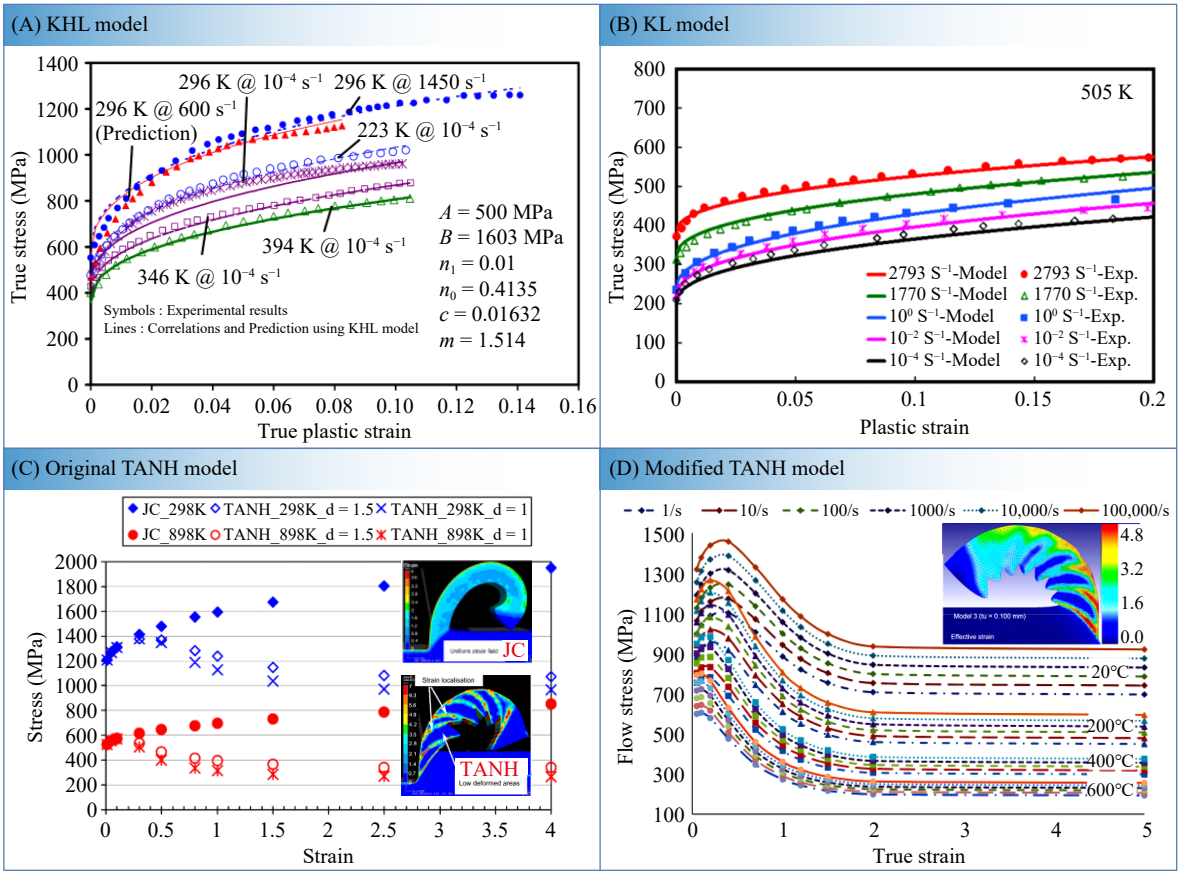


Fig. 6 Calculated flow stresses by KHL model, TANH model and the modified models. (A) KHL model for DP 800 steel [22]. (B) KL model for Al 2024-T35 [73]. (C) Original TANH model for Ti–6Al–4V [100]. (D) Modified TANH model under varied thermomechanical conditions [58].

TANH model by proposing three enhanced versions: a temperature-independent basic form; a form incorporating temperature-dependent flow softening parameters; and a complete form that includes both temperature-dependent parameters and a strain softening term. They introduced the control parameter s to more precisely adjust the shape of the hyperbolic tangent function, as illustrated by the flow stress curve of the third modified model in Fig. 6D. Owing to its accurate characterization of shear localization in titanium alloys, the TANH model has been widely adopted in research on the cutting processes of such materials. Recently, Bakhshan et al. [102], Niu et al. [103], and Zhou et al. [104] applied the TANH model to simulate the chip formation for Ti–6Al–4V alloy. Collectively, these studies confirm the effectiveness and reliability of the TANH model in predicting material deformation behavior during the cutting of titanium alloys. Nevertheless, its application to other material systems remains to be further expanded.

In summary, as significant developments of the JC model, the KHL and TANH constitutive models each offer distinct advantages and have their own applicable scopes in modeling metal cutting processes. The series of improved KHL models demonstrate good robustness and material applicability across a wide range of working conditions, particularly at high strain rates and elevated temperatures. They are well suited for describing the mechanical behavior of materials such as BCC metals, high-strength steels, and titanium alloys under extreme deformation conditions. In contrast, the TANH model effectively captures the flow softening behavior of materials at high strains, offering notable advantages in simulating the cutting processes of materials prone to shear localization, such as titanium alloys, and provides more accurate characterization of specific failure behaviors [102,104–106].

2.1.1.3 Other phenomenological models

In addition to the models discussed above, research on material constitutive modeling encompasses several representative types of phenomenological plastic models. One such example is the power law model [107], which

expresses the relationship between flow stress and thermo-mechanical field variables in the form of a power function. This model features a relatively small number of parameters that can be directly calibrated through experimental data fitting, offering concise mathematical expressions and straightforward parameter identification [108]. Temperature effects are typically described using a fifth-order polynomial. Due to its uncoupled formulation, the model is relatively easy to implement numerically; however, its predictive accuracy is limited when simulating working conditions involving complex multi-field couplings, such as those encountered in cutting processes. Another notable type is the strain path dependence model, which accounts for the influence of deformation history on the mechanical response of materials, making it suitable for describing plastic behavior under complex loading paths such as nonproportional loading. Studies have shown that this model is applicable to the numerical simulation of cutting processes for materials such as low-carbon steel and titanium alloys, and effectively captures path-dependent plastic characteristics. The modeling framework proposed by Maekawa et al. [109] exemplifies this approach and provides an effective tool for analyzing relevant engineering problems. Other influential phenomenological constitutive models include the Fields–Backofen (FB) model [110], the Molinari–Ravichandran (MR) model [111] and the Voce–Kocks (VK) model [112], among others. For further details, readers are referred to the corresponding references.

Phenomenological plasticity models express flow stress as a function of variables such as strain, strain rate, and temperature, providing a practical and efficient framework for simulating metal cutting processes. Models represented by the JC model and its derivatives (KHL and TANH) offer several advantages, including a concise mathematical form, clear physical interpretation of parameters, and ease of calibration through macroscopic mechanical tests, which have facilitated their widespread application in engineering practice [22,113,114]. However, the empirical nature of phenomenological models also imposes inherent limitations. Their predictive capability is largely constrained by the range of experimental data used for parameter calibration; when applied to extreme working conditions or complex stress paths beyond the calibrated range, prediction accuracy may deteriorate significantly. Moreover, the commonly adopted multiplicative form combining strain hardening, strain rate sensitivity, and thermal softening fails to capture the underlying coupling mechanisms among these physical processes and lacks a direct representation of microstructural evolution, such as DRX [79,115]. These limitations highlight the drawbacks of relying solely on macroscopic empirical relationships.

2.1.2 Physics-based constitutive models

Metal cutting is a complex process involving the intersection of multiple disciplines, such as mechanics, materials science, and heat transfer. Phenomenological constitutive models primarily rely on mathematical formulations to accurately describe the thermomechanical properties of materials, including the stress–strain relationships under varying conditions of plastic strain, strain rate, and temperature. With the integration of materials science and fundamental mechanical theories, physics-based constitutive models have been increasingly employed to predict microstructure evolution during metal cutting. These models not only capture the stress–strain response but also account for microstructural changes, such as dislocation slip, twinning-induced grain refinement, DRX, and phase transformations. Both phenomenological and physics-based constitutive models are grounded in the physical mechanisms underlying material deformation, encompassing mechanical behavior and microstructural evolution from the perspective of materials science. In the field of numerical modeling of metal cutting processes, physics-based constitutive models are typically defined as those capable of predicting microstructure evolution during deformation, including changes in dislocation density [79,116], grain size [19,78,115,117], and phase transformation [118–120].

Based on the degree of coupling between flow stress and microstructure evolution, physics-based constitutive models can be divided into two main categories: purely physical models [82,121,122] and semi-physical models [59,75,115,123,124]. For most purely physical models, the flow stress at plastic stage is determined by the dislocation density, grain boundaries and phase transformation [82,123,125]. For semi-physical models, flow stress is typically characterized as a function of strain, strain rate, and temperature. In addition, these models are capable of predicting microstructural features such as dislocation density and grain size. Based on whether microstructural evolution exerts an influence on flow stress, semi-physical models can be further divided into two subtypes. In the first subtype, physical quantities serve only as outputs and do not affect the flow stress; the core framework remains phenomenological, while microstructural attributes, such as dislocation density and grain size, are computed in a supplementary manner. In the second subtype, physical factors, including grain size, directly influence the flow stress, thereby establishing a coupling between microstructure evolution and the phenomenological constitutive framework.

2.1.2.1 Purely physical models

Purely physical models are grounded in theories such as

thermodynamics, dislocation mechanics, and slip dynamics. They take into account microstructural characteristics such as texture, grain size, and dislocation density, establishing physical quantities as internal variables that influence flow stress [26]. Table 3 lists several typical examples of purely physical models. These models generally account for various work hardening mechanisms active during plastic deformation. Yield strength and flow stress are characterized by factors such as dislocation accumulation, the Hall–Petch effect associated with grain refinement, phase transformation, and solution strengthening [29,32,61,126–128], as shown in Fig. 4.

The Zerilli-Armstrong (ZA) model, as a typical physical model originally formulated by Zerilli and Armstrong [24] based on dislocation mechanisms, marked a pivotal transition from purely phenomenological descriptions toward physically informed constitutive laws. This framework partitions flow stress into athermal and thermally activated components. A key innovation lies in its incorporation of crystal structure effects, yielding distinct constitutive relations for face-centered cubic (FCC) and body-centered cubic (BCC) materials, while accounting for strain hardening, strain rate sensitivity, and thermal softening. Regarding its application, Jaspers and Dautzenberg [131] observed that while the ZA model outperformed the JC model in simulating the machining of AISI 1045 steel, its predictive accuracy was comparatively lower for AA6082-T6 aluminum alloy. Childs [132] and Childs and Rahmad [133] incorporated the ZA model into a comprehensive machining analysis framework, which substantially improved the prediction accuracy for cutting forces, shear angles, and stresses in carbon steels. Their modification, which incorporated the peak strain and accounted for both hardening and softening regimes, led to enhanced predictions of flow stress under elevated thermal conditions.

Considering the physical mechanism during plastic deformation, thermally activated mobile dislocations in a metal interact with various obstacles, giving rise to phenomena such as work hardening, recovery, and grain boundary sliding [129]. Building upon the foundational work of Kocks [134], Estrin and Mecking [135], and

Table 3 Physical constitutive models.

References	Constitutive equation	Description
Estrin et al. [122]	$\begin{cases}\tau = fM\left(\alpha Gb\sqrt{\rho_w}\right)\left(\frac{\dot{\gamma}_w}{\dot{\gamma}_0}\right)^{1/m} + (1-f)M\left(\alpha Gb\sqrt{\rho_c}\right)\left(\frac{\dot{\gamma}_c}{\dot{\gamma}_0}\right)^{1/m} \\ \dot{\rho}_c = \alpha^* \frac{2}{3\sqrt{3}}\frac{\sqrt{\rho_w}}{b}\dot{\gamma}_w - \beta^*\frac{4\dot{\gamma}_c}{bd\sqrt{1-f}} - k_0\left(\frac{\dot{\gamma}_c}{\dot{\gamma}_0}\right)^{-1/n}\dot{\gamma}_c\rho_c \\ \dot{\rho}_w = \frac{4\beta^*\dot{\gamma}_c\sqrt{1-f}}{bdf} + \frac{2\beta^*\dot{\gamma}_c(1-f)\sqrt{\rho_w}}{fb\sqrt{3}} - k_0\left(\frac{\dot{\gamma}_w}{\dot{\gamma}_0}\right)^{-1/n}\dot{\gamma}_w\rho_w \\ f = f_\infty + (f_0 - f_\infty)\exp\left(-\frac{\gamma^r}{\gamma_f^r}\right) \\ d = \frac{K}{\sqrt{f\rho_w + (1-f)\rho_c}}\end{cases}$	The dislocation density model explicitly distinguishes materials into two phases: dislocation cell walls and cell interiors, defining their respective dislocation densities and evolution laws. It is suitable for simulating plastic deformation in high-stacking-fault-energy metals (such as aluminum and iron)
Follansbee and Kocks [129], Nemat-Nasser et al. [82], Anurag and Guo [130]	$\begin{cases}\sigma = \sigma_G + \sigma_{\text{th}} \\ \sigma_G = m\alpha Gb\sqrt{\rho_i} \\ \sigma_{\text{th}} = g(T,\dot{\varepsilon}) = \hat{\sigma}\left\{1 - \left[-\frac{k}{G_0}T\left(\ln\frac{\dot{\varepsilon}}{\dot{\varepsilon}_0}\right)\right]^{1/q}\right\}^{1/p}\end{cases}$	The MTS model describes the flow stress as the sum of an athermal stress component and a thermally activated stress component
Wedberg et al. [61]	$\begin{cases}\sigma_y = \sigma_G + \sigma_{\text{th}} + \sigma_{\text{drag}} \\ \sigma_{\text{drag}} = G\left(C_e + C_p\frac{T}{300}\right)\dot{\varepsilon}^p\end{cases}$	Incorporating the dislocation drag term
Imbrogno et al. [32]	$\begin{cases}\sigma = \sigma_G + \sigma_{\text{th}} + \sigma_{\text{HP}} \\ \sigma_{\text{HP}} = \alpha_G^0\tanh\left(\frac{d}{D^{-0.5}}\right)^{\nu}/\sqrt{D}\end{cases}$	Incorporating the Hall–Petch grain boundary strengthening term
Liu et al. [126,127]	$\sigma = \sigma_G + \sigma_{\text{th}} + \sigma_{\text{HP}} + \sigma_D$	Incorporating the dislocation drag and Hall–Petch grain boundary strengthening terms
Rinaldi et al. [29]	$\begin{cases}\sigma_{\text{pl}} = \sigma_G + \sigma_{\text{TH}} + \sigma_{\text{HP}} + \sigma_D + \sigma_{\text{TW}} \\ \sigma_{\text{TW}} = M\beta_{\text{TW}}Gb\left(\frac{1}{D} + \frac{1}{2t}\cdot\frac{f_{\text{TW}}}{1-f_{\text{TW}}}\right)\end{cases}$	Incorporating the twinning induced material strengthening term
Xu et al. [106]	$\sigma_{\alpha+\beta} = f_\alpha\sigma_\alpha + f_\beta\sigma_\beta$	Incorporating phase transformation and DRX effects for laser-assisted machining of Ti−6Al−4V alloy
Wang et al. [128]	$\overline{\sigma} = a_1\times\sigma_m + a_2\times\sigma_t + a_3\times\sigma_{\alpha+\beta}$	Incorporating grain refinement, nano-twinning, and phase-ratio evolution effects

Mecking and Kocks [136], Follansbee and Kocks [129] introduced the Mechanical Threshold Stress (MTS) model in 1988. This constitutive framework employs the mechanical threshold stress as a central internal state variable to characterize the stress required to overcome obstacles. The flow stress is decomposed into a thermally activated component (σ_{th}), which depends on temperature and strain rate, and an athermal component (σ_G), which arises from long-range barriers. The MTS model offers a unified description of material flow behavior, distinguished by its physically grounded interpretation of strain rate sensitivity and temperature dependence. Its applicability has been demonstrated in studies on the rheological behavior of tantalum, tantalum-tungsten alloys, and Ti–6Al–4V by Nemat−Nasser and Isaacs [137] and Nemat−Nasser et al. [82]. Moreover, some researchers have incorporated vacancy concentration as an internal variable to capture microstructural evolution, with successful applications in orthogonal cutting simulations for stainless steels [138] and Ti–6Al–4V [121].

As physics-based modeling methods move toward a more comprehensive integration of microscopic mechanisms, an increasing range of strengthening and evolution phenomena is being incorporated into their constitutive frameworks. For instance, Imbrogno et al. [32] introduced a Hall–Petch term to account for grain boundary strengthening. By coupling this with models for dislocation density evolution and DRX, they successfully predicted the grain size and dislocation density in Waspaloy during cutting. To enhance predictive accuracy under high strain rate and elevated temperature conditions, mechanisms such as dislocation drag [79], twinning-induced strengthening [29], and solid-solution strengthening [139] have been progressively integrated. Liu et al. [126,127] incorporated grain size effects and a dislocation drag term into their model, enabling accurate predictions of flow stress alongside the evolution of average dislocation density and grain size (Fig. 7A). Rinaldi et al. [29] introduced a twinning strengthening

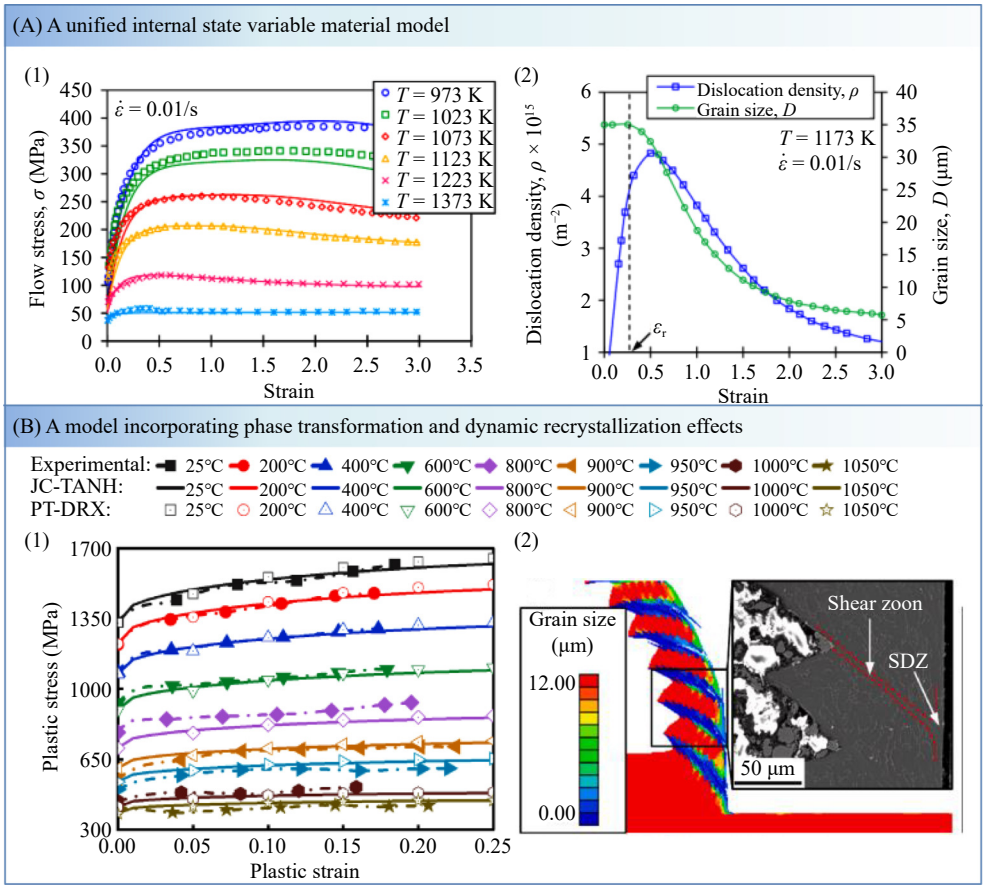


Fig. 7 Mechanical response and simulated results from purely physical models. (A) A unified internal state variable model: comparison of flow stress between experiment and simulation at different temperatures, and predicted evolutions of dislocation density and grain size [126]. (B) A model incorporating phase transformation and dynamic recrystallization effects: experimental flow stress–strain curves compared with two models and the simulated grain size evolution [106].

term correlated with twin lamella spacing and dynamically recrystallized grain size, describing its evolutionary influence through a strain-driven twin volume fraction equation. In the context of Ti–6Al–4V machining, Malakizadi et al. [139] decomposed the flow stress into four distinct contributions: lattice friction, grain refinement strengthening (Hall–Petch), solid-solution strengthening (encompassing both substitutional and interstitial elements), and dislocation strengthening. This model was coupled with evolution laws for the α-phase volume fraction and grain size. A notable advantage is that its calibration requires only six sets of SHPB data, thereby reducing parameterization costs. However, due to premature dislocation saturation and the omission of drag stress at high strains, it tends to underpredict cutting forces at higher cutting speeds. Complementing these efforts, other studies [29,140] have coupled the MTS model with the Estrin dislocation density model to synergistically leverage the strengths of both approaches.

A pioneering two-dimensional dislocation density model was proposed by Estrin et al. [122] originally developed for materials exhibiting a well-defined dislocation cell structure. Designed to capture work hardening behavior under large-strain deformation, the model was validated through simulations of cutting processes in pure metals. In this approach, the material is treated as a composite system comprising cell walls with high dislocation density and cell interiors with relatively lower dislocation density. The macroscopic mechanical response is linked to the evolution of microscale dislocation densities via the rule of mixtures. As research progressed, this modeling framework was systematically extended to three-dimensional formulations [141]. By introducing an empirical function that describes the evolution of cell wall volume fraction with strain—a critical microstructural parameter—and embedding it within a viscoplastic, self-consistent polycrystalline plasticity framework [141], the model achieved a unified description and predictive capability for large-strain hardening behavior under arbitrary strain paths. This advancement significantly broadened the model's applicability and generalizability. Within this theoretical framework, subsequent investigations have extended its application to machining simulations across diverse materials [142]. Investigations on aluminum alloys and pure copper have shown that large plastic strains, combined with relatively low cutting speeds and deformation temperatures, promote the formation of ultrafine-grained and even nanocrystalline structures [143]. Later, Ding and Shin [144] applied the model to orthogonal cutting of commercially pure titanium, establishing a quantitative relationship between dislocation cell size and total dislocation density, thereby enabling the prediction of dynamic grain refinement within the deformation zone. Such models, which employ dislocation density as the primary state variable, require calibration of physical parameters—including coefficients for dislocation generation and annihilation in the evolution equations. This typically necessitates microstructural data for parameterization and yields microstructural information as model outputs.

Normally, dislocation, phase transformation and twinning will contribute to the increase of the yield strength for metals [71,125,145–147]. Addressing the extreme thermomechanical conditions involving phase transformation, Xu et al. [106] developed a constitutive model specifically for laser-assisted machining of Ti–6Al–4V alloy, incorporating both phase transformation and DRX mechanisms. Using the TANH model, they generated stress–strain datasets under elevated temperatures and high strain rates to calibrate the parameters of their Phase Transformation–Dynamic Recrystallization (PT-DRX) model, including the kinetic equations for phase evolution and DRX parameters, as illustrated in Fig. 7B(1). The resulting model successfully captured the evolution of grain size [Fig. 7B(2)]. Wang and Liu [128] proposed a microstructure-sensitive model that integrates grain refinement, deformation twinning, and phase transformation mechanisms to simulate the flow stress behavior during high-speed machining of Ti–6Al–4V. Their study elucidated the distinct contributions of these mechanisms to the hardening behavior of titanium alloys under high strain rate cutting conditions. They found that grain refinement–induced flow stress elevation dominated the post-machining hardening response; however, this contribution diminished with further increases in cutting speed (exceeding 300 m/min) due to grain growth promoted by elevated cutting temperatures. At intermediate cutting speeds (approximately 200 m/min), deformation twinning emerged and contributed significantly to work hardening. Notably, the flow stress associated with the β-phase had a negligible influence on the overall hardening behavior of Ti–6Al–4V.

Purely physical models interpret material deformation and hardening behaviors based on microstructural evolution principles rooted in materials science. However, since such models incorporate physically meaningful parameters such as dislocation density, most of their input values are derived from material characterization techniques—including EBSD, TEM, and XRD [148,149]. As a result, these parameters are generally more difficult to obtain than those in phenomenological models. Moreover, the predictive accuracy of purely physical models is challenging to

validate under diverse loading conditions, particularly for the high strain rates and elevated temperatures encountered in machining processes. Under the extreme deformation conditions typical of material cutting, the integration of coupled mechanisms—such as DRX and phase transformation—remains incomplete in these models. In addition, their predictive capability is significantly influenced by the initial microstructural state of the material. Collectively, these limitations hinder the practical application of purely physical constitutive models in industrial-scale simulations.

2.1.2.2 Semi-physical models: physical variables as outputs

The evolution of microstructure, including the grain size, dislocation density and phases, is related to the loading strain, strain rate and temperature conditions. That is, most microstructure prediction models are determined by the material related parameters and also the loading strain, strain rate and temperature. The semi-physical models are another typical model which can predict the dislocation density, grain size and phase transformation by the output of strain, strain rate and temperatures of phenomenological models. As aforementioned, depending on whether microstructural evolution affects the flow stress, the semi-physical models can be classified as two types: microstructure output model [56,102,115,150] and microstructure dependent flow stress prediction model [59,117,151,152].

For microstructure output semi-physical model, parameters of phenomenological flow stress empirical formulations are typically identified via mechanical characterization, including quasi-static and high-strain-rate mechanical testing. Such models adopt plastic strain, strain rate, and temperature as input variables to characterize the stress response under thermomechanical loading. On this basis, the calibrated constitutive parameters are further incorporated into microstructure evolution frameworks—such as the Johnson-Mehl-Avrami-Kolmogorov (JMAK) model [19,115,153] and dislocation density evolution models [121,154,155]—to predict microstructural features including grain size, dislocation density, and phase transformations. Nevertheless, within this constitutive setup, microstructural quantities serving as outputs from the microstructure model do not exert a reciprocal influence on the flow stress behavior. The coupling relationship between the phenomenological constitutive model and the semi-physical microstructure prediction model is illustrated in Fig. 8.

The JMAK model is fundamentally based on the core premise of quantifying the recrystallized volume fraction, which is defined as a function of temperature, strain, and strain rate. When combined with the initial grain size, this premise enables the prediction of microstructural evolution [56]. Nevertheless, the conventional JMAK formulation is insufficient in capturing more complex morphological characteristics, such as grain morphology. In practical applications, the JMAK model is often integrated with the Zener-Hollomon parameter [150], which encapsulates the coupled effects of temperature and strain rate on deformation behavior through an exponential formulation [156]. The Arrhenius equation [157] has been widely adopted to characterize the interdependent relationship among strain rate, flow stress, and temperature. Rotella et al. [81] established a correlation between deformation conditions and recrystallized grain size by means of the Zener−Hollomon parameter, thereby successfully predicting microstructural alterations in AA7075-T651 alloy during machining. Their findings indicated that both cutting velocity and tool nose radius exert a significant influence on the integrity of the machined surface and subsurface. In the research on titanium alloy machining, Bai et al. [56] employed the TANH model to characterize flow behavior while coupling it with the JMAK framework to predict both the volume fraction of DRX and the average grain size. Sadeghifar et al. [115] utilized the JC model to simulate plastic flow in Ti–6Al–4V alloy, subsequently employing the JMAK model to examine how cutting parameters influence machining-induced grain size evolution. Similarly, a dual-scale modeling approach was proposed, combining the TANH constitutive model for macroscopic material response with an incremental microstructural model encompassing dislocation density evolution, JMAK kinetics, and the Hall–Petch relationship for Ti–6Al–4V alloy [102]. The thermal and mechanical field variables were coupled in a unidirectional manner, in which microstructural evolution outcomes were not directly incorporated back into the TANH constitutive equations. This methodology enabled high-fidelity predictions of both serrated chip formation and microstructural evolution during TC4 alloy machining.

Denguir et al. [154] developed a constitutive model that comprehensively incorporates strain hardening, strain rate sensitivity, and thermal softening effects, while also integrating the influences of DRX and stress triaxiality [52,159]. To realize microstructural predictions, this constitutive model was coupled with the Estrin dislocation density framework. Normalized depth profiling of dislocation density distributions indicated that the subsurface had the lowest dislocation density at an undeformed chip thickness of 0.05 mm and a tool rake angle of 30°, while the highest surface dislocation density

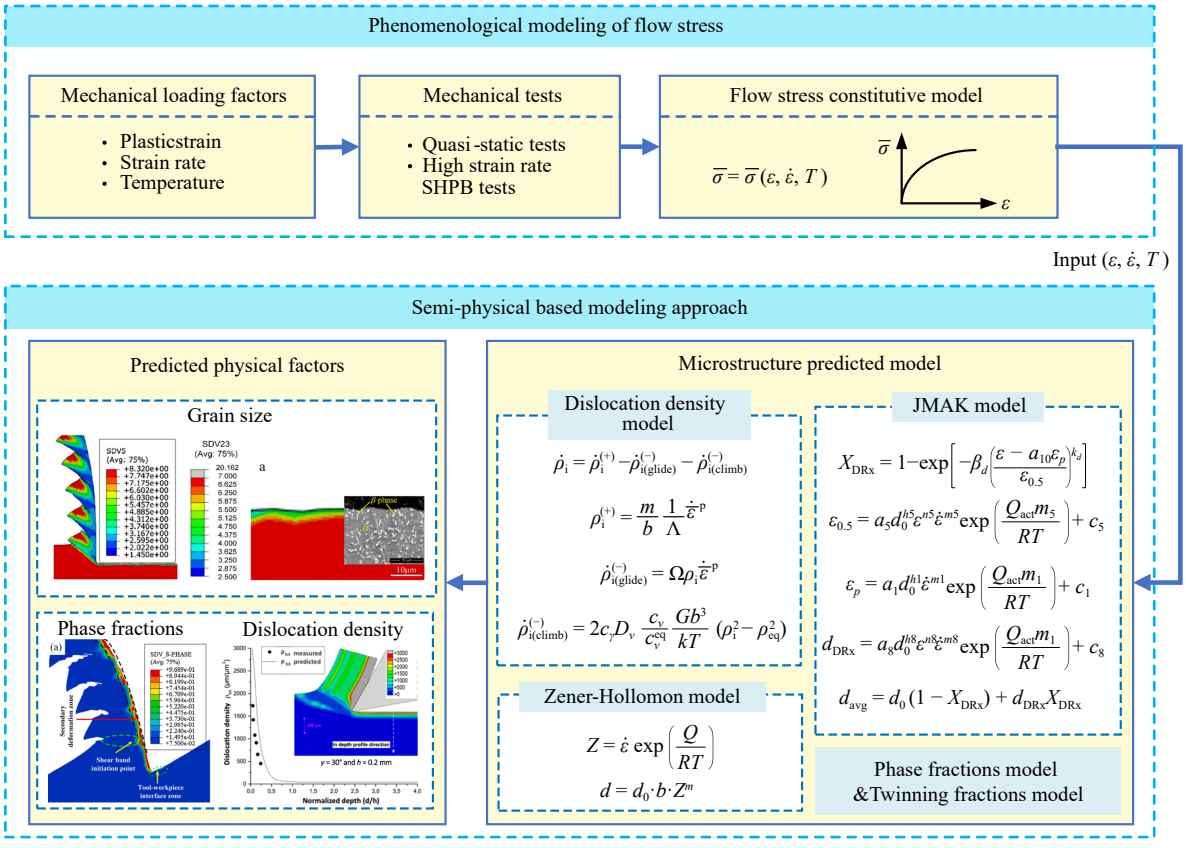


Fig. 8 Semi-physical models in which physical quantities act only as output variables. Reprinted from Ref. [15,59,154,158].

appeared at 0.2 mm undeformed chip thickness, where the deformation-affected material layer reached its maximum at a 20° rake angle [154]. Although there were localized differences between the simulated and experimental values under certain parameter combinations, the overall variation trends of dislocation density with cutting conditions were consistent with the experimental observations.

Phase transformation is a crucial physical phenomenon during the machining of engineering alloys (e.g., steels, aluminum alloys, titanium alloys, and nickel-based superalloys), mainly triggered by high temperatures, rapid heating rates, and subsequent quenching effects. The mechanisms regulating these transformations are closely related to the material's properties and crystallographic structures. Obvious phase transformation characteristics have been found in the shear bands of serrated chips, along the tool-chip interface, and within the white layers formed on machined surfaces [120,160]. To investigate machining-induced phase transformation in Ti–6Al–4V alloy, Pan et al. [120] developed a physics-based finite element model integrated with the Avrami equation. Their simulation results indicated that increasing cutting speed and feed rate leads to higher temperatures, which facilitates the transformation to the β phase and increases its volume fraction on the machined surface. For simulating rapid heating and cooling during high-speed machining of Ti–6Al–4V, Wang et al. [161] established phase transformation models based on transformation dynamics. Ullah et al. [15] developed a thermo-metallo-mechanical finite element model to simulate phase transformations during the high-speed milling of Ti–6Al–4V. They incorporated phase transition kinetics via a user subroutine. The simulations revealed significant phase evolution during rapid thermal cycles. The β phase volume fraction increased markedly at elevated cutting speeds and feed rates due to intensified heating.

Twinning is a distinct crystallographic process during plastic deformation, in which a part of a crystal undergoes uniform shear along specific crystallographic planes, forming a mirror-symmetric orientation and lamellar twin bands. This phenomenon is commonly observed under high strain rate and cryogenic conditions [36]. Together with conventional dislocation slip, twinning plays an indispensable role—especially in metals with limited slip systems (e.g., magnesium and titanium)—by providing additional deformation modes to accommodate strain along different orientations. During deformation, twin boundaries act as intrinsic barriers to

impede dislocation motion, which promotes microstructural refinement and significantly enhances the material's work hardening capacity [162–164]. Wang et al. [165] combined orientation imaging microscopy with a visco-plastic self-consistent (VPSC) framework to investigate crystallographic texture evolution during Ti–6Al–4V machining, with a particular focus on deformation twinning. The VPSC model incorporated five slip families and twinning mechanisms in the hexagonal close-packed titanium structure. Simulation results showed that a strong C fiber shear texture was generated and it was mainly attributed to the activation of multiple slip systems (especially the second-order pyramidal <c+a> slip). The research provides a modeling basis for understanding the role of twinning in crystallographic texture evolution and deformation behavior during titanium alloy machining.

Over all, the characteristics of the semi-physical models with outputting physical parameters predict the physical microstructure parameters by the output of strain, strain rate and temperature by the phenomenological model. Achieving accurate prediction of the microstructure while ensuring the accuracy of flow stress prediction is the primary objective pursued by such models.

2.1.2.3 Semi-physical models: physical variables coupled in phenomenological frameworks

The semi-physical model, which outputs physical parameters, combines the simplicity of phenomenological constitutive models with the accuracy of flow stress prediction under varying temperature, strain, and strain rate conditions. Furthermore, it enables the prediction of physical parameters and microstructural evolution, offering both engineering applicability and the capability for physical mechanism analysis in metal cutting simulations. However, the effect of microstructure evolution on flow stress is often neglected. Normally, grain refinement and increased dislocation density enhance material strength through the mechanisms of grain boundary strengthening and dislocation strengthening [69,70,125,146,149]. To account for the influence of microstructure on plastic behavior, semi-physical models incorporating physical variables and coupled work hardening models were proposed as another type of semi-physical model. These models integrate physical strengthening mechanisms within a phenomenological modeling framework, as illustrated in Fig. 9.

Numerous investigations have integrated the DRX volume fraction into phenomenological constitutive frameworks. Yameogo et al. [153] introduced a dual-stress superposition hybrid model, employing the JC formulation for non-recrystallized zones while adopting a modified TANH model incorporating a DRX softening term for fully recrystallized regions, thereby enabling the simulation of titanium alloy machining processes. Shu et al. [124] developed an enhanced JC constitutive model that accounts for DRX effects during cutting of Inconel 718 alloy. Parameter a_5 in the DRX kinetics model was recalibrated based on Oxley's parallel-sided shear zone theory to ensure consistency with processing conditions. Two additional parameters, designated b and k, were introduced to account for the influence of DRX behavior on flow stress. The predictive capability of the proposed model was substantiated through orthogonal cutting experiments and corresponding numerical simulations. To accurately capture microstructural evolution during machining, Liu et al. [27] proposed an incremental formulation of the JMAK model, establishing a modified JC framework that explicitly incorporates DRX phenomena.

To characterize the influence of grain size on yielding behavior, Khan et al. [152] incorporated the Hall–Petch relationship into the KHL constitutive model. This

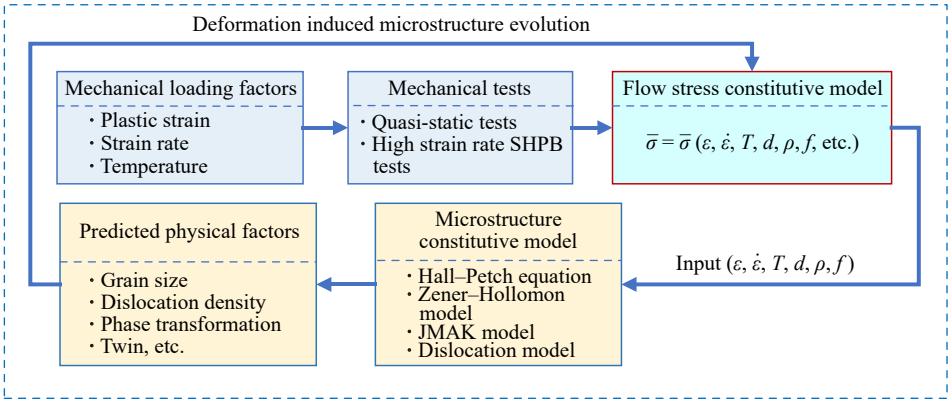


Fig. 9 Phenomenological-physical coupled modeling approach.

modification substantially enhanced the model's predictive capability regarding the mechanical response of ultrafine-grained and nanocrystalline materials, with subsequent validation through experimental observations. The resulting framework simultaneously accounts for strain hardening, strain rate sensitivity, and grain size effects, rendering it suitable for simulating mechanical behavior under high strain rate deformation as well as microstructurally dependent responses. Nevertheless, the applicability of this model under conditions of extremely high strain rates or exceptionally fine grain sizes remains subject to uncertainty. Building upon this foundation, Farrokh and Khan [78] developed the Khan–Liang–Farrokh (KLF) model, a constitutive framework capable of simulating post-yield material response across a broad spectrum of grain sizes—ranging from coarse-grained to nanocrystalline materials—under various strain rates (from quasi-static to dynamic) and temperatures (from cryogenic to elevated). This model effectively captures the evolution of work hardening behavior as a function of both grain size and temperature. Chen et al. [59,117] proposed a grain size and temperature dependent JCM-ms plastic model and carried out cutting simulation for Ti–6Al–4V alloy with different edge geometries and cooling conditions. Subsequently, Jin et al. [166] employed this modified formulation to predict the distribution of grain size, plastic deformation and the nanoindentation hardness in surface milling burnishing process (SMBP) treated Ti–6Al–4V alloy.

Although constitutive models can be categorized as phenomenological, physical, or semi-physical, their fundamental purpose remains consistent: to mathematically characterize the relationship between flow stress and mechanical loading conditions, as well as the evolution of material microstructure. Essentially, any constitutive model serves as a mathematical representation of mechanical behavior and the foundational principles governing material deformation [72,167]. Thus, the basis of all constitutive modeling lies within the domain of physical science. Different types of constitutive models have been developed, each emphasizing specific advantages tailored to the objectives of the numerical simulations used in cutting processes. Purely physical models can deeply reveal deformation mechanisms under conditions of large strain, high strain rate, and high temperature, offering unique advantages in describing microstructural evolution such as DRX, grain refinement, and twinning behavior. However, the parameter calibration of such models relies on material microstructure characterization results, including EBSD, TEM, and XRD [168,169], with high costs and difficulties in parameter acquisition. Additionally, these models are sensitive to the initial material state, limiting their widespread application in industrial-level cutting simulations. Semi-physical models, on the other hand, allow for the convenient acquisition of model parameters for predicting plastic flow stress through mechanical testing, achieving a better balance between engineering practicality and physical mechanism representation. Among them, models where physical quantities serve only as outputs integrate phenomenological constitutive models with frameworks such as the JMAK model and dislocation density evolution models, enabling simultaneous analysis of macroscopic responses and microstructural evolution with high computational efficiency [121,153,154,170]. Meanwhile, microstructure-dependent plastic flow stress prediction models directly incorporate physical quantities like grain size and recrystallization fraction into constitutive equations, significantly enhancing the accuracy of predicting work hardening, thermal softening, and related mechanical behaviors.

With advancements in advanced material characterization techniques, such as *in situ* EBSD and high-resolution TEM, future physics-based constitutive models will be able to integrate more physical mechanisms, including crystal plasticity theory, and achieve more precise parameter calibration. The combination of online monitoring and characterization methods provides opportunities for real-time study of microstructural evolution during cutting processes, which will greatly advance research on machining deformation mechanisms and enhance the level of digital manufacturing technology. A key challenge in the research of physics-based constitutive models lies in how to maintain the accuracy of microstructure prediction while simultaneously ensuring the reliability of stress–strain relationships under varying conditions of strain, strain rate, and temperature—that is, guaranteeing prediction accuracy for macroscopic mechanical performance under different thermomechanical coupling conditions, including the accuracy of main cutting force and feed force predictions. The organic integration of macroscopic and microscopic mechanical properties with material microstructure prediction represents an important direction for the future development of numerical simulation technology.

2.1.3 Parameter determination, calibration and optimization for plastic constitutive models

The accuracy of material constitutive model parameters is critical to the reliability of numerical simulations in cutting processes. Establishing a scientific and comprehensive system for parameter acquisition, calibration, and optimization serves as the essential

prerequisite for achieving high-precision simulations. Currently, the solution and optimization of plastic constitutive parameters have formed a multi-level, multi-dimensional technical framework encompassing three primary approaches: calibration based on standard mechanical tests [72,75,77], inverse identification optimization combining simulation with experimental measurements [171–173], and data-driven machine learning modeling [174–176]. These methods complement one another in terms of application scenarios, accuracy levels, and implementation costs, collectively addressing the parameter calibration requirements under complex cutting conditions.

2.1.3.1 Direct calibration based on standard mechanical tests

Parameters calibration of constitutive model via standard mechanical tests, which relies on mechanical experimental data for model parameter calibration, is fundamental for obtaining constitutive parameters. During metal machining, workpiece materials experience complex deformation (from room-temperature quasi-static to high-temperature, high-strain-rate states with variable stress triaxiality and Lode angle), so calibration experiments must accurately reflect the machining-related strain, strain rate, temperature and multi-axial stress states [177]. As shown in Fig. 10A, the cutting process is a dynamic process involving high strain and high strain rate, requiring the collaboration of quasi-static and dynamic tests to complete the calibration of constitutive model parameters. Conventional mechanical tests adopt a combination of quasi-static and dynamic experiments to obtain stress-strain data, supporting direct parameter calibration: in the quasi-static stage, tensile and compression tests conforming to ASTM standards are adopted, and cylindrical compression tests are carried out with a universal material testing machine to determine the basic parameters of classical constitutive models such as the JC model, with the relevant test schematic shown in Fig. 10B [178]; in the dynamic stage, the SHPB technique based on the theory of elastic stress wave propagation is widely utilized to test the metal plastic flow behaviors within a strain rate range of 10^3–10^4 s^{-1}, as shown in Fig. 10C [75,179,180]. For higher strain rate conditions (10^6–10^8 s^{-1}), impact tests, rod-on-rigid-anvil

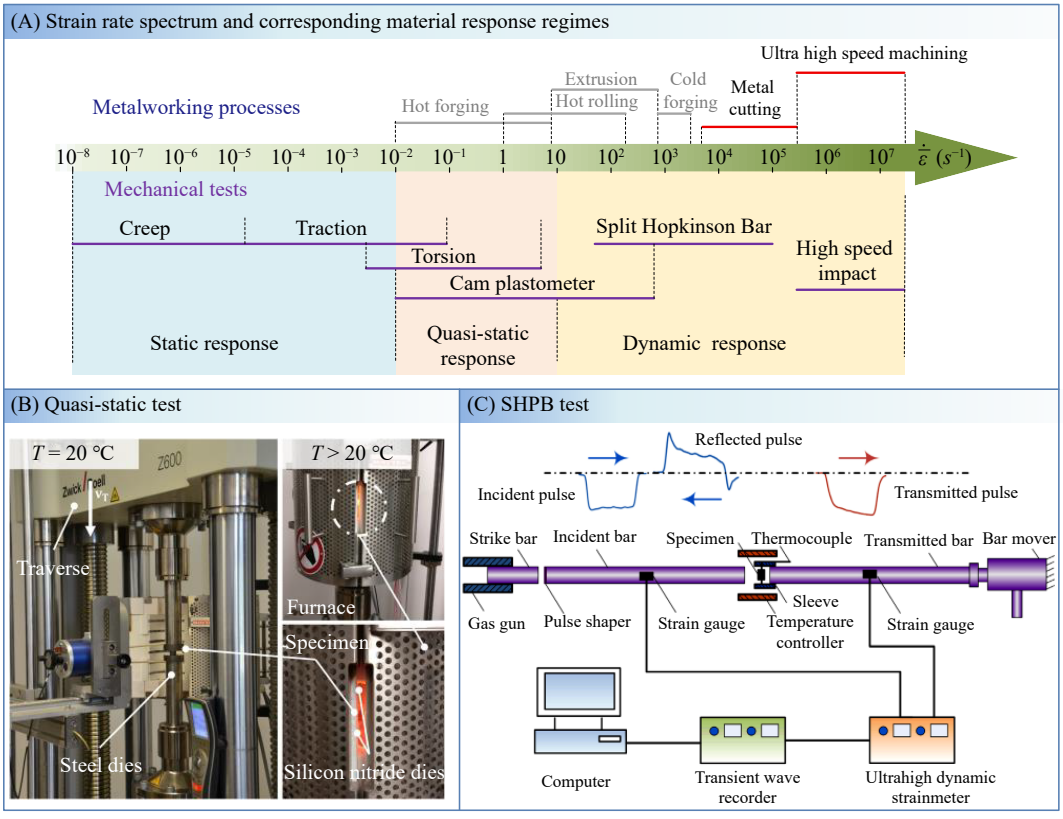


Fig. 10 Characterization methods for constitutive model parameters under various strain rates. (A) Strain rate spectrum and corresponding material response regimes in metalworking processes. Reproduced with permission from Ref. [181]. (B) Quasi-static compression test apparatus [178]. (C) Schematic diagram of the SHPB system [75].

tests, Taylor impact experiments and other methods can be adopted. Although these methods cannot directly derive flow stress curves, parameter calibration can be realized by matching the deformation morphology of specimens [76].

2.1.3.2 Parameter determination method via inverse identification and algorithmic optimization

Another widely used approach for determining plastic model constants is inverse identification combined with algorithmic optimization. This method moves beyond the constraints of isolated mechanical tests by iteratively solving for optimal constitutive parameters. It uses measured macroscopic cutting responses—such as cutting force and temperature—as targets, integrating them with numerical simulations [182,183]. The core principle involves constructing a constitutive model that includes parameters to be calibrated, which are then iteratively adjusted through finite element simulations to minimize the discrepancy between simulated predictions and experimental measurements. With the aid of digital image correlation technology, strain, strain rate, and temperature distributions within the workpiece material can be directly obtained during cutting experiments. This expands the available target data, overcomes the calibration limitations inherent in traditional thermo-mechanical tests, and enhances parameter adaptability [171]. To address the limitations of conventional single-objective fitting approaches, multi-objective optimization algorithms have emerged as a key area of advancement. When combined with intelligent algorithms such as genetic algorithms for multi-condition parameter fitting, these methods account for diverse mechanical behavior characteristics, significantly improving model prediction accuracy and generalization capability [173,184]. Current parameter optimization strategies are generally classified into three categories: gradient-based methods, gradient-free methods (soft computing), and hybrid optimization strategies, offering a range of technical path-ways for achieving accurate parameter identification [185].

2.1.3.3 Data-driven constitutive modeling using machine learning

As a cutting-edge data-driven modeling approach, machine learning offers a new paradigm for plastic constitutive modeling and parameter optimization. Its core advantage lies in the ability to directly learn complex mapping relationships between material responses and loading conditions from experimental data, thereby reducing reliance on predefined forms of constitutive laws. Machine learning methods are generally categorized into supervised learning, unsupervised learning, and reinforcement learning, enabling modeling and prediction directly from experimental test data without relying on traditional constitutive laws [176,186,187]. Among them, artificial neural networks are the predominant tool for metal plasticity modeling and are widely used in manufacturing processes such as forming, drawing, and hot stamping [188]. They can either function as standalone predictive models or be coupled with CPFEM and conventional constitutive models to capture complex mechanical behaviors—such as unconventional strain hardening, the Bauschinger effect, and anisotropic plasticity—that are difficult to describe with traditional phenomenological models [189]. Recurrent neural networks can further incorporate loading path history to achieve accurate prediction of path-dependent plastic behavior [190].

In summary, machine learning methods provide flexible data-driven modeling capabilities that open new avenues for plastic constitutive modeling. Although a mature data-driven constitutive modeling framework has not yet been established in the field of machining analysis, relevant applications in computational mechanics have demonstrated significant promise. Future work focused on accelerating algorithmic efficiency and expanding multiaxial experimental datasets will further improve model applicability and generalization under complex loading conditions.

2.2 Damage models for metal cutting simulation

Machining of metals involves material separation, which can be considered as a complex physical process. It is normally governed by the theories of ductile fracture which is considered as the ability of a material to accept large amount of deformation without fracture [52,191,192]. In the field of damage mechanics, the ductile damage criteria can be characterized by the strain, stress or mixed strain−stress [191]. When modeling metal cutting processes, it is insufficient to consider only the plastic constitutive behavior of the material, which is manifested as strain hardening or softening in the stress-strain response. Accurate prediction of chip formation, surface integrity, and the in-service performance of machined components, particularly under the high strain rates encountered in applications such as aerospace engines and automotive components subjected to impact loading, requires incorporating damage models that capture damage accumulation and fracture failure behavior [107,193]. While conventional shear theory exhibits limitations in explaining certain cutting phenomena, fracture mechanics theory provides a powerful complement for understanding the material separation process considering the strain, stress and the stress state [194], as indicated in Fig. 11.

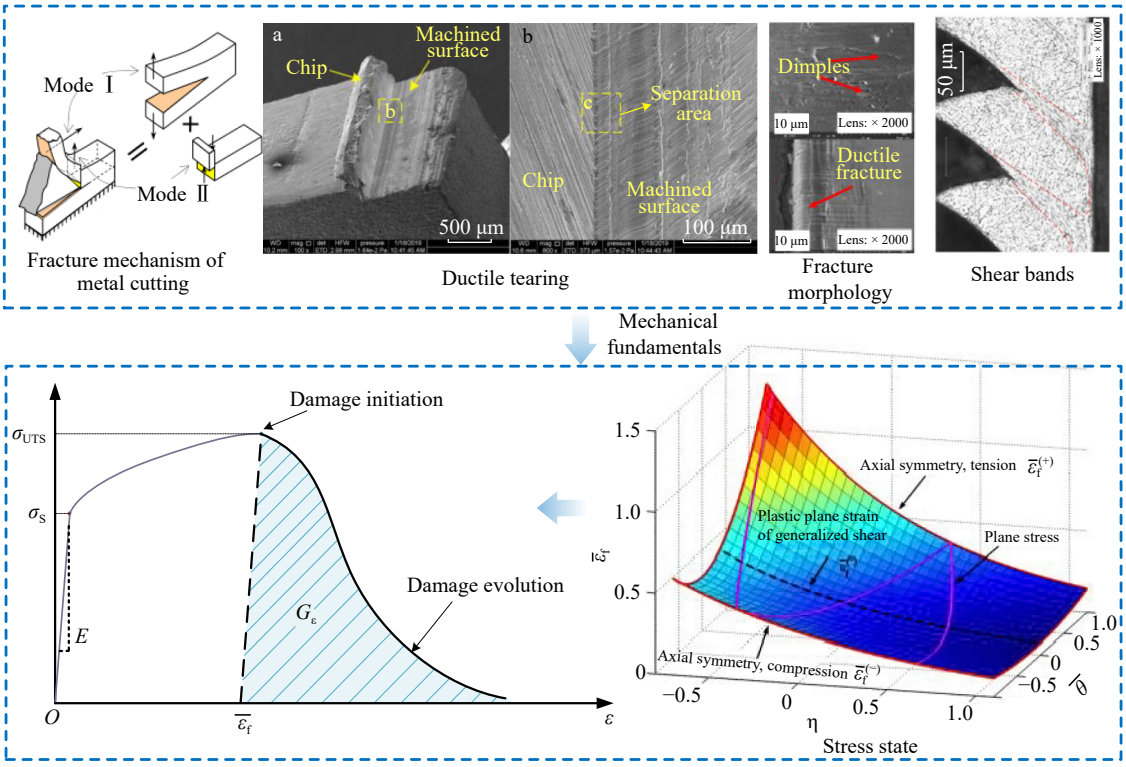


Fig. 11 Fracture mechanics fundamentals involved in metal cutting processes. Reprinted from Ref. [17,30,52,65,195].

2.2.1 Fundamentals of effect of stress state on ductile fracture

Ductile fracture in metals is fundamentally a damage accumulation process. Under external loading, plastic deformation promotes the nucleation of micro voids at microstructural inhomogeneities. These micro voids subsequently undergo growth driven by hydrostatic tensile stresses and eventually coalesce through plastic instability mechanisms within the intervening matrix, specifically internal necking or shear localization, ultimately leading to macroscopic fracture. Stress triaxiality and the normalized Lode angle parameter serve as critical state variables that govern the ductile fracture behavior of materials by characterizing the prevailing stress state [52,192].

The stress state exerts a decisive influence on the ductile fracture behavior of materials [159,196]. Research by Bai and Wierzbicki [52] demonstrated that stress triaxiality (η) and the Lode angle parameter ($\bar{\theta}$) are two critical parameters governing material fracture. Fig. 12 illustrates the corresponding η and $\bar{\theta}$ values for various classical specimen types and tests, establishing relationships between different loading conditions and stress states [192]. To enhance predictive capabilities under complex stress states, the extended Mohr−Coulomb (MC) criterion [197] incorporates both parameters, substantially improving prediction accuracy for shear fracture and fracture behavior under multiaxial stress conditions. This model offers the capability to predict fracture plane orientation while requiring only two parameters determined through fracture tests, rendering it highly amenable to engineering applications. However, certain predictive deviations still exist under high stress triaxiality conditions, and the model shows significant parameter sensitivity. This necessitates its integration with multi-mechanism damage frameworks to expand its range of applicability. Similarly, Roth and Mohr [198] proposed a strain rate-sensitive Hosford−Coulomb (HC) fracture initiation model, successfully predicting ductile fracture initiation conditions for DP590 and TRIP780 steels through combined tensile testing and numerical simulation, thereby providing an effective tool for failure analysis under complex stress states. Both fracture criteria incorporate stress triaxiality and Lode angle parameters, endowing them with considerable generalizability.

Stress state related fracture investigations have been conducted on various materials, such as 2024-T351 aluminum alloy [52], 5A06 aluminum alloy sheet [199], and Ti–6Al–4V alloy [196]. The fracture behavior exhibits pronounced dependence on stress triaxiality. Taking Ti–6Al–4V alloy as an illustrative example, Wang et al. [196] revealed that while elevated strain rates

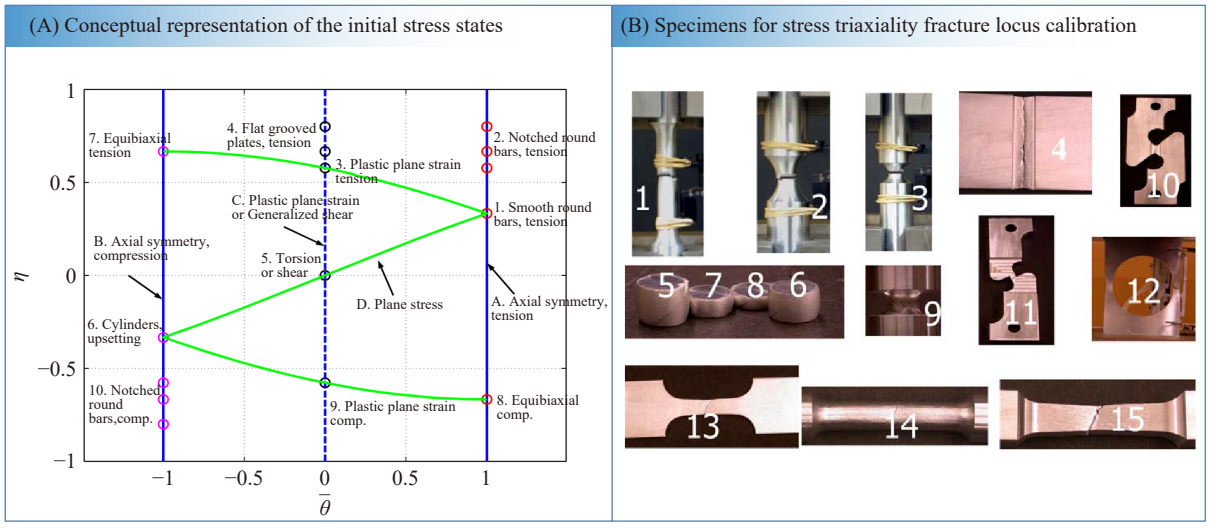


Fig. 12 Initial stress states for fracture and experimental verification. (A) Conceptual representation of initial stress states [52]. (B) Specimens for calibrating the fracture locus across a wide range of stress triaxiality [197].

promote material embrittlement, the influence of stress triaxiality proves more decisive. Upon reaching sufficiently high magnitudes, whether tensile or compressive, stress triaxiality exerts a dominant influence on fracture behavior, rendering strain rate effects negligible. Systematic transitions in fracture mechanisms and associated microstructural morphologies are observed across varying stress triaxiality regimes [200]. Under negative triaxiality conditions with a value of $\eta = -0.31$, wherein the material experiences a combined compression shear stress state, the resulting fracture surface exhibits relative planarity with microstructural evidence predominantly indicating transgranular fracture [200]. At low positive triaxiality corresponding to $\eta = 0.035$ under pure shear loading, the fracture morphology reveals mixed mode characteristics, comprising both transgranular and intergranular features. With further elevation of triaxiality to 0.50, the prevailing tension shear stress state promotes intergranular fracture as the principal failure mechanism. In summary, these studies establish a micromechanical foundation for understanding fracture behavior during cutting.

2.2.2 Fracture mechanisms and models in metal cutting

Metal cutting is a complex process involving large deformations, high strain rates (10^3-10^6 s^{-1}), and material separation. During this process, the external energy applied to the cutting system causes the formation of chips due to the material separation from the bulk material. The process of physically separating a solid into two or more parts involves fracture [201]. Chip formation in metal cutting is mainly induced by the shear-compressive stress state within the first deformation zone (i.e., the primary shear plane) [202,203]. Here, the material is subjected to extremely high shear stress and strain rate, and the stress triaxiality varies with the different loading strain rates [200]. Micro-voids nucleate within the shear band, grow elongated, and rapidly connect and coalesce through the shear band, thus leading to chip formation.

When machining difficult-to-machine materials such as titanium alloys, this process occurs periodically, resulting in serrated chips. Ductile fracture occurs near the free surface of the chip, where the stress state transitions from shear to one accompanied by a tensile component. The spatial distribution and dynamic evolution of the stress state during cutting are critical factors governing material fracture behavior and chip morphology. Accurate characterization of stress triaxiality and the Lode angle parameter enables deeper understanding and prediction of serrated chip formation mechanisms, thereby providing a theoretical foundation for cutting process optimization. Xu et al. [16] demonstrated that high-speed machining of Ti–6Al–4V induces significant stress gradient distributions within the deformation zone, as illustrated in Fig. 13A. With increasing cutting speed, the compressive stress intensity in the vicinity of the tool tip systematically diminishes, corresponding to an elevation in stress triaxiality, while the free surface of the chip exhibits increasingly tensile-dominated characteristics, reflected by positive growth in triaxiality values. Concurrently, the Lode angle parameter displays obvious spatial heterogeneity: the central region of the shear band exhibits sensitivity to velocity variations, with this parameter decreasing as cutting speed increases, whereas boundary regions near the tool tip and free surface demonstrate monotonically increasing trends. This

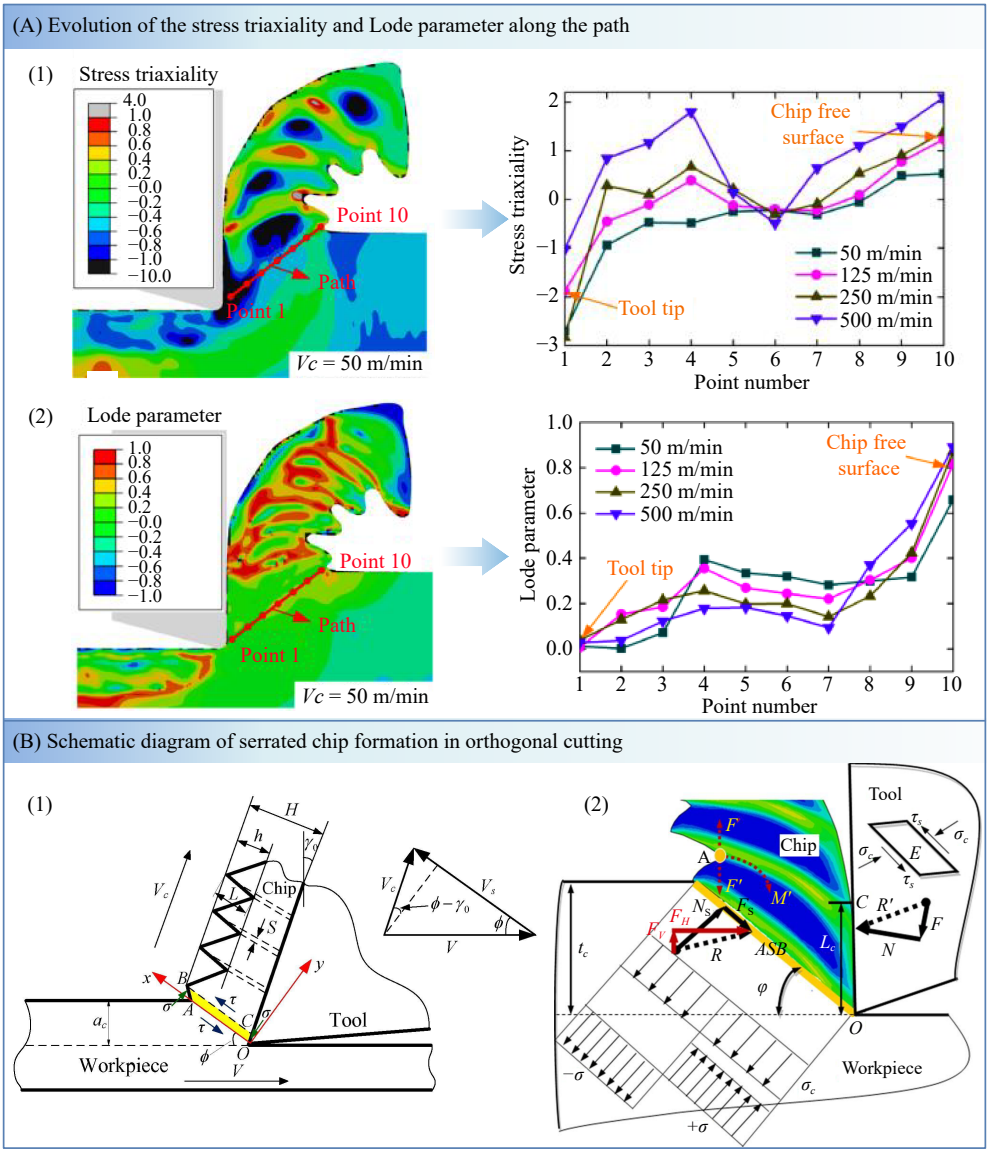


Fig. 13 Stress state distribution during metal cutting processes. (A) Stress state distribution in the deformation zone at different cutting speeds in metal cutting simulation [16]. (B) Fracture mechanics characteristics of serrated chips [14,204].

dynamic evolution of the stress state directly influences damage initiation strain in the material, thereby governing the formation and evolution of serrated chips. Wang and Liu [14] established a model describing stress triaxiality distribution along the primary deformation zone, as shown in Fig. 13B(1), and validated the dominant role of stress triaxiality in determining fracture modes through high-speed cutting experiments coupled with SEM fractographic analysis. According to Zhang et al. [204], in the high-speed cutting process of Ti–6Al–4V alloy, the peak stress triaxiality is found at the intersection of the chip segmentation free surface and the adiabatic shear band near the primary shear zone, and the stress triaxiality and strain intensity in chips will increase with cutting speed. The stress state characteristics associated with serrated chip formation during machining are depicted in Fig. 13B(2).

Since the early 1980s, numerical investigations into the fracture behavior of engineering structural materials have attracted growing attention across industrial sectors. Entering the 2000s, the demand for accurate numerical simulation of fracture and damage evolution has become particularly pressing in automotive, aerospace, aluminum processing, and steel manufacturing applications [191]. The fracture model is the fundamentals for modeling of metal fracture. Based on differences in modeling approaches, fracture models can be categorized into physically based micromechanical models and

phenomenologically based models calibrated through experimentation. Physically based fracture models characterize damage evolution by describing the nucleation, growth, and coalescence of micro-voids [205]. However, their engineering applicability remains constrained due to the reliance on microstructural characteristics that are difficult to quantify with sufficient accuracy. In contrast, phenomenological fracture models, which can easily be calibrated using macroscopic experimental data, enable effective prediction of ductile fracture with high computational efficiency and relatively easy implementation in commercial finite element codes. Table 4 presents a selection of representative fracture models.

The Taylor test, first proposed in 1948 [206], is used to determine the dynamic yield stress of materials by launching a flat-nosed cylindrical specimen against a rigid stationary wall. In 1985, the JC damage model was developed and the failure parameters were calculated based on different tests with different pressure-stress ratios [207]. This model expresses equivalent fracture strain as a multiplicative function of stress triaxiality, strain rate, and temperature, thereby incorporating both strain rate and thermal effects. Its representation of fracture strain dependence on stress triaxiality traces back to the seminal theoretical work by Rice and Tracey on void growth [208]. Parameter calibration for this model requires systematic experimental procedures: parameters D_1–D_3 can be identified via mechanical tests under various stress states (as shown in Fig. 14), which establish the relationship between stress triaxiality and fracture strain; parameter D_4 is calibrated by comparing

Table 4 The typical damage models.

References	Model	Constitutive equation	Description
Bai and Wierzbicki [197]	MC	$\bar{\varepsilon}_f = \left\{\frac{A}{c_2}\left[1-c_\eta(\eta-\eta_o)\right]\left[c_\theta^s+\frac{\sqrt{3}}{2-\sqrt{3}}(c_\theta^{ax}-c_\theta^s)\left(\sec\left(\frac{\bar{\theta}\pi}{6}\right)-1\right)\right]\right.$ $\left.\times\left[\sqrt{\frac{1+c_1^2}{3}}\cos\left(\frac{\bar{\theta}\pi}{6}\right)+c_1\left(\eta+\frac{1}{3}\sin\left(\frac{\bar{\theta}\pi}{6}\right)\right)\right]\right\}^{-\frac{1}{n}}$	Considering the stress triaxiality and the Lode angle parameter
Roth and Mohr [198]	Hosford–Coulomb	$\bar{\varepsilon}_f^{pr}[\eta,\bar{\theta}] = b(1+c)^{\frac{1}{n}}\times$ $\left(\left\{\frac{1}{2}\left((f_1-f_2)^a+(f_2-f_3)^a+(f_1-f_3)^a\right)\right\}^{\frac{1}{a}}+\right.$ $\left.c(2\eta+f_1+f_3)\right)^{-\frac{1}{n}}$ $b=\begin{cases}b_0 & \text{for } \dot{\bar{\varepsilon}}_p < \dot{\varepsilon}_0\\ b_0\left(1+\gamma\ln\left[\frac{\dot{\bar{\varepsilon}}_p}{\dot{\varepsilon}_0}\right]\right) & \text{for } \dot{\bar{\varepsilon}}_p \geqslant \dot{\varepsilon}_0\end{cases}$	Incorporating stress triaxiality, Lode angle parameter, and strain rate effects; Suitable for predicting ductile fracture under various stress states and strain rates
Johnson and Cook [207]	JC	$\bar{\varepsilon}_f = [D_1+D_2\exp(D_3\eta)][1+D_4\ln\dot{\varepsilon}^*][1+D_5\ln T^*]$ $T^* = \frac{T-T_r}{T_m-T_r},\ \dot{\varepsilon}^* = \dot{\varepsilon}/\dot{\varepsilon}_0$	Considering stress triaxiality, strain rate, and temperature effects; Widely used for metal materials under large strains, high strain rates, and high temperatures
Wang and Liu [14]	Modified Bao–Wierzbicki	$\bar{\varepsilon}_f = \varepsilon_f^0\left(1+D_4\ln\frac{\dot{\bar{\varepsilon}}}{\dot{\varepsilon}_0}\right)\left(1+D_5\frac{T-T_r}{T_m-T_r}\right)$ $\dot{\bar{\varepsilon}} = \frac{\dot{\gamma}}{\sqrt{3}} = \frac{V_s}{\sqrt{3}S} = \frac{V\cos\gamma_0}{\sqrt{3}S\cos(\varphi-\gamma_0)}$ $T = T_r+\Delta T = T_r+\frac{\mu\zeta\int_0^\gamma \tau(\gamma,\dot{\gamma},T)\,d\gamma}{\rho c}$	Applicable to high-speed machining scenarios; Characterizes the influence of strain rate and temperature on fracture; Based on the Bao-Wierzbicki model
Cockcroft and Latham [218]	Cockcroft–Latham	$\int_0^{\bar{\varepsilon}_f}\sigma_1\,\mathrm{d}\bar{\varepsilon} = C$	This criterion is based on the accumulation of maximum principal tensile stress. It is simple to implement and is commonly used in metal forming to predict fracture by cumulative plastic work
Oh et al. [211]	Modified Cockcroft–Latham	$D_{cr} = \int_0^{\bar{\varepsilon}^f}\frac{\langle\sigma_1\rangle}{\bar{\sigma}}\mathrm{d}\bar{\varepsilon}_{pl}$	Normalizes the maximum principal stress with equivalent stress
Chen et al. [59,217]	/	$\bar{\sigma}_f = \bar{\sigma}(\varepsilon,\dot{\varepsilon},T,d)(1-D)$ $D = \frac{1-\exp\left(-a\int_0^{\varepsilon_f}\frac{\bar{\sigma}_y}{G_\varepsilon}\mathrm{d}\bar{\varepsilon}\right)}{1-\exp(-a)}$ $G_\varepsilon = \frac{G_f}{L} = \int_{\bar{\varepsilon}_{oi}}^{\bar{\varepsilon}_f^{pl}}\sigma_y\mathrm{d}\bar{\varepsilon}^{pl}$	This criterion is based on energy density and can reduce the mesh dependence during machining

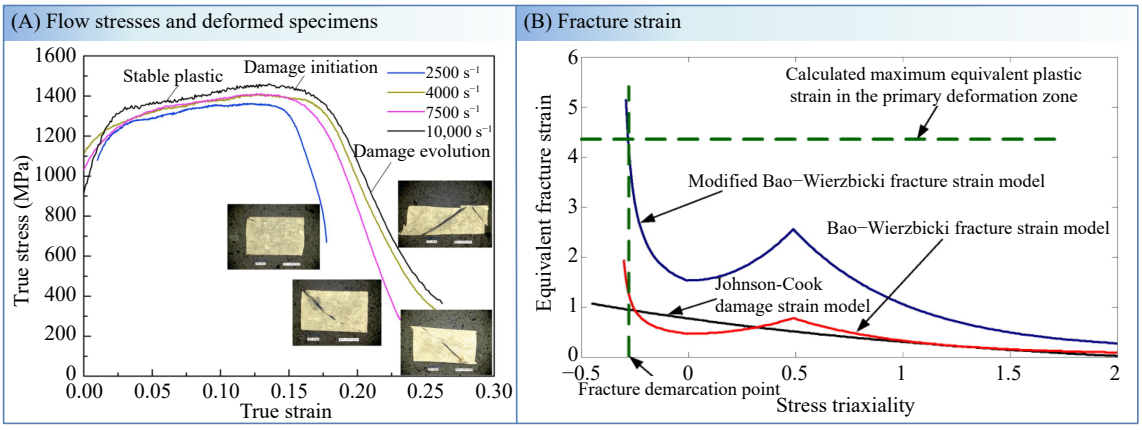


Fig. 14 Initial fracture stress and strain in metal cutting. (A) Experimental flow curves [201]. (B) Relationship between initial fracture strain and stress triaxiality with different models [14].

dynamic Split Hopkinson Bar test results with quasi-static data to capture strain rate sensitivity; and parameter D_5 is evaluated through elevated temperature Hopkinson bar tests to assess thermal softening effects. This calibration methodology enables the JC damage model to accommodate a wide range of loading conditions, leading to its extensive application in numerical simulations of metal cutting processes. Khan and Liu [96] investigated the fracture characteristics of aluminum alloy AA5083-H116, though the model's representation of negative strain rate sensitivity proved inadequate. Subsequently, Chen et al. [201] conducted SHPB tests to investigate the ductile damage behavior of Ti–6Al–4V alloy under high strain rates ranging from 2500 to 10,000 s^{-1} and wide temperature ranges (20–900 ℃), as illustrated in Fig. 14A. Shear band crack formation was observed and the failure initiation strain associated with crack generation was quantified by the SHPB results.

The Bao-Wierzbicki fracture criterion is distinguished by its incorporation of a negative stress triaxiality cutoff value of −1/3, below which material failure does not occur [192,209,210]. This model effectively prevents spurious element deletion and erosion phenomena while accurately predicting fracture modes under various impact loading conditions, demonstrating considerable applicability. However, parameter calibration for its full-range formulation remains complex, necessitating integration of diverse experimental data from tensile, compressive, and shear testing modalities. Building upon this foundation, Wang and Liu [14] developed a modified Bao-Wierzbicki model tailored for high-speed cutting conditions. This enhanced formulation incorporates strain rate and temperature effects as correction factors, enabling more accurate description of material failure behavior under dynamic loading. Their findings indicate that both strain rate and temperature exert positive influences on fracture strain, with heightened sensitivity observed within the negative stress triaxiality regime. Fig. 14B presents the fracture strain versus stress triaxiality curves for the three fracture models.

The Cockcroft−Latham (CL) fracture criterion employs accumulated plastic strain modified by the maximum principal tensile stress as a damage indicator, rendering it particularly suitable for forming processes characterized by low stress triaxiality, such as forging and extrusion [191]. Oh et al. [211] introduced a modification to the CL model by normalizing the maximum principal tensile stress with respect to the equivalent stress, thereby transforming the damage indicator into a dimensionless quantity. This reformulation ensures that damage accumulation no longer depends on the absolute magnitude of individual stress components but rather reflects the relative influence of the stress state through the ratio of maximum principal tensile stress to equivalent stress. This modification aligns more closely with the synergistic interactions among stress field components that govern fracture processes in metallic materials.

Beyond the aforementioned criteria formulated in terms of stress and strain, a separate class of fracture models based on energy principles has been developed. The fracture work W_f is commonly employed to represent the fracture resistance or toughness of engineering alloys [212], as illustrated in Fig. 15A. Dolinski et al. [213] proposed an energy-based failure criterion wherein failure initiation occurs when the total strain energy density W within a material element reaches a critical threshold W_{crit} (Fig. 15A). This critical value is determined by integrating experimental dynamic stress-strain curves. This damage model combined with the JC plasticity model, was utilized to predict the onset and propagation of dynamic shear localization for metals. For machining simulation, Mabrouki et al. [195] defined the fracture energy G_f according to the crack energy theory

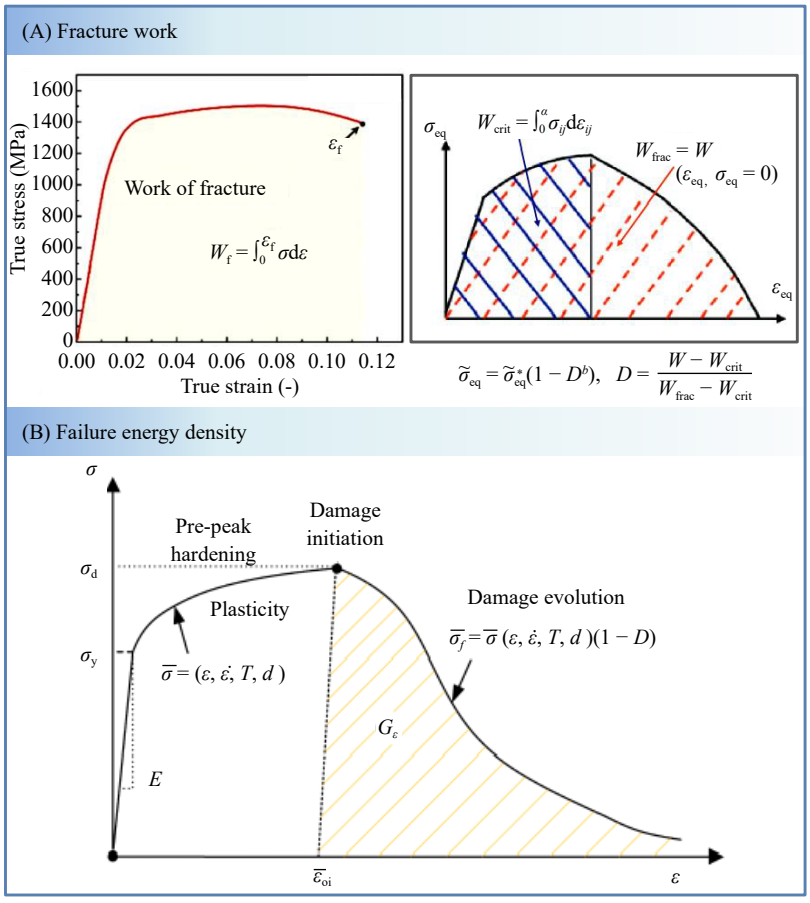


Fig. 15 Representation of fracture work and failure energy density in flow stress curves within failure criteria. (A) Fracture work [212,213]. (B) Failure energy density [59].

developed by Hillerborg et al. [214] in 1976, establishing an energy-based failure evolution model that was later used to simulate orthogonal cutting of the aerospace aluminum alloy AA2024-T351. However, it has been reported that simulation accuracy, including the prediction accuracy of cutting force, is significantly influenced by the characteristic length of the mesh element [215,216]. Since 2011, Chen et al. [30,59,201,217] have developed an energy-density-based failure evolution model at the damage evolution stage (Fig. 15B). The model maintains flow stress throughout the damage evolution stage and is capable of alleviating mesh dependence in cutting simulations. This approach effectively enhances the prediction accuracy of cutting forces and chip morphologies under various mesh densities.

Although damage models based on loading conditions including stress triaxiality can effectively establish correlations between fracture behavior and stress state, their parameters are typically calibrated through experiments conducted under specific loading paths. When applied to cutting processes characterized by non-proportional loading and complex deformation trajectories, the predictive stability of these models remains subject to inherent limitations. Future model development necessitates continued advancement in understanding the physical mechanisms governing material damage and failure under extreme cutting conditions, encompassing high strain rates, elevated temperatures, and complex stress paths. Concurrent efforts should be directed toward developing comprehensive damage frameworks that harmonize physical accuracy, parameter calibration accessibility, and computational robustness, thereby further enhancing the reliability of process simulations in metal cutting applications.

2.3 Summary

Material constitutive models, including plastic and fracture (damage) constitutive models, are the core foundation for ensuring the accuracy of metal cutting simulations, as they can accurately describe the dynamic mechanical behavior and fracture characteristics of

metallic materials under the high strain, high strain rate, and high temperature coupling effects involved in machining.

Plastic constitutive models, which describe the relationship between loading conditions (strain, strain rate, temperature, and stress state) and material mechanical behavior, are categorized into phenomenological, physics-based, and semi-physical models. Phenomenological models, represented by the JC, KHL, and TANH models, are widely used in engineering practice due to their concise mathematical forms and ease of parameter calibration via macroscopic mechanical tests. Among them, the JC model offers the best balance between simplicity and efficiency but suffers from limited accuracy under extreme conditions due to its decoupled formulation. The KHL model improves rate sensitivity description at low temperatures with increased parameter demands. The TANH model effectively captures flow softening and shear localization but involves more complex fitting. Physics-based models, such as the ZA and MTS models, focus on microstructural evolution (e.g., dislocation density, grain size) but face challenges in parameter acquisition due to their reliance on microstructural characterization techniques. Semi-physical models balance engineering practicality and physical mechanism representation, either outputting microstructural parameters (e.g., via coupling with the JMAK model) or integrating physical variables (e.g., grain size, DRX fraction) into phenomenological frameworks to enhance prediction accuracy. Overall, the main objectives of the plastic model are to achieve high prediction accuracy for plastic flow behavior and to be capable of predicting microstructure evolution based on the fundamentals of material and physical sciences. Further work on the constitutive modeling should focus on improving the prediction accuracy of flow stress and microstructure evolution.

Damage models are indispensable for accurately predicting chip formation, surface integrity, and material separation during cutting, as plastic models alone cannot capture damage accumulation and fracture failure. The review emphasizes the decisive role of stress state (characterized by stress triaxiality and normalized Lode angle parameter) in ductile fracture behavior, with fracture models classified into phenomenological and physics-based categories. Phenomenological damage models, such as the JC damage model, Bao-Wierzbicki criterion, and CL criterion, are widely applied due to their computational efficiency and ease of calibration. Additionally, energy-based fracture models, which use fracture work or strain energy density as critical thresholds, provide an alternative approach to capturing fracture behavior, with modified models addressing mesh sensitivity issues in cutting simulations. With the development of numerical modeling approaches, improving the damage/failure prediction accuracy under complex loading conditions—including strain, temperature, strain rate, and stress state—is crucial for the industrial application of numerical modeling for metal machining or in-service conditions.

Additionally, data-driven calibration demonstrates potential, yet current models have notable shortcomings. Future research should focus on integrating physical mechanisms while improving calibration accessibility and computational robustness.

3 Numerical Modeling Methods for Chip Formation

To address the limitations of conventional experimental methods in observing transient cutting phenomena, numerical modeling has become an indispensable research tool for revealing chip formation mechanisms and predicting process responses [36]. For metal machining simulation, numerical modeling—including the finite element method (FEM) and other approaches—has developed rapidly since the 1970s [3]. Among various numerical methods, FEM and FEM-integrated approaches are the most widely used techniques for simulating material removal processes in machining [26,36]. This work reviews FEM-based and FEM-hybrid modeling methods, with a focus on how different modeling strategies influence cutting performance and underlying deformation mechanisms.

3.1 Continuum scale-based numerical methods

The first fundamental theory for FE simulation was presented by Courant in 1943 [219]. A breakthrough for the FEM came with the publication of the book “The Finite Element Method in Structural and Continuum Mechanics” in 1967 [220].

Numerical methods grounded in continuum mechanics provide the dominant framework for simulating metal cutting processes. By treating both the workpiece and the tool as continuous media, these methods solve the conservation equations of mass, momentum, and energy to predict macroscopic responses such as cutting forces, temperature fields, chip morphology, and residual stresses [2,50]. Among these approaches, the FEM has become the most widely adopted and extensively developed numerical technique, owing to its maturity and versatility in handling complex geometries, nonlinear material behavior, and strongly coupled boundary

conditions [102,178]. Meanwhile, the finite volume method, as the prevailing approach in computational fluid dynamics, plays an important role in addressing phenomena involving fluid behavior, including cutting fluid flow, cooling effects, and chip curling and fracture. In summary, continuum-scale methods, particularly FEM, form the backbone of macroscopic cutting process modeling, with their effectiveness rooted in rigorous conservation laws and adaptability to complex machining conditions.

Three principal finite element formulations are commonly employed for simulating chip formation: the Lagrangian (LAG) method, the arbitrary Lagrangian–Eulerian (ALE) method, and the coupled Eulerian–Lagrangian (CEL) method. As the mesh is fully coupled with material points, the LAG method is capable of capturing the plastic deformation characteristics by mesh distortion, including the plastic flow direction during machining [30,166]. However, owing to the severe plastic deformation inherent in cutting, the LAG method often relies on sacrificial layer techniques or element deletion algorithms governed by physical or geometric criteria to realize chip separation [as shown in Fig. 16A(1)] [11,95,195,215,221]. Although the LAG method employing the sacrificial layer technique facilitates chip separation from the workpiece during simulation, it struggles to accurately predict thrust forces, and machined surface integrity (e.g. surface plastic flow), owing to the discrepancy in material failure behavior between the sacrificial layer and the workpiece. In recent years, several researchers have developed sacrificial-layer-free modeling approaches for machining simulation by assigning identical plastic and failure properties to the entire workpiece. Chen et al. [59,117] developed a JCM-ms plasticity model and an energy-density-based failure model to simulate the machining of Ti–6Al–4V alloy under various tool geometries and cooling/lubrication conditions using a separation-free LAG approach [Fig. 16A(2)]. Compared with the LAG method employing separation layers, the proposed strategy achieved significantly higher prediction accuracy for thrust force and surface plastic deformation and grain refinement. Similarly, Hu et al. [94,222] systematically evaluated the performance of the separation-free LAG method and the separation-layer-based LAG method in predicting chip morphology, cutting forces, and residual stresses. In essence, while the LAG method offers direct tracking of material history, its practical application often requires additional strategies to manage chip separation, with separation-free variants showing promise for improved accuracy.

The ALE formulation [154,223–225] was developed to reconcile the precise tracking capability of the LAG method with the mesh stability of the Eulerian method in accommodating large deformations. ALE permits mesh motion independent of material movement, enabling dynamic remeshing or nodal repositioning to accommodate deformation while maintaining adequate mesh quality. Two variants of the ALE formulation exist, namely purely Lagrangian domains and coupled Lagrangian–Eulerian domains, as illustrated in Fig. 16B. In cutting simulations, the ALE method is commonly adopted in regions subjected to severe shear deformation, such as the primary shear zone, while Lagrangian meshes are retained for the tool and workpiece substrate [226], thus enabling computationally efficient and stable simulations. The ALE approach allows the simulation of steady-state continuous chip formation without introducing explicit fracture criteria to characterize material flow. Nevertheless, the ALE formulation involves complex mesh-update algorithms, presents relatively low computational efficiency, and faces challenges in modeling localized fracture related to highly serrated chip formation in difficult-to-machine materials [227]. Therefore, although ALE effectively balances mesh stability and deformation tracking, its computational overhead and limitations in simulating severe localized fracture remain notable drawbacks.

The CEL method [228,230–232] explicitly partitions the computational domain into Eulerian regions, describing material flow such as that of the workpiece, and Lagrangian regions, representing components such as the tool or workpiece substrate, as depicted in Fig. 16C. Material flows through the Eulerian mesh, inherently circumventing Lagrangian mesh distortion. The CEL method typically demonstrates stable performance in outputting field variables including strain and temperature, and enables simulation of segmented chip formation in three-dimensional orthogonal cutting, as shown in Fig. 16C. However, the CEL method presents several limitations. When the workpiece is modeled as an Eulerian domain, the direct incorporation of microstructural features such as grain orientation becomes challenging. Three-dimensional simulations incur significant computational costs and low efficiency, while the applicability of two-dimensional models is restricted. Both the ALE and CEL approaches circumvent issues of element distortion and material loss, yet they cannot reproduce serrated chip formation without the use of damage constitutive models. Compared with ALE, the CEL method helps avoid mesh distortion while maintaining stable time increments [233]. Furthermore, CEL exhibits distinct advantages in modeling stress-dependent flow behavior [16]. In summary, while CEL offers robust handling of large deformation and stable time integration, its limitations in incorporating

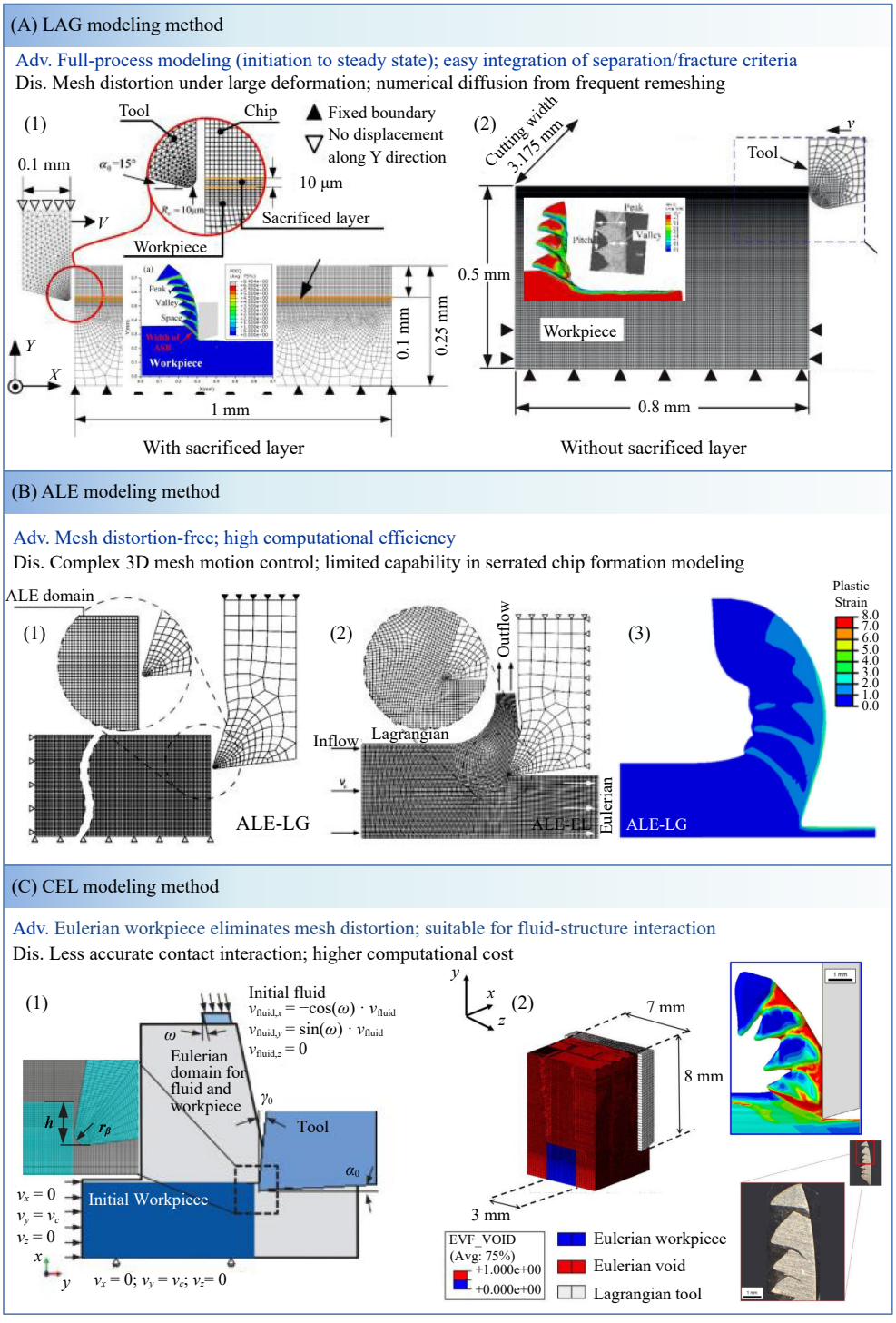


Fig. 16 Boundary conditions and predicted results of typical finite element methods for metal cutting simulation. (A) LAG [13,59]. (B) ALE [226]. (C) CEL [228,229].

microstructural details and high computational cost must be carefully considered based on the specific simulation objectives. Meanwhile, it is difficult for the CEL method to capture microscopic deformation mechanisms such as ASBs in serrated chips and the plastic flow direction near the machined surface layer.

In summary, each of the above modeling methods has its own advantages in handling large deformation behaviors in machining processes. The main direction for future improvement of simulation modeling methods is

how to obtain more information about the plastic deformation and microstructure evolution while ensuring simulation accuracy and computational efficiency.

3.2 Particle-based numerical methods

Particle-based numerical methods fundamentally circumvent the reliance on fixed meshes by discretizing the continuum into systems of interacting particles, offering inherent advantages for modeling extreme deformation scenarios.

Introduced by Gingold and Monaghan [234] in 1977, smoothed particle hydrodynamics (SPH) has become the most widely adopted particle method. This approach discretizes the governing partial differential equations through an ensemble of particles endowed with material properties, which interact via smoothing kernel functions. Such a formulation naturally accommodates large deformations without the mesh distortion constraints that plague conventional LAG methods. Between 2007 and 2015, numerous researchers applied SPH to simulate high-speed machining [235], single-grain cutting [236], and chip formation processes. Afrasiabi et al. [53] simulated orthogonal cutting of Ti–6Al–4V, validating their approach through comparison with finite element methods while evaluating both effectiveness and computational efficiency, as illustrated in Fig. 17A. Addressing two principal challenges in thermal modeling for metal cutting—namely convergence characteristics and boundary condition implementation—they subsequently proposed refinements [41]: employing higher-order Laplacian operators to enhance solution accuracy for heat conduction equations, and implementing robust surface detection algorithms to impose more physically realistic thermal boundary conditions. Validation through orthogonal cutting simulations demonstrated excellent agreement between numerical results and experimental measurements. Overall, SPH provides a fundamentally mesh-free solution for large-deformation cutting simulations, yet its early formulations often overlooked critical thermal interactions, such as heat transfer from the workpiece to the tool, prompting the development of hybrid strategies.

While SPH effectively handles large deformation conditions, heat transfer from the workpiece to the cutting tool is commonly neglected [236]. To synergistically combine the advantages of finite element and SPH methodologies, researchers have developed hybrid modeling approaches that integrate SPH with finite element formulations. Zhang et al. [237] established cross-domain thermal conduction coupling between the workpiece, modeled using SPH, and the tool, represented through a transient finite element model, as depicted in Fig. 17B. Model validity was confirmed through parametric sensitivity analysis and comparative studies with commercial software. This hybrid approach substantially improved computational efficiency, with simulated tool temperatures demonstrating favorable agreement with experimental measurements. Similarly, Zahedi et al. [238] employed this hybrid methodology to

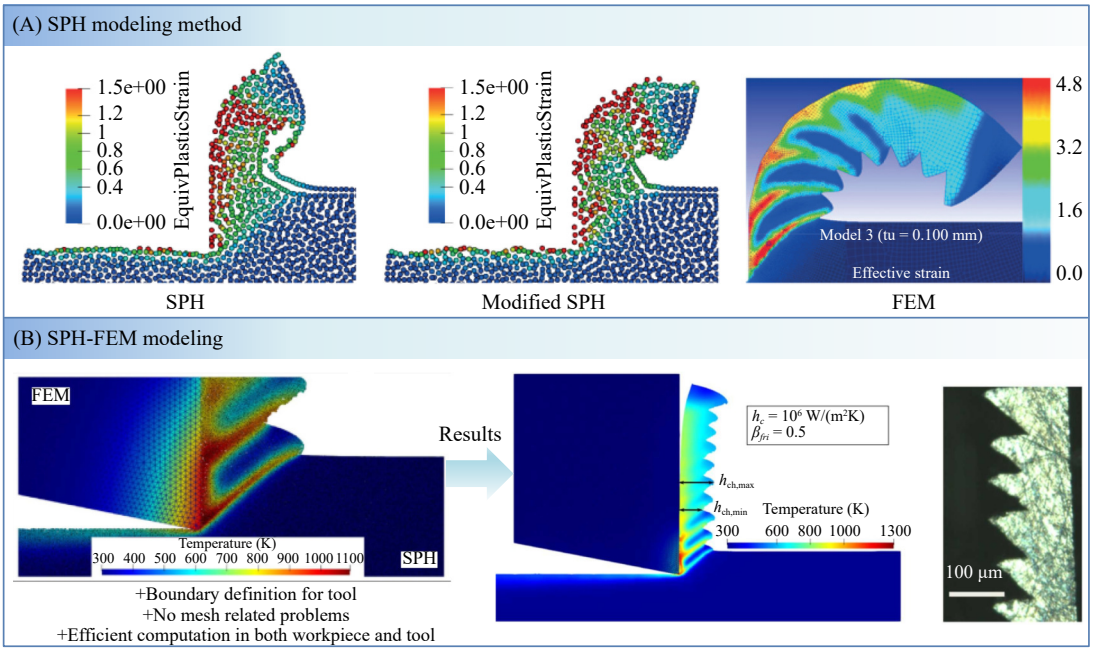


Fig. 17 Modeling of metal cutting processes using SPH and coupled SPH-FEM methods. (A) Comparison of SPH, modified SPH, and FEM for chip formation simulation [53]. (B) SPH-FEM coupled modeling for temperature distribution and serrated chip prediction [237].

elucidate the influence of crystallographic orientation on cutting performance in face-centered cubic metals. Nevertheless, the computational accuracy of the SPH method depends significantly on kernel function selection and particle distribution density. Insufficient resolution may precipitate issues such as particle penetration or stress oscillations. Regarding constitutive description, SPH typically employs simplified bilinear hardening models, which exhibit limited accuracy in capturing the nonlinear hardening effects commonly encountered in metal cutting. Furthermore, the method demonstrates suboptimal convergence characteristics, necessitating the introduction of artificial viscosity to maintain numerical stability when handling dynamic contact problems, thereby increasing computational burden [41]. Although GPU-based parallel computing techniques partially alleviate efficiency concerns, current industrial applications of SPH remain limited, with the method predominantly confined to academic research contexts. In essence, while hybrid SPH-FEM approaches effectively address the thermal and efficiency limitations of pure SPH, the method's reliance on kernel functions, artificial viscosity, and simplified constitutive models continues to constrain its accuracy and industrial applicability.

Beyond the SPH method, molecular dynamics (MD) and the discrete element method (DEM) also find specific applications in metal cutting simulation [2]. MD method reveals microscopic mechanisms such as dislocation evolution and phase transformation during cutting at the atomic scale by solving Newton's equations of motion for atomic ensembles [239,240]. This approach constitutes a fundamental tool for investigating nanometric cutting mechanisms and is particularly suitable for studying ultra-precision machining processes. However, the computational scale remains constrained by the number of atoms, limiting simulations to nanometer-scale cutting phenomena. The DEM method [241] idealizes materials as assemblies of numerous discrete particles, simulating macroscopic mechanical behavior through defined relationships governing contact forces and displacements between particles. This methodology proves especially applicable for simulating fracture and fragmentation processes in brittle materials, cutting mechanisms in powder materials, and material disintegration behavior under extreme deformation. In problems involving extensive generation of discontinuous interfaces, DEM exhibits inherent modeling advantages over continuum-based approaches [242]. Thus, MD and DEM extend particle-based methods to atomic and discontinuous scales respectively, each addressing specific cutting phenomena that continuum or mesh-based methods cannot readily capture—MD for nanoscale deformation mechanisms and DEM for brittle fracture and granular flow. The MD approach is commonly applied for modeling of the nano-cutting or nanoscale material deformation mechanism. More detailed research for MD simulation is beyond the scope of this work and readers are referred to Ref. [243] for more information.

3.3 Multiscale numerical methods

3.3.1 Particle finite element method

The Particle Finite Element Method (PFEM) is a kind of numerical technique that seamlessly integrates particle-based methodologies within the finite element framework [244]. The PFEM was firstly developed in 2004 by Oñate et al. [245] and Idelsohn et al. [246]. It was specifically developed to overcome the severe mesh distortion challenges encountered by conventional finite element methods when solving problems involving large deformations, free-surface flows, and material separation [247].

In this approach, the material is discretized as an ensemble of Lagrangian particles that carry all relevant physical information. A finite element mesh is then regenerated at each time step based on the current positions of these particles, enabling dynamic mesh adaptivity and full topological reconfiguration of the computational domain. Bakhshan et al. [102] employed the inherent particle insertion mechanism of PFEM to effectively simulate serrated chip formation within a purely Lagrangian framework and the distribution of grain size was predicted, as illustrated in Fig. 18A. Subsequently, they employed this method to conduct a comparative study of dislocation density distributions in conventional and ultrasonic machining, as shown in Fig. 18B. This simulation was achieved without requiring predefined failure criteria or sacrificial layers, while robustly addressing mesh distortion issues throughout the entire analysis process. Frequent remeshing based on particle positions is helpful to eliminate mesh distortion issues common in large-deformation analyses. However, most cutting simulations with remeshing technique are difficult to capture the plastic flow in the deformation zones by the element distribution.

3.3.2 Crystal plasticity finite element method

Most finite element simulations for metal deformation prediction consider single-crystal and bicrystal materials as isotropic. To characterize the crystalline anisotropy, including the orientation dependent change, crystallographic texture, strength, the plastic and damage behaviors, crystal plasticity finite element (CPFE)

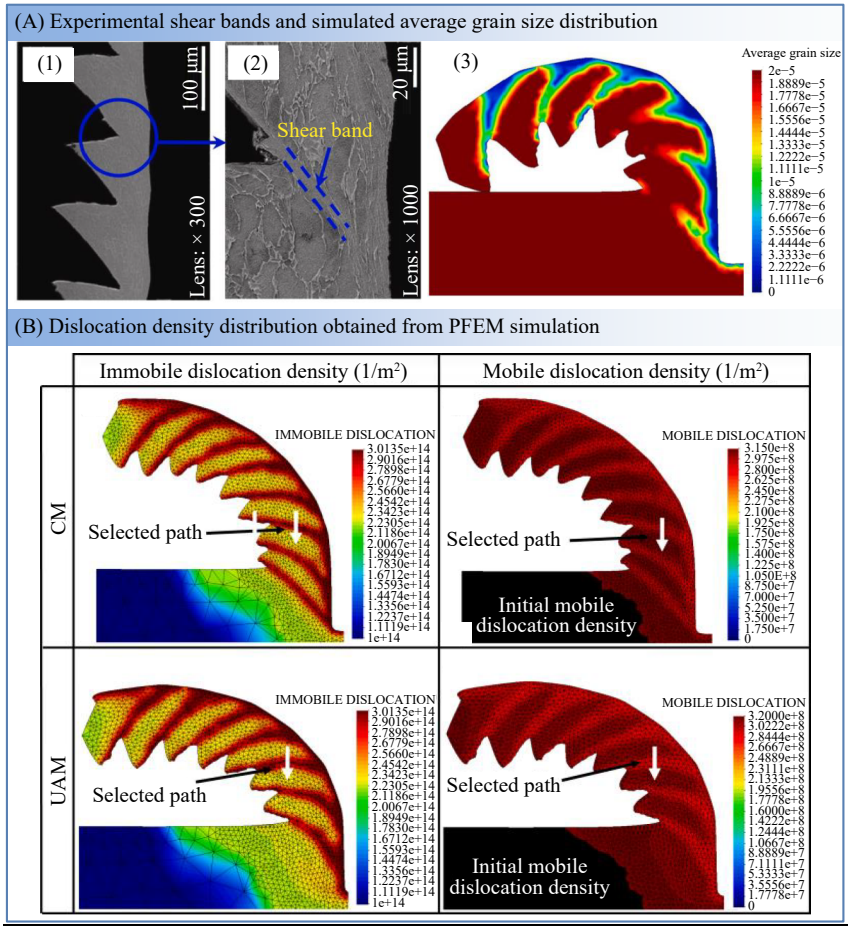


Fig. 18 PFEM simulation of serrated chip formation. (A) Experimental shear bands and simulated average grain size distribution [102]. (B) Immobile and mobile dislocation density distributions under CM and UVAM [151].

method was developed firstly in the field of material science [248–250]. The CPFE method, which combines crystal plasticity theory with the classical FEM, was first proposed by Peirce et al. in 1982 [251]. This method is capable of characterizing dislocation motion on activated slip systems, thereby revealing the relationship between the internal microstructure and the plastic deformation of workpieces under external loading [43].

Previous research employing the CPFE method has primarily focused on elucidating deformation mechanisms, analyzing intragranular texture evolution, and examining strain hardening and fracture responses, mainly through fundamental mechanical tests such as tension, compression, torsion, and bending [252]. With its ongoing development, the CPFE method now offers significant potential for modeling quasi-static and approximately proportional loading scenarios. Its particular strength lies in linking explicit representations of crystallographic texture and its evolution to the fundamental microstructural origins of macroscopic anisotropy [252,253]. For instance, using a CPFE approach that integrates slip, twinning, and fracture interactions, Tong et al. [252] simulated the grain size effect in progressive microforming. The CPFE method outperforms traditional FEM, which exhibits discontinuous strain fields, by more accurately predicting strain concentration and material flow in critical areas like the shear and dead zones, as shown in Figs. 19A(1)–19A(3), thereby highlighting its strength in revealing microstructural deformation details. By developing a crystal plasticity model that incorporates both geometrically necessary dislocation evolution and misfit strain-induced plasticity, Zan et al. [253] simulated the response of single-crystal micropillars and polycrystalline specimens within hydride-matrix composites. This modeling approach revealed the effects of hydrides and their accompanying misfit strain on localized plastic deformation, stress concentration, and dislocation density distribution in zirconium alloys, as shown in Figs. 19A(4)–19A(5).

Extreme conditions encountered in machining simulations, such as cutting processes featuring large

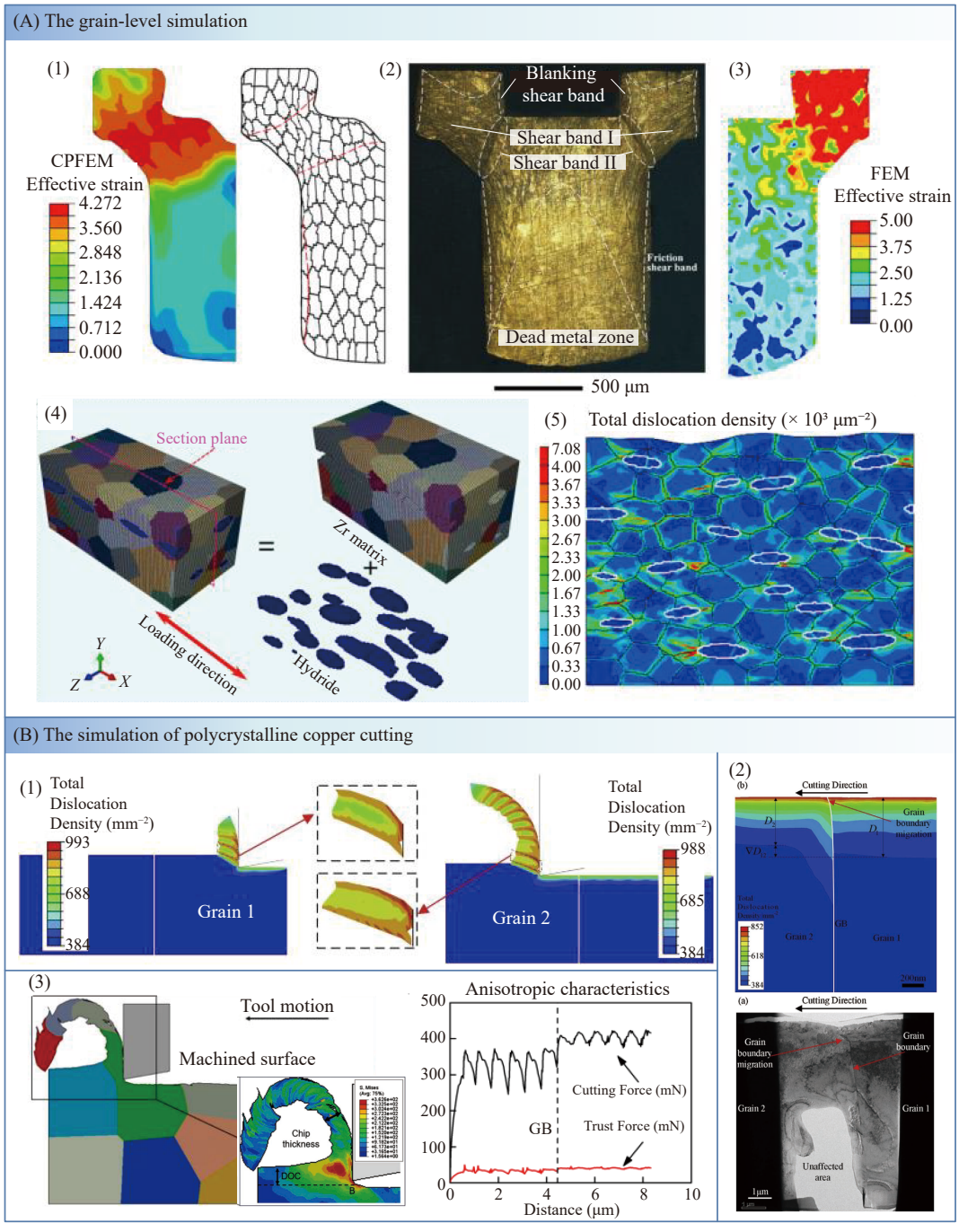


Fig. 19 Modeling using CPFE method. (A) Investigation of grain-level deformation mechanisms [252,253]. (B) Grain-scale deformation, microstructural evolution, and cutting force anisotropy in diamond cutting of copper revealed by CPFE simulation and TEM characterization [42,43,256].

deformations, high strain rates, and intricate thermomechanical–microstructural coupling, pose substantial demands on CPFE modeling. Overcoming the associated challenges in model formulation and computational efficiency remains an open issue, and research in this area is still in its nascent stage. Liu et al. [254] applied CPFE method to analyze the dislocation-slip-dominated mechanism in micro-cutting of single-crystal copper. By incorporating a damage criterion based on shear strain, their model accurately captures anisotropic material responses and predicts orientation-dependent cutting forces, asymmetric chip formation, and subsurface deformation fields. Lee et al. [255] investigated material anisotropy in ultra-precision

diamond turning of single-crystal aluminum using CPFE model incorporating crystallographic slip dynamics via Schmid's law. Wang et al. [42] applied CPFE to simulate copper cutting processes. By determining crystal orientations via EBSD and implementing a user material subroutine (UMAT) to capture grain-level anisotropic plastic deformation, their model quantitatively revealed the machining anisotropy effects induced by high-angle grain boundaries (HAGBs), including fluctuating cutting forces [Fig. 19B(3)] and increased surface roughness. To further understand grain boundary effects on machining response, a CPFE simulation of diamond cutting of bi-crystal Cu with a misorientation angle of 20° was conducted [256], as shown in Fig. 19B(1). The simulation captures the deformation heterogeneity across the grain boundary and its influence on cutting force and chip morphology. Complementing the simulation, cross-sectional TEM characterization of bi-crystal Cu after diamond cutting is presented in Fig. 19B(2). The comparison between CPFE simulation and TEM characterization demonstrates good agreement, validating the capability of CPFE to capture grain-scale deformation mechanisms at the grain boundary. However, CPFE simulations face challenges in intuitively representing the grain refinement process at the microscopic scale. To precisely characterize microstructural evolution, Zhang et al. [43] developed a multiscale coupled framework that integrates CPFE with cellular automaton simulation techniques. This framework was used to investigate microstructural evolution during ultra-precision diamond cutting of polycrystalline copper, revealing correlations between stress–strain distribution and grain refinement mechanisms. Fig. 19B(3) presents simulation results for machining assisted by ultrasonic elliptical vibration.

In summary, significant advancements have been achieved in CPFE modeling for machining processes, spanning from single-crystal to polycrystalline metals and covering macro–micro coupled mechanical behaviors. CPFE models have been successfully applied to reveal the dominant effects of crystallographic orientation and dislocation slip on anisotropic cutting responses, including cutting forces, chip formation, and subsurface deformation. Integrated approaches combining CPFE with EBSD characterization and user-defined material subroutines have enabled quantitative evaluation of machining anisotropy induced by grain boundaries and microstructural heterogeneities. To overcome the limitations of conventional CPFE in characterizing microstructural evolution such as grain refinement, multiscale and hybrid frameworks (e.g., CPFE–CA) have been developed, which establish clear correlations between thermomechanical conditions, stress–strain localization, and grain refinement mechanisms under extreme machining environments [43,257]. Nevertheless, developing physically consistent constitutive models that can accurately predict both macroscopic mechanical responses and microstructural crystalline anisotropy under large deformation, high strain rate, and strong thermo-microstructural coupling conditions remains a critical challenge for the future application of CPFE method in advanced machining processes.

3.3.3 Cellular Automata method for microstructure simulation

The fundamental theory of Cellular Automata (CA) was first proposed by John von Neumann in 1951 [258], while the formal concept of "Cellular Automata" was introduced in 1965 [259]. The CA method is widely used to simulate dynamic evolution processes such as material deformation, microstructure growth and physical field propagation using simple local interaction rules. In recent years, the ZH, JMAK, and Hall–Petch equations have been incorporated into finite element-based cutting simulations to predict the resulting grain size distribution. These models allow macroscopic prediction of grain size evolution. However, such approaches fail to capture the complex dynamic mechanisms underlying recrystallization and grain refinement. Based on dislocation density evolution theory, the CA method [260] has been widely applied to simulate microstructural evolution, and has proven to be an effective approach for modeling mesoscale microstructure development during thermoplastic deformation [35].

Multiscale simulation that couples finite element and CA methods has emerged as a powerful strategy for revealing microstructural evolution within chips and machined surfaces during metal cutting processes, as demonstrated in Figs. 20A–20C. In general, the strain, strain rate, and temperature distributions predicted via FEM are adopted as input variables for the CA model. This integrated multiscale framework bridges macroscopic thermomechanical fields and mesoscopic microstructural kinetics, thereby enabling accurate prediction and mechanistic analysis of microstructure changes during machining. Shen et al. [261] pioneered the application of the CA model for predicting microstructural evolution in machining operations. Using aluminum alloy 1100 as the material platform, they first extracted dynamic thermomechanical loading histories under various orthogonal cutting conditions through finite element simulations (Fig. 20A), subsequently employing a CA model constructed to simulate dislocation density evolution. This modeling framework integrated multiple microstructural evolution

mechanisms, including severe plastic deformation, dynamic recovery, DRX, and thermally activated grain growth. Zhou et al. [262] further applied microstructural evolution simulations to explore grain refinement behavior. Their results indicated that, within the studied range of cutting parameters, the degree of grain refinement in both ASBs and machined surface layers is enhanced with increasing cutting speed and feed rate. Importantly, the controlling mechanisms underlying the effects of cutting speed and feed rate are distinct, which provides valuable guidance for optimizing cutting parameters to improve the mechanical properties of machined parts. Overall, the coupled FE–CA multiscale approach offers an effective pathway to uncover microstructural evolution mechanisms and support performance-oriented machining optimization.

Despite the successful applications of CA methods in analyzing machining-induced microstructural evolution, conventional CA models established on discontinuous dynamic recrystallization (DDRX) theory suffer from critical limitations when applied to high-speed machining scenarios involving ultra-high strain rates and severe plastic deformation [35]. These traditional models fail to fully characterize the complex recrystallization behavior under extreme thermo-mechanical loading, thereby restricting accurate prediction of microstructural evolution in high-speed cutting processes. To address this gap, Zhang et al. [35] developed an advanced CA model incorporating both discontinuous and continuous dynamic recrystallization mechanisms (Fig. 20B), which enabled quantitative simulation of dislocation density evolution, grain deformation, and recrystallization processes in oxygen-free high-conductivity copper during high-speed cutting. Their work clarified the dominant grain refinement mechanism driven by DRX: high strain rates promote grain refinement by accelerating dislocation density accumulation, while high temperatures activate dynamic recovery and grain growth; the synergistic interaction between these competing effects eventually generates fine equiaxed grain structures within the deformed chip. Liu et al. [45] further advanced the modeling framework by adopting preloading conditions (with an initial grain size of 100 μm) and evolutionary states from prior deformation stages as initial inputs, realizing full-process simulation of microstructural evolution from preloading to unloading. Liu et al. [263] subsequently proposed a physics-based continuous dynamic recrystallization (CDRX) model for machining applications, which captured sub-grain nucleation, grain rotation, and grain boundary migration behaviors, and systematically analyzed microstructural evolution within shear bands. The reliability of this model was fully validated by comparing the simulated microstructural morphology, grain size, and dislocation density with experimental data. Collectively, these studies demonstrate that incorporating cDRX and multi-physics field coupling into CA modeling effectively compensates for the deficiencies of traditional models, laying a solid foundation for high-precision prediction of microstructural evolution in high-speed and heavy-plastic deformation machining processes.

Currently, simulation results derived from CA models often yield discontinuous grain or microstructure distributions, which are inconsistent with the realistic microstructural evolution observed in actual cutting processes. In practice, materials undergo continuous microstructural transformations driven by smoothly varying physical fields, including temperature and stress gradients. Accordingly, realizing continuous and gradient-consistent predictions of machining-induced microstructures, as illustrated in Fig. 20D, has become a key objective for further advancing this field.

3.4 Summary

This section systematically summarizes the numerical modeling framework for chip formation in metal cutting, clarifying the characteristics and applicable scales of continuum-, particle-, and multiscale methods as listed in Table 5. Continuum approaches represented by FEM—including LAG, ALE, and CEL schemes—are well-established for predicting macroscopic field variables and thermomechanical responses, yet suffer from mesh distortion and limited capability in capturing microstructural evolution. Particle methods such as SPH, MD, and DEM excel in simulating large deformation, fracture, and nanoscale phenomena, but are restricted by high computational cost and oversimplified constitutive models.

Multiscale methods including PFEM, CPFE, and FEM–CA coupling represent the frontier, bridging macro- and mesoscale behaviors to link microstructural evolution with macroscopic cutting performance. Notably, using multiscale simulations to reveal microstructural gradient distributions and DRX mechanisms has become a key trend for understanding grain refinement and optimizing surface integrity. Despite these advances, CA models often produce discontinuous microstructures, while CPFE faces challenges under high strain-rate thermo-microstructural coupling, revealing inherent trade-offs between accuracy, efficiency, and physical completeness. Future research should focus on integrated multiscale models with gradient-consistent microstructure prediction and high-fidelity constitutive descriptions for extreme cutting conditions.

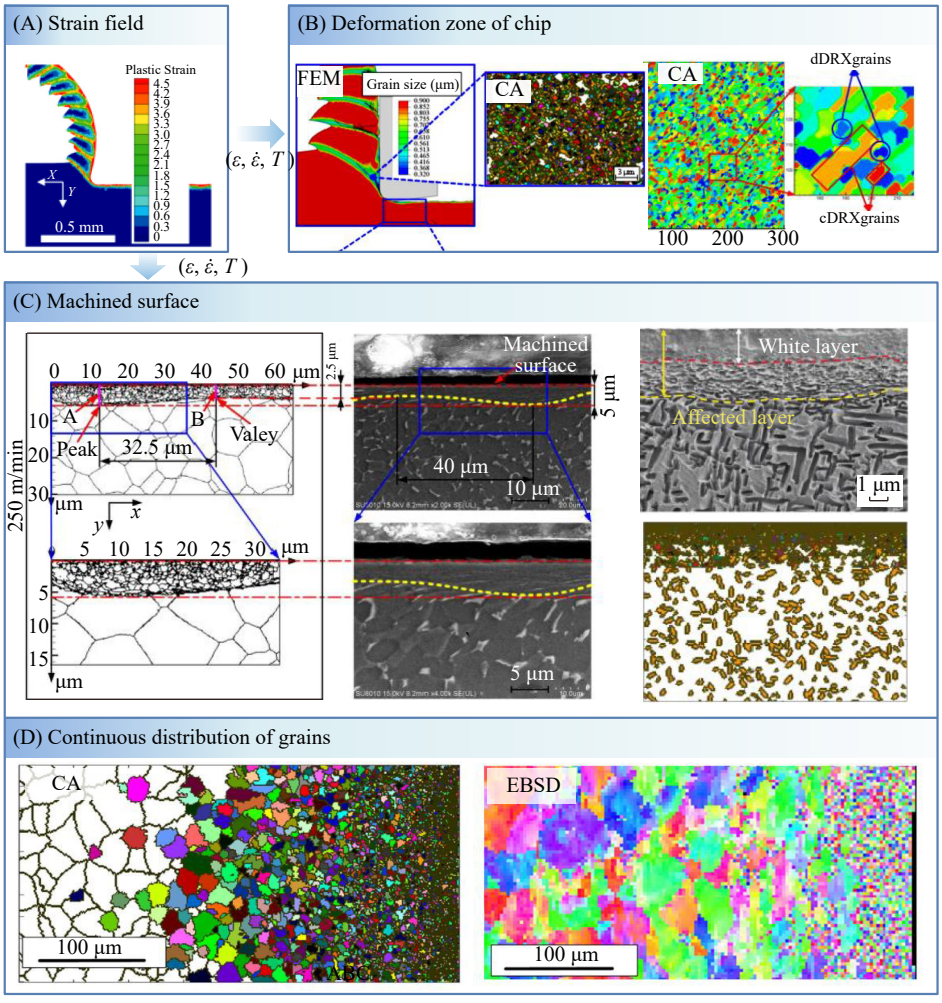


Fig. 20 Modeling of machining using CA method. (A) Physical field distribution used as deformation input for chip formation simulation [263]. (B) Microstructure evolution in the cutting zone [35,264]. (C) Microstructure evolution on the machined surface [55,264]. (D) Continuous distribution simulation with the CA model and EBSD validation [54].

Table 5 Classification of numerical modeling methods for chip formation.

Category	Method	Description
Continuum scale-based	FEM (formulations: LAG, ALE, CEL)	Macroscopic predictions: forces, temperature, stress, plastic flow; mesh distortion; weak in microstructure tracking
Particle-based	SPH/DEM/MD	Handling large deformation, fracture, atomic-scale events; high computational cost; simplified constitutive laws
Multiscale	PFEM/CPFEM/CA	Linking macro- and meso-scale behaviors; connecting microstructure evolution to cutting performance; tradeoffs among accuracy, efficiency, and physical fidelity

4 Modeling of cutting mechanics and surface integrity

Science-based modeling for machining simulation dates back to the 1940s–1960s. Typical works include the shear plane theory proposed by M.E. Merchant [9], Lee and Shaffer [265] and the shear zone theory proposed by Oxley et al. [266], both of which characterize the physical mechanisms in the primary shear zone during cutting. In the 1970s, computer-based FEM approaches were proposed [267]. In 1995, the CIRP Scientific Technical Committee (STC) "Cutting" established a working group on "Modeling of Machining Operations" under the chairmanship of Professor C.A. van Luttervelt [268]. The keynote paper by this working group states that the main objective of machining operation modeling is to predict machining performance, thereby enabling control of the cutting process to optimize productivity, machined surface quality, and machining costs [269]. To

date, the primary goal of cutting modeling remains to enhance predictive capabilities—including predictions of strain, strain rate, temperature, cutting forces, chip morphology, tool wear, and machined surface integrity (encompassing microstructure evolution)—while simultaneously improving prediction accuracy.

4.1 Modeling of physical fields, chip morphology and tool wear

4.1.1 Physical fields

Due to the high strain rates inherent in cutting processes, experimental methods face significant limitations in capturing microscopic and instantaneous physical parameters. Numerical modeling offers an effective alternative for predicting these multi-physical parameters. Consequently, accurate modeling of the physical fields involved in metal cutting serves as the foundation for understanding and predicting machining phenomena. By developing numerical models—particularly finite element simulations that couple mechanical, thermal, and material constitutive behaviors—it becomes possible to elucidate the complex physical processes within the cutting zone and to quantitatively predict key variables, including cutting force, temperature, stresses, strain, and strain rate, as well as mechanical and microstructure characteristics [177]. Physical fields (Fig. 21) govern chip morphology, tool wear, surface integrity, and machining efficiency, thereby providing a scientific basis for process optimization and control.

Cutting force is one of the most crucial parameters in process system design, tool optimization, and condition monitoring. Its magnitude and fluctuation characteristics are comprehensively affected by tool geometry (e.g., rake angle and edge radius), workpiece material

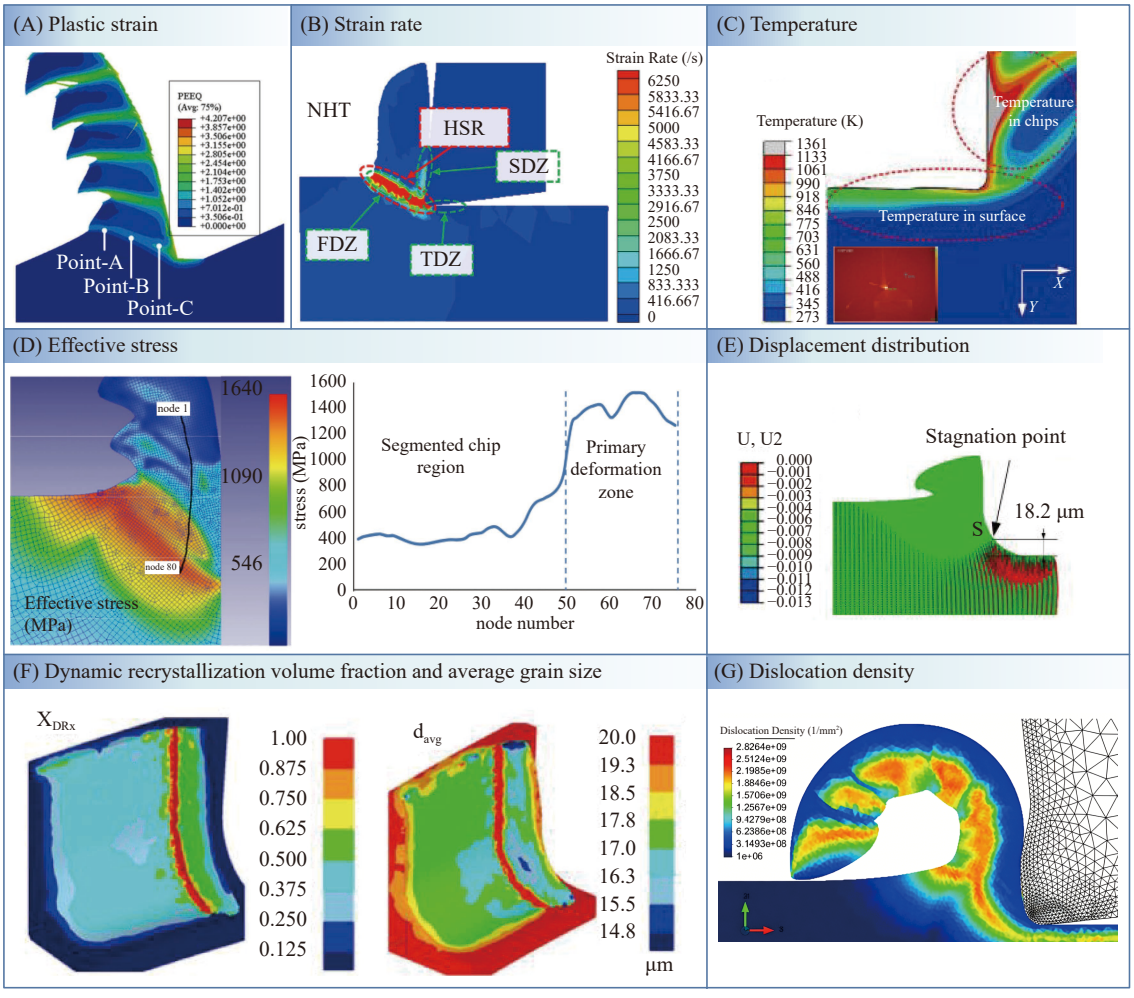


Fig. 21 Simulation of fundamental physical fields. (A) Equivalent plastic strain [18]. (B) Strain rate [274]. (C) Temperature [55,275]. (D) Effective stress [58]. (E) Displacement distribution [59]. (F) Dynamic recrystallization volume fraction and average grain size [276]. (G) Dislocation density [277].

microstructure, cooling and lubrication conditions, and process parameters [51]. Currently, the mainstream modeling approach is thermo-mechanically coupled finite element simulation based on material constitutive and friction models. Sun [270] recorded cyclic cutting forces using a dynamometer and simultaneously observed periodic features of both the chip and the workpiece surface via scanning electron microscopy and laser scanning microscopy. The study revealed that the wavy morphology of the chip and machined surface arises from periodically distributed dimples or slip bands under different cutting conditions. By correlating the time-domain characteristics of the cutting force with the spatial characteristics of the surface morphology, this work provided important insights into the force–surface coupling mechanism during chip segmentation. Although cutting force prediction is a basic function achievable in current cutting simulations, accurately predicting the directional components (e.g., principal cutting force and thrust force) under varying cutting conditions—including different cutting edge geometries—remains challenging [30,59,95,117]. This task involves the proper selection of material constitutive models and material failure models, and is one of the key factors determining the accuracy of simulating plastic deformation during chip formation and machined surface generation.

The cutting temperature, generated by plastic deformation in the shear zone and by friction between the tool and workpiece, significantly affects chip formation, tool wear, and machined surface integrity. The finite element numerical method can simulate the entire process of heat generation—from plastic deformation work and frictional work—along with heat conduction within the workpiece, chip, and tool, as well as dissipation to the environment or cooling medium, thereby obtaining a transient three-dimensional temperature field. The accuracy of temperature prediction heavily depends on the plastic behaviors and the thermophysical properties of the material (e.g., the variation of thermal conductivity and specific heat capacity with temperature) and boundary conditions (e.g., the friction and heat transfer coefficients at the tool–chip interface and cooling conditions). Theraroz et al. [271] proposed an improved analytical temperature model for orthogonal cutting, which accounts for both the edge radius and the flank wear length, and introduces the coupling relationship between them—specifically, the change in edge radius caused by wear. This modified model was validated experimentally, and the predicted results showed good agreement with measured temperatures. Through finite element simulation, the flow behavior of material in the primary shear zone and the secondary deformation zone can be visualized, and quantitative data on high-resolution stress, strain, and strain-rate fields can be obtained. These field variables provide the fundamental basis for analyzing chip formation mechanisms (such as adiabatic shear or thermomechanical shear instability and material damage), and for predicting work hardening and residual stress distribution on the workpiece surface layer [3,272,273]. Overall, the prediction accuracy of both cutting force and temperature is influenced by the constitutive model and friction model used in numerical modeling.

4.1.2 Chip morphology

Chip formation involves plastic shear or shear localization in the primary deformation zone, which is closely related to variations in cutting forces, tool–chip thermomechanical contact behavior, and tool life [272]. Pioneering research on chip formation, particularly on the mechanism of continuous chip formation, has been conducted since the early 1950s [278]. With the advancement of computer technology (after the 1970s), numerous studies have applied the FEM to investigate chip formation mechanisms during cutting, especially for segmented chips [30,58,100,273,279]. As a direct representation of the material's cutting response behavior, numerical modeling of chip morphology is of crucial significance for revealing material removal mechanisms, validating multi-physical field coupled simulation models, and guiding process optimization, owing to its macroscopic shape and microstructural characteristics [280] (as depicted in Fig. 22). Research indicates that steady-state plastic flow generally results in continuous ribbon-shaped chips, whereas periodic adiabatic shear instability leads to the formation of serrated chips [193,204].

Several studies have investigated the effects of process conditions on chip formation and the associated microstructure evolution within chips. For instance, Zhang et al. [281] observed microcracks and fold-like morphologies at the serration peaks in their study of Invar 36 alloy. This fan-shaped chip morphology is accompanied by surface quality deterioration and accelerated tool wear [Fig. 22A(3)]. Liang et al. [280] revealed the regulation mechanism of the vibration field on material deformation behavior by comparing chip morphologies of CuZn37 alloy under high-frequency ultrasonic vibration-assisted cutting and conventional cutting. As understanding of the underlying mechanisms deepens, it has become possible to actively control chip morphology by adjusting cutting parameters (e.g., speed and feed rate) and tool geometry (e.g., rake angle and chip breaker structure). For example, Xu et al. [16] found that increasing cutting speed promotes chip serration in Ti−6Al−4V, as stress triaxiality near the cutting edge becomes less negative, reducing the strain at damage initiation. Three-dimensional simulations using the CEL

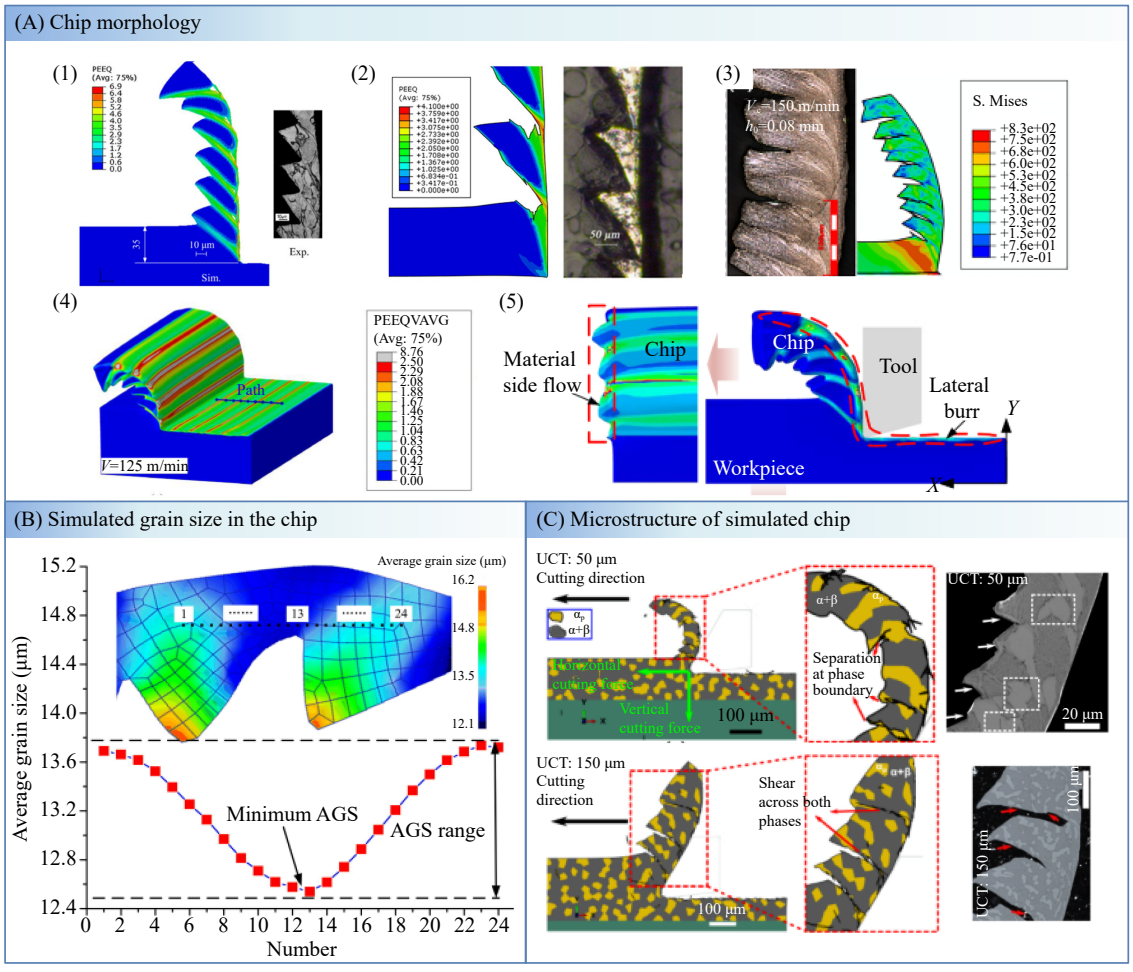


Fig. 22 Chip morphology and its correlation with cutting mechanism and microstructure. (A) Different chip morphologies [16,30,204,281]. (B) Numerically predicted average grain size (AGS) distribution between adjacent sawteeth in the chip [56]. (C) Microstructure-related chip morphology [282].

approach can effectively predict lateral burr formation, as shown in Figs. 22A(4)–22A(5). Studies indicate that a larger width of cut allows greater material side flow, resulting in increased chip width and lateral burr formation on the machined surface. Zan et al. [282] successfully simulated the morphological evolution from continuous deformation to serration under different undeformed chip thicknesses by constructing a mesoscopic finite element model that incorporates the two-phase grain structure of Ti–6Al–4V (Fig. 22C). Chip morphological features, such as shear band spacing and curl radius, serve as key observational indicators for verifying the rationality of material constitutive models, damage criteria, and friction boundary conditions [68]. Relevant studies on chip machining simulation and prediction cover the analysis of chip formation mechanisms, identification of key indicators, active control strategies, and influencing factors, thereby providing important support for the optimization of cutting processes.

Currently, chip morphology research, through the integration of multiscale experimental and simulation approaches, has established effective correlations among macroscopic morphology, microstructure, and material constitutive behavior. It thus serves as a core foundation for process optimization and machining defect prediction. Future developments may include real-time process–morphology mapping technologies that enable prediction and active control of chip morphology via online monitoring and machine learning, while also quantitatively establishing the influence of distinct chip morphologies on machined surface integrity.

4.1.3 Tool wear

Tool wear is a critical factor influencing tool costs, surface quality, and machining efficiency in metal cutting processes [283,284]. As progressive wear increases edge

roundness, the residual stress distribution on the workpiece surface alters, potentially leading to higher surface roughness and microcrack initiation [285]. Concurrently, the reduction in tool stiffness may induce chatter, further compromising machining stability. When machining difficult-to-cut materials such as Ti–6Al–4V and Inconel 718, their inherently low thermal conductivity and poor machinability impede heat dissipation from the cutting zone, thereby exacerbating tool wear under elevated temperature conditions [286]. This issue becomes particularly pronounced during high-speed machining [284].

Understanding tool wear mechanisms is essential for improving machining performance, and researchers have generally pursued two main approaches: experimental and numerical. Numerous researchers have investigated tool wear mechanisms in metal cutting through experimental approaches [287]. To quantitatively predict wear progression, Zhuang et al. [288] developed a two-stage wear rate finite element model for TiAlN-coated tools during Inconel 718 machining, revealing that both rake and flank faces are susceptible to adhesive wear during cutting. Adhered chip debris readily promotes built-up edge formation, subsequently inducing edge chipping and other failure modes [289]. Flank wear simulations and corresponding results are presented in Figs. 23A–23C. Wang et al. [290] constructed a multi-mechanism finite element tool wear model encompassing

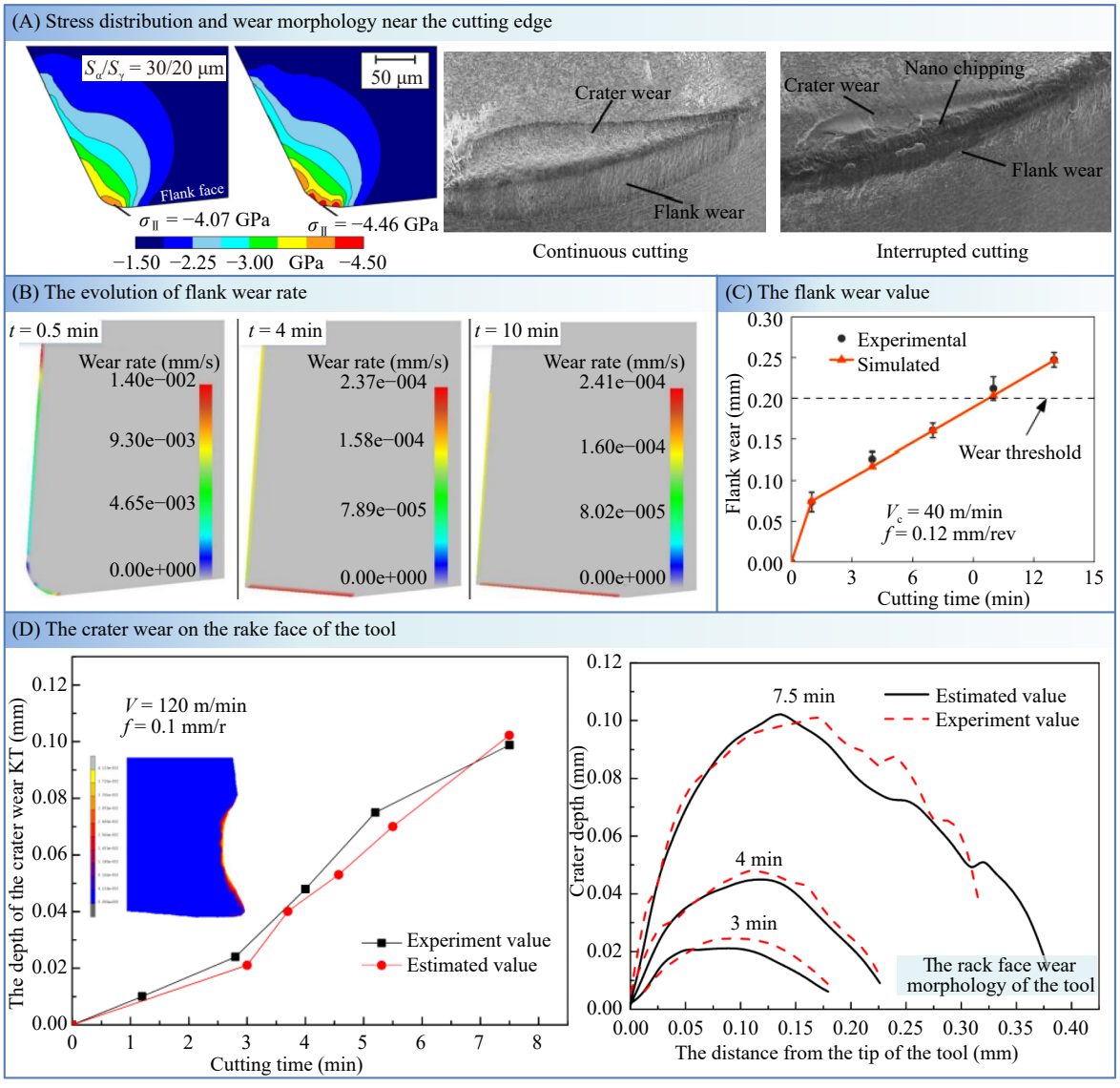


Fig. 23 Simulation of tool wear. (A) Stress distribution and wear morphology near the cutting edge [57]. (B) Evolution of flank wear rate during Inconel 718 machining [288]. (C) Comparison between experimental and simulated flank wear values in Inconel 718 machining [288]. (D) Crater wear morphology on the tool rake face during high-speed dry machining of Ti–6Al–4V [290].

abrasive wear, adhesive wear, and diffusion wear, validating its reliability in predicting wear morphology and dimensions under specific cutting conditions through experimental comparison, as illustrated in Fig. 23D. Their investigation indicated that for high-speed dry machining of Ti–6Al–4V, appropriate parameters for cemented carbide tools should be maintained within the ranges of cutting speed 90–150 m/min and feed rate 0.10–0.20 mm/r. Overall, numerical simulation not only compensates for the limitations of experimental methods but also provides a predictive basis for parameter optimization and tool life extension, representing a promising direction for future research.

In finite element simulations, the choice of friction model critically determines the accuracy of tool wear predictions. The thermomechanical load gradients induced by frictional behavior constitute primary drivers of tool wear, while wear progressively modifies tool geometry, subsequently influencing contact conditions and frictional behavior [36,60,177]. Simulations typically account for the evolution of rake face wear (crater wear), flank wear, and cutting edge wear with different edge geometries [59,291,292]. Furthermore, simulations effectively evaluate the influence of various cooling and lubrication strategies, including dry cutting, cryogenic cooling, high-pressure cooling, minimum quantity lubrication, and nanofluid lubrication, on tool wear, facilitating the selection of appropriate cooling approaches to extend tool life [117]. Additionally, tool wear influences machined surface integrity, with simulation models capable of predicting evolutionary trends in surface topography, subsurface microstructure, residual stress distribution, and surface hardness gradients across different wear stages, thereby providing critical foundations for process optimization and surface quality control.

Future research on tool wear should integrate the insights from experimental observations and numerical simulations to address the persistent challenges highlighted above, that is, the adverse effects of wear on surface quality, machining stability, and tool life, especially when processing difficult-to-cut materials. While simulation-based approaches have demonstrated clear advantages in compensating for the limitations of experimental methods, further advances are needed in multiphysics coupling, multiscale modeling, and data-driven integration, with particular emphasis on friction and wear mechanisms under extreme machining conditions. Comprehensive simulation models that incorporate the synergistic effects of coatings, surface textures, and lubrication will be developed. At the same time, high-precision experimental calibration combined with machine learning optimization will enable accurate tool life prediction and intelligent process control. Collectively, these efforts will not only deepen the understanding of wear-induced alterations in residual stress, stiffness, and surface integrity but also promote the ultimate realization of green, efficient, and intelligent manufacturing [60].

4.2 Prediction of machined surface integrity

Surface integrity refers to the comprehensive quality state of the surface and subsurface layers generated by material removal processes. The earliest technical concept of surface integrity, dating back to 1964, was defined as a surface condition whether inherent or enhanced, resulting from machining or other surface generation operations [293,294]. The researchers who proposed this concept also established testing methodologies for evaluating surface integrity, thereby laying the foundation for subsequent studies in this field. As illustrated in Fig. 24, surface integrity encompasses not only surface topography (including roughness and defects) but also subsurface microstructural and mechanical properties, such as residual stresses and microhardness, covering both macroscopic and microscopic characteristics [49,295]. Note that machined surface integrity is a consequence of the combined influence of microstructural changes and mechanical properties, and it usually refers to the post-machining (*ex-situ*) state. Actually, surface integrity needs to comprehensively consider the combined effects of the in-process (*in-situ*) state and the post-machining (*ex-situ*) state on microstructural evolution and mechanical properties [17]. These attributes directly influence the service performance of components, including contact conditions and fatigue life, making surface integrity a critical indicator that links machining processes to component functional behavior.

Regarding evaluation methodologies, diverse experimental analysis techniques have provided multidimensional characterization data for surface integrity while also establishing foundations for modeling validation [8]. In recent years, with advances in computational technology, numerical simulation has demonstrated significant value in predicting surface integrity. Through integration of sophisticated material constitutive models and incorporation of physical behaviors such as dislocation slip, phase transformation, DRX, simulations enable systematic prediction of key machining-induced indicators including residual stresses and microstructural alterations [40]. This kind of surface integrity prediction provides an effective approach to studying the formation mechanism of machined surfaces from the fundamental principles of physical and materials science. A key challenge that must be addressed in the prediction of machined surface integrity is how to maintain the predictive accuracy of simulation models with respect to material and mechanical properties, while

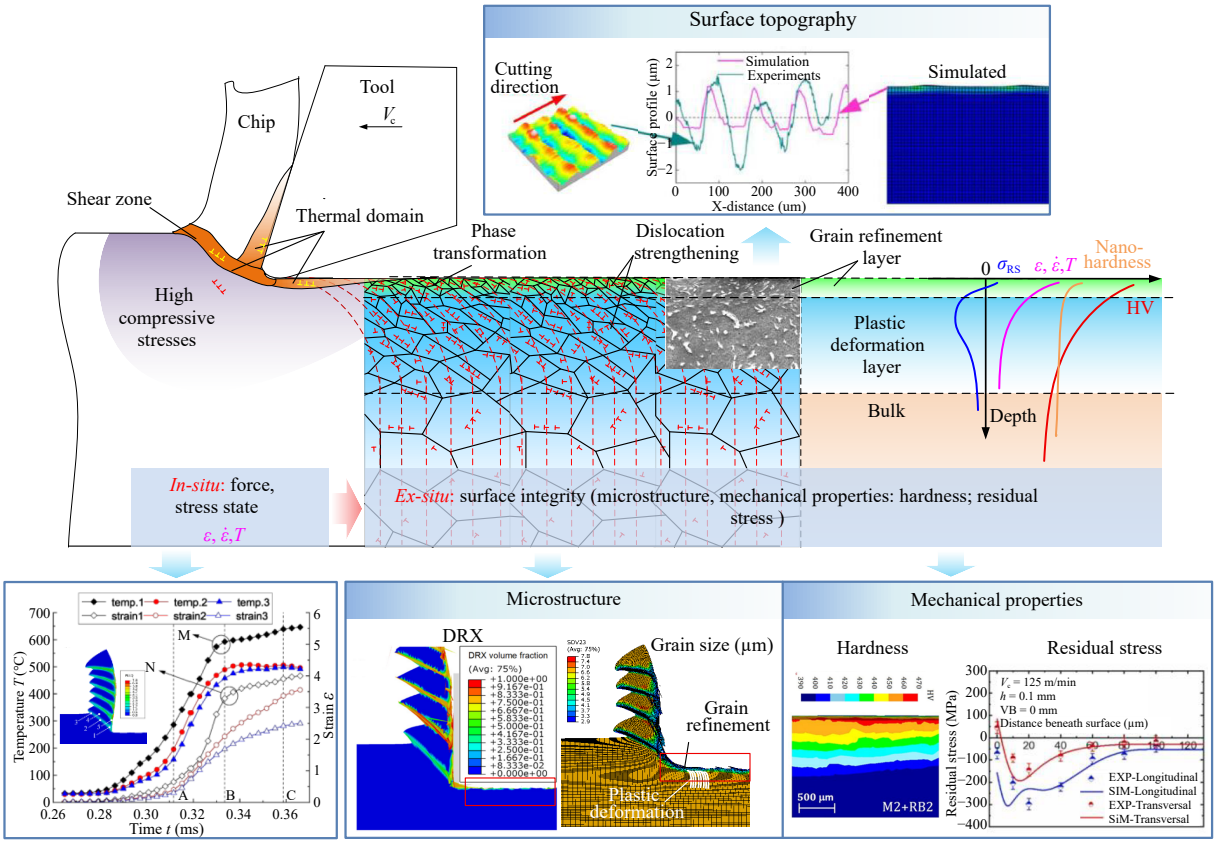


Fig. 24 Simulation of surface integrity in metal cutting processes. Reprinted from [13,16,296,297].

simultaneously achieving multi-scale, multi-physical predictions of macro/micro machined surface and subsurface physical information.

4.2.1 Surface topography

Surface topography is a comprehensive product of the mechanical-thermal loads during machining, which includes not only measurable geometric features such as roughness and texture [Fig. 25A(3)], but also physical defects and subsurface material conditions such as voids and tearing [Fig. 25B(1)] [298].

Characterization of surface topography is typically performed using instruments like surface profilometers or

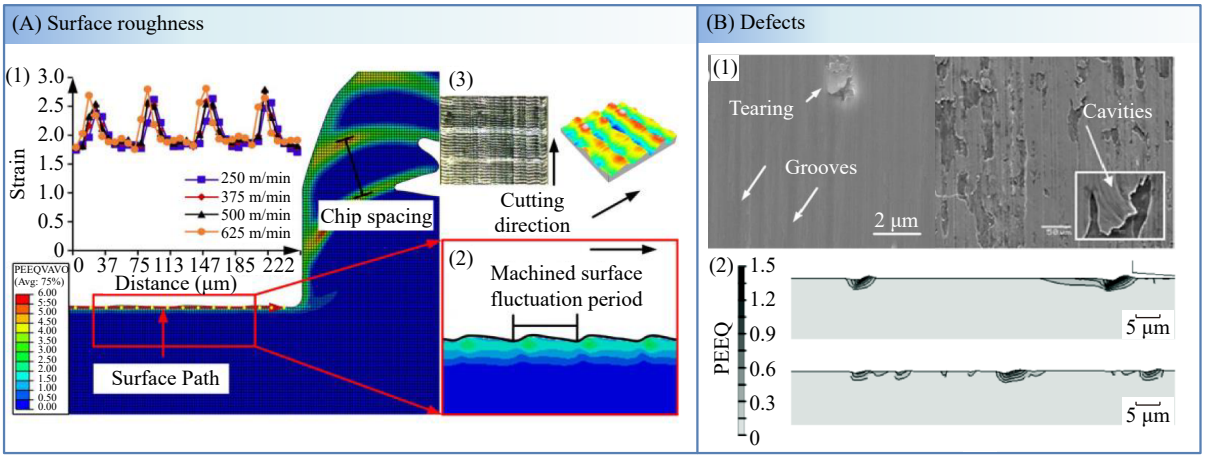


Fig. 25 Surface topography. (A) Surface topography of machined surface [55]. (B) Experimental and simulated surface defects [280,303,305].

confocal optical microscopes, which generate three-dimensional topographic images and surface roughness parameters [299]. Cutting parameters have a direct influence on surface roughness. Studies indicate that the average surface roughness (Ra) generally decreases with increasing cutting speed [49]. For instance, Chen et al. [47] conducted orthogonal cutting experiments on Ti–6Al–4V alloy under various cooling conditions and found that within an uncut chip thickness range of 10–50 μm, its effect on surface roughness is not significant. Furthermore, finite element simulations have enabled the prediction of machined surface topography. For example, Imbrogno et al. [32] successfully predicted the machined surface topography of Waspaloy and validated their predictions against experimental results. Xu et al. [55] observed that during high-speed cutting of Ti–6Al–4V, the formation of serrated chips leads to periodic distributions of morphological and physical characteristics on the machined surface. A clear correlation exists between chip spacing and the period of surface undulation, which is further confirmed by statistical measurements, as shown in Fig. 25A.

Excessive mechanical and thermal loads induced by improper cutting parameters can trigger various surface defects during machining, such as cavities [300], micro-cracking [301], surface tearing [44], material redeposition [302]. These defects pose significant risks in safety-critical components and must therefore be mitigated by optimizing cutting conditions. Revealing the underlying defect formation mechanisms is crucial for effective surface quality control. Finite element simulation offers a powerful approach to model heterogeneous plastic flow and fracture behavior during cutting, thereby predicting defect initiation. However, this imposes high demands on model accuracy. Early work by Simoneau et al. [303,304] observed dimple-type defects on machined surfaces of 1045 steel. The formation of these dimples is essentially caused by the asymmetric evolution and dissipation of cutting energy at specific grain boundaries. Using a finite element model combined with plastic dissipation energy analysis, they successfully predicted the formation mechanism of surface dimples in micro-cutting, as illustrated in Fig. 25B(2).

In summary, the prediction of machined surface topography and defects relies heavily on the synergistic use of advanced characterization techniques and high-fidelity finite element simulations. Future efforts should focus on developing multi-scale, physics-informed models that integrate material heterogeneity and dynamic thermal-mechanical coupling, enabling real-time, in-process surface quality prediction and control.

4.2.2 Subsurface microstructure

In recent decades, metallurgical alterations on machined surfaces have attracted increasing attention and have gradually become recognized as critical surface integrity parameters governing surface properties and performance [306]. During machining processes, workpiece materials are exposed to thermal, mechanical, and chemical energy inputs, leading to strain hardening and DRX phenomena. Through strain hardening, materials may experience hardening accompanied by reduced ductility, while DRX can produce hardening with enhanced ductility. These thermal effects involving elevated temperatures and rapid quenching, combined with mechanical effects characterized by high stresses and strains, constitute the primary drivers of microstructural modifications, phase transformations, and plastic deformation. Numerical simulation of microstructure evolution encompasses aspects such as dislocation density evolution and texture development, and the resulting microstructure fundamentally determines the macroscopic behavior and mechanical response of materials [7].

Grain refinement in machining predominantly arises from DRX behavior. Traditionally, DRX has been represented as DDRX for predicting grain refinement during processing, while CDRX has often been overlooked; only recently has CDRX received increased attention as novel experimental techniques have enabled investigation of DRX mechanisms during machining [263]. White and dark layers govern the distribution of residual stresses and influence the mechanical properties of machined surfaces, substantially affecting workpiece performance [39]. The white layer typically manifests as a hard, brittle region that facilitates crack initiation and propagation on workpiece surfaces, consequently limiting the fatigue strength of finished components in numerous applications [307,308]. Most studies model the grain refinement by the DRX theory, such as the classical ZH model, JMAK model [13,150,151,170,264]. When machining under severe cutting conditions, such as those involving large undeformed chip thicknesses and tool wear, the resulting elevated mechanical loads induce severe plastic deformation in the workpiece, potentially leading to grain refinement within the machined surface layer [307]. This machining-induced grain-refined layer is designated as the white layer due to its characteristic appearance following etching [38]. Bakhshan et al. [102] presented a numerical modeling framework that integrates the PFEM with microstructural evolution schemes to predict grain size variations during orthogonal cutting of Ti–6Al–4V alloy. The evolution of dynamically recrystallized grain size is incrementally developed and incorporated into the PFEM through internal state variables as homogeneous field distributions. The JMAK model is employed to predict grain size evolution resulting from DRX phenomena

induced by severe plastic deformation during machining. The predicted grain size distributions within machined surfaces are quantitatively compared with experimental measurements, demonstrating satisfactory agreement, as shown in Fig. 26A. This validation confirms the capability of the proposed coupled approach to reliably simulate grain refinement mechanisms and resulting grain size alterations during TC4 machining processes.

For high-speed machining of titanium alloy, a modified DRX model incorporating large plastic strain as a control variable was proposed to overcome limitations of the conventional ZH model, and an incremental formulation captures the continuous evolution of grain size; EBSD validation reveals that grain size gradually increases along the depth direction, indicating that strain rate dominates the DRX process over temperature effects on machined surfaces [309] (Fig. 26B). In addition, predictive investigations on white layer formation during machining of AISI 52100 steel and nickel superalloys have been reported [37,38,311]. Furthermore, the influence of cutting step distance on chip grain refinement and work hardening in Ti–6Al–4V machining reveals that residual strain from preceding passes induces variations in grain size and microhardness within the chip free surface during subsequent operations [312].

Stored energy serves as a key indicator for characterizing microstructural evolution during machining. Energy dissipation constitutes a critical factor determining machined surface integrity, as plastic deformation induces accumulation of internal energy in the form of lattice defects, primarily dislocations, and this stored energy differs fundamentally from elastic strain energy in that it is not released upon unloading [313]. Tang et al. [310] proposed that stored energy within the

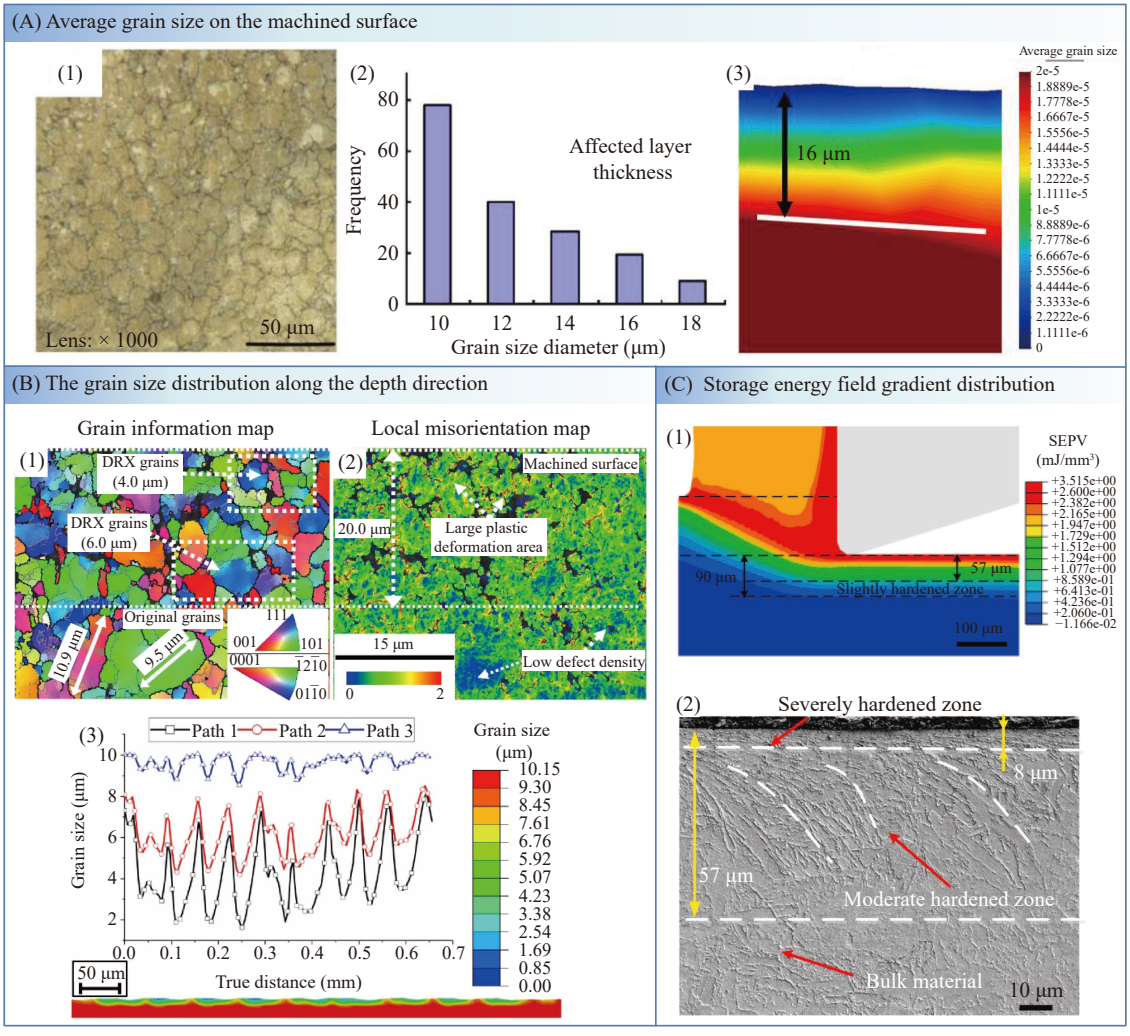


Fig. 26 Prediction of grain size and grain refinement layer. (A) Comparison of average grain size on the machined surface between experimental measurements and numerical simulation results [102]. (B) Grain size gradient of the machined surface in the depth direction [309]. (C) Prediction of grain refinement layer via the gradient of stored energy field [310].

cutting deformation zones can serve as a key indicator for characterizing microstructural evolution, particularly grain refinement. By establishing a stored energy prediction model based on material hardening behavior and microstructural changes, the subgrain size distribution in orthogonal cutting was successfully simulated; TEM and EBSD analyses verified that stored energy effectively predicts the refined grain structure [310]. Additionally, the stored energy field correlates well with hardness and stress distributions, offering a practical way to assess deformation-induced grain refinement via hardness measurements, further highlighting the role of stored energy in capturing grain refinement mechanisms during cutting processes (Fig. 26C) .

Dislocation slip and deformation twinning are the primary deformation mechanism for metals [67]. Currently, the majority of researchers employ experimental techniques to analyze dislocation density on machined surfaces. A multi-faceted experimental approach was used to investigate microstructural evolution and grain refinement in Inconel 718 during high-speed machining, employing EBSD to map grain orientation and boundary characteristics, and TEM with precession electron diffraction (PED) to provide detailed analysis of dislocation structures; this enabled quantification of geometrically necessary dislocation (GND) density, as shown in Fig. 27A [64]. It was found that DRX is not the primary factor behind hardness increase; rather, areas beneath the DRX layer exhibit significant crystallographic slip, thereby increasing dislocation density, and numerical modeling effectively linked these dislocations to material hardening and recovery, with simulated dislocation concentrations aligning with experimentally observed slip bands (Fig. 27B) [32]. A three-dimensional finite element model developed for high-speed turning of AA7075-T6 can predict variations in dislocation density under different cooling conditions; simulations indicate that cryogenic machining results in a higher predicted dislocation density than other conditions because low temperatures suppress recovery effects on the machined surface, thereby preserving the dislocations generated during deformation (Fig. 27C) [314]. Over all, the distribution of dislocation density reflects a metal's resistance to plastic deformation and is highly correlated with its mechanical strength, such as yield strength and micro-hardness [315]. Therefore, investigating dislocation density provides a crucial strategy for understanding the relationship between microstructural evolution and mechanical behavior during machining.

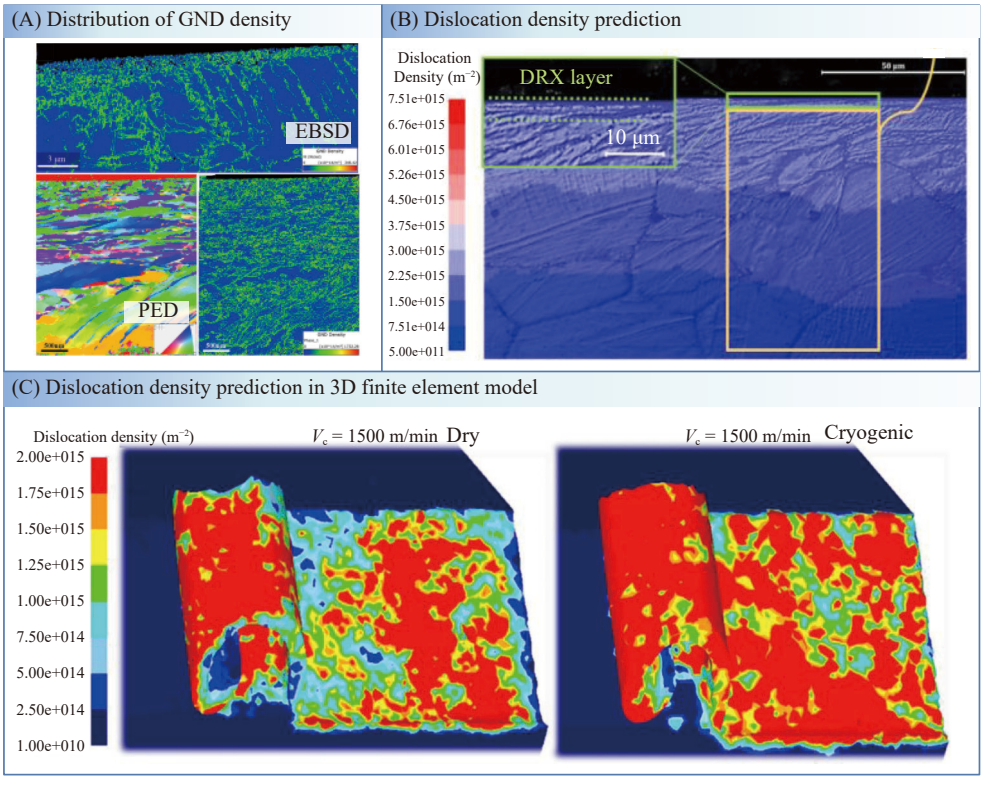


Fig. 27 Examination and simulation of dislocation density. (A) GND distribution within the machined subsurface characterized by experiments [64]. (B) Numerical prediction of dislocation density and corresponding experimental validation [32]. (C) Three-dimensional finite element prediction of dislocation density under different cooling conditions [314].

Phase transformation is also recognized as a significant factor influencing metallurgical alterations. Under high cutting speeds, the short interaction time between tool and workpiece results in phase transformation characteristics on machined surfaces that differ from those observed in conventional heat treatment and forming processes [316]. Ullah et al. [15] investigated the dynamic phase transformation behavior of Ti–6Al–4V during high-speed milling, with the simulated results of phase volume fraction and corresponding XRD experimental verification presented in Fig. 28A. Their study revealed that during the rapid heating stage, the β-phase volume fraction increased dramatically with elevated cutting speed and feed rate, reaching up to 96.38% at 350 m/min, while the subsequent rapid cooling facilitated the reversion of transformed β phase back into α' phase, highlighting the material's sensitivity to thermal fluctuations. XRD analysis of machined surfaces further confirmed these phase alterations, showing that β-phase peak intensities decreased with varying milling parameters due to grain refinement from severe plastic deformation, which directly influenced the phase volume fractions. For NiTi alloys, machining-induced phase transformation is sensitive to temperature and stress; higher cutting speed leads to higher temperature, which further promotes martensitic transformation on the machined surface, resulting in a larger and deeper martensite volume fraction (Fig. 28B) [317]. In summary, recent studies have demonstrated that phase transformation during high-speed machining can be effectively modeled using microstructure-based constitutive laws within finite element frameworks, capturing dynamic changes in phase volume fractions (e.g., α↔β, martensitic transformation) that are validated by experimental measurements such as XRD. Future research should focus on developing coupled multi-mechanism models that integrate phase transformation, DRX, dislocation slip, and twinning into a unified theoretical and computational framework, enabling comprehensive prediction of microstructural evolution under extreme thermomechanical conditions [318]. Such coupled models will be essential for understanding the interplay between different metallurgical mechanisms and for optimizing machining processes to achieve desired surface integrity.

With the advancement of material characterization techniques, an increasing number of methods have become available to study grain deformation mechanisms during machining. Advanced characterization techniques are paving the way for crystal plasticity-based simulations. Among them, transmission Kikuchi diffraction (TKD) is primarily used for high-resolution characterization of microstructural evolution in the subsurface layer after cutting, such as observing grain refinement and texture evolution, as shown in Fig. 29. By providing crystal orientation information, TKD correlates micro-deformation mechanisms (e.g., slip plane activation) with macroscopic cutting parameters (e.g., shear angle), thereby revealing the plastic deformation and phase transformation mechanisms involved in material removal. Given the high-resolution crystal orientation data that TKD provides, CPFE simulation is

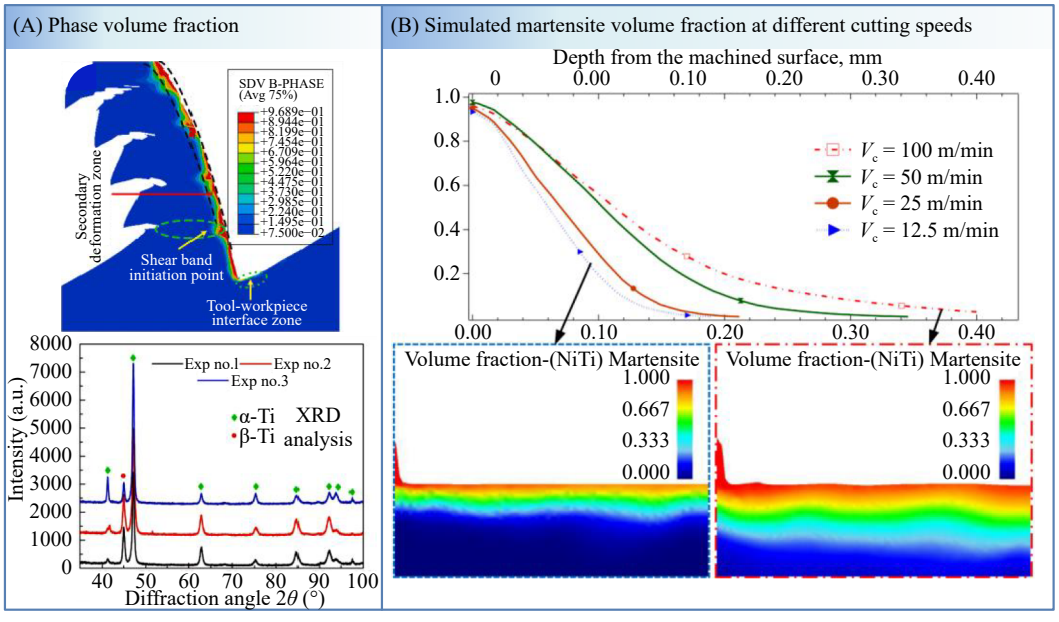


Fig. 28 Prediction of phase fraction. (A) Simulated results of phase volume fraction and XRD experimental verification [15]. (B) Simulated martensite volume fraction and its distribution depth from the machined surface at different cutting speeds [317].

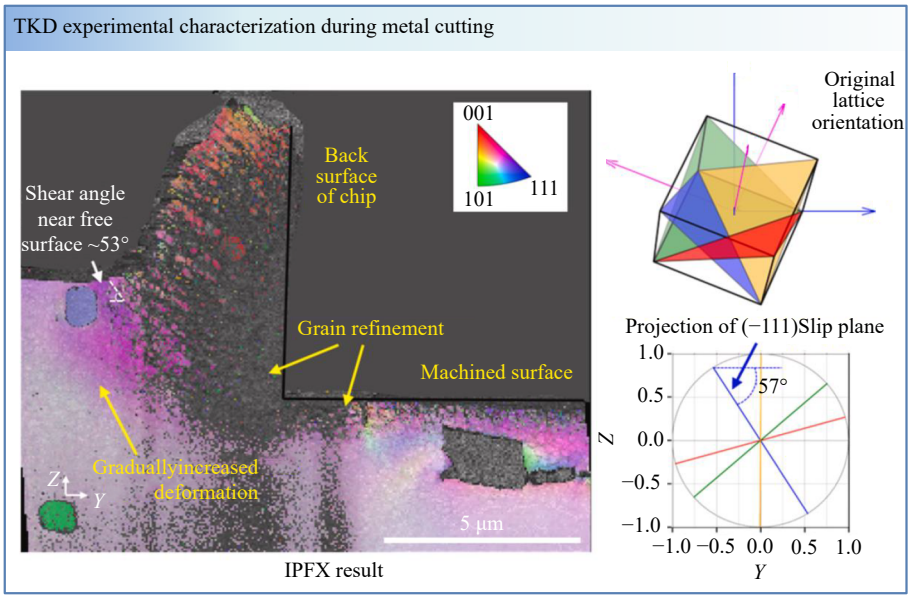


Fig. 29 TKD experimental characterization of machining-induced microstructures [48].

expected to become the mainstream approach. A key research direction for advancing numerical simulation of machined surface integrity is to integrate CPFE analysis to more comprehensively and accurately predict grain evolution and deformation mechanisms during machining, and to achieve effective integration and high prediction accuracy with microstructural characterization. Furthermore, ensuring the accuracy of flow stress predictions under varying temperatures and strain rates, while maintaining the fidelity of physical parameters obtained from microstructural characterization, is critical for guaranteeing the reliability of macro-micro mechanical and microstructural predictions in materials science.

4.2.3 Subsurface mechanical properties

4.2.3.1 Hardness

Work hardening behavior is an important physical phenomenon in metal cutting processes. It refers to the increase in yield stress caused by rising plastic strain, and serves as a key factor reflecting the machined surface integrity. The first technique for characterizing the hardness of metals was proposed in 1900 by Brinell [319]. After that, with the development of hardness test technology, hardness becomes one of the most important mechanical behaviors for metals. Based on the theoretical analysis and experimental characterization, a well-known empirical relationship between the hardness H_v and yield stress σ_y follows the form of $H_v \approx 3\sigma_y$ [320,321]. Normally, hardness increases due to grain boundary strengthening and dislocation strengthening, as an increase in grain boundaries or dislocations impedes dislocation movement under further loading. Note that the hardness of the machined surface can be regarded as an *ex-situ* physical state, since the in-process cutting involves high temperatures that reduce mechanical strength [17]. The strains induced in the workpiece microstructure by the material removal process can cause significant alterations in its elastoplastic mechanical behavior at both the micro and nano scales. Consequently, microhardness and nano-hardness serve as important indicators of surface integrity, providing quantitative measures of the surface metallurgical state and influencing the service performance of machined components [298].

Fig. 30A presents typical numerical prediction of microhardness on machined surfaces, with results validated through experimental measurements. Chen et al. [322] developed a calculated microstructure-sensitive hardness model for treating of Al−Cu−Mg alloy by high-pressure torsion. The model effectively predicts hardness variations on both the surface and subsurface, confirming that higher burnishing forces combined with finishing operations lead to increase in hardness. The strengthening mechanism was theoretically analyzed by considering the effects of dislocation accumulation, grain refinement, solid solution strengthening, precipitation strengthening, solute clusters and element segregation [296]. For metal cutting processes, most of FE models employ the DRX prediction models (e.g. JMAK model) and the Hall–Petch equation to predict the grain refinement and micro-hardness [34,46,323]. In addition, some researchers have applied physics-based constitutive models that consider the effects of dislocation strengthening and Hall–Petch

relation-based grain boundary strengthening to predict the micro-hardness [32,296]. Mustafa et al. [323] proposed a predictive model for grain size refinement and microhardness enhancement during high-speed milling of Inconel 718. The study revealed significant grain refinement on the machined surface and within the segmented chips, driven by DRX under intense thermomechanical loading. The refined grain structure directly increases microhardness, consistent with the Hall–Petch relationship. Chen et al. [59] investigated the effect of edge radius on subsurface hardness in orthogonal cutting of titanium alloy and reported that the micro-hardness of the machined surface is highly related to the degree of plastic deformation. That is, severe shear plastic deformation at the machined surface generates a thicker grain refinement layer and also leads to higher surface hardness.

Some researches modeled the nano-hardness by considering the grain refinement in machining based on the Hall–Petch relation. Umbrello et al. [31] established a correlation between α lamellar thickness and nano-hardness to develop a 3D cutting process for dry and cryogenic machining of titanium alloy. The predicted nano-hardness results demonstrated favorable agreement with experimental measurements, as illustrated in Fig. 30B(2). Jin et al. [166] established a relationship between the nano-indentation hardness and the yield strength of Ti–6Al–4V alloy ($HN = 4.6\sigma_y$). Based on a grain-size-dependent plastic model, they modeled the nano-indentation hardness distribution of the workpiece subjected to a surface milling-burnishing process, and the simulated nano-indentation hardness showed good agreement with the experimental results, as shown in Fig. 30B(1). Meanwhile, from a physical and materials science perspective, researchers have analyzed the grain refinement mechanisms arising from CDRX and geometric DRX during machining, along with their effects on mechanical performance evaluated through micro-pillar compression testing. The hardening mechanisms associated with different DRX phenomena were systematically investigated via microstructure characterization (Fig. 31) [325]. Although various modeling approaches can be used to predict the micro-hardness distribution in machining, the underlying strengthening or work hardening mechanisms still require further investigation using numerical modeling methods.

The above studies consistently demonstrate that, through appropriate physical models (e.g., the Hall–Petch relationship) and numerical simulations, the hardness evolution on machined surfaces and sub-surfaces can be

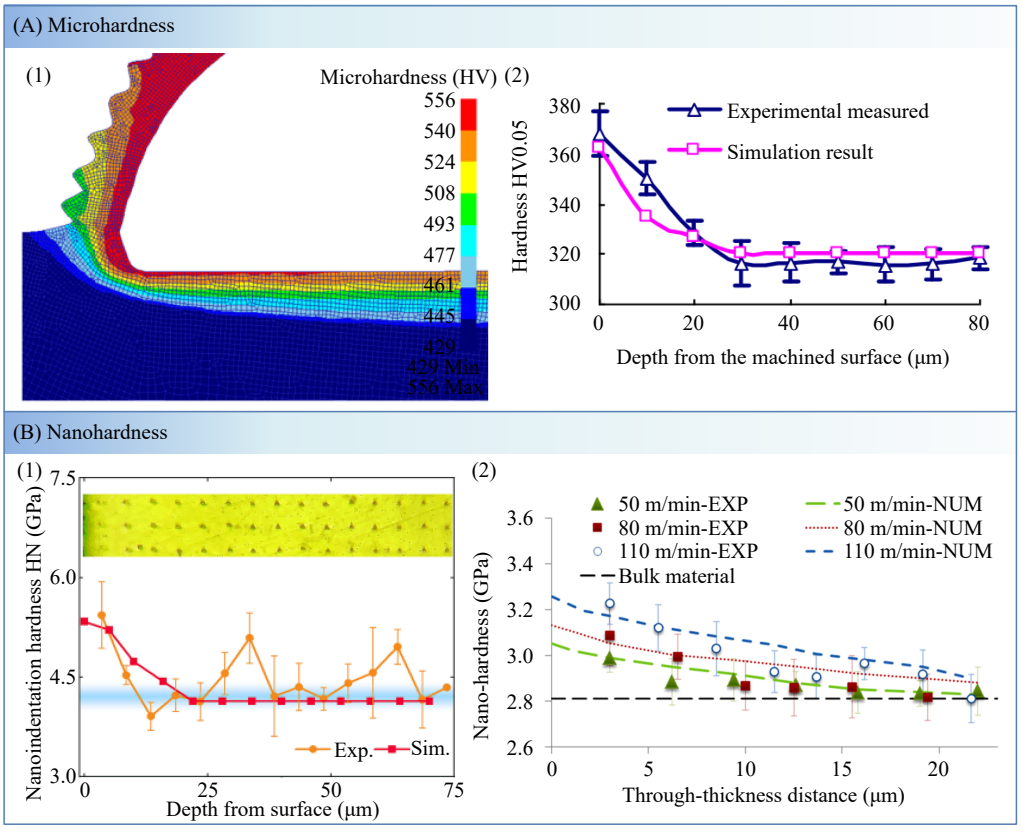


Fig. 30 Micro-hardness and nano-hardness prediction. (A) Microhardness [34,324]. (B) Nanohardness [31,166].

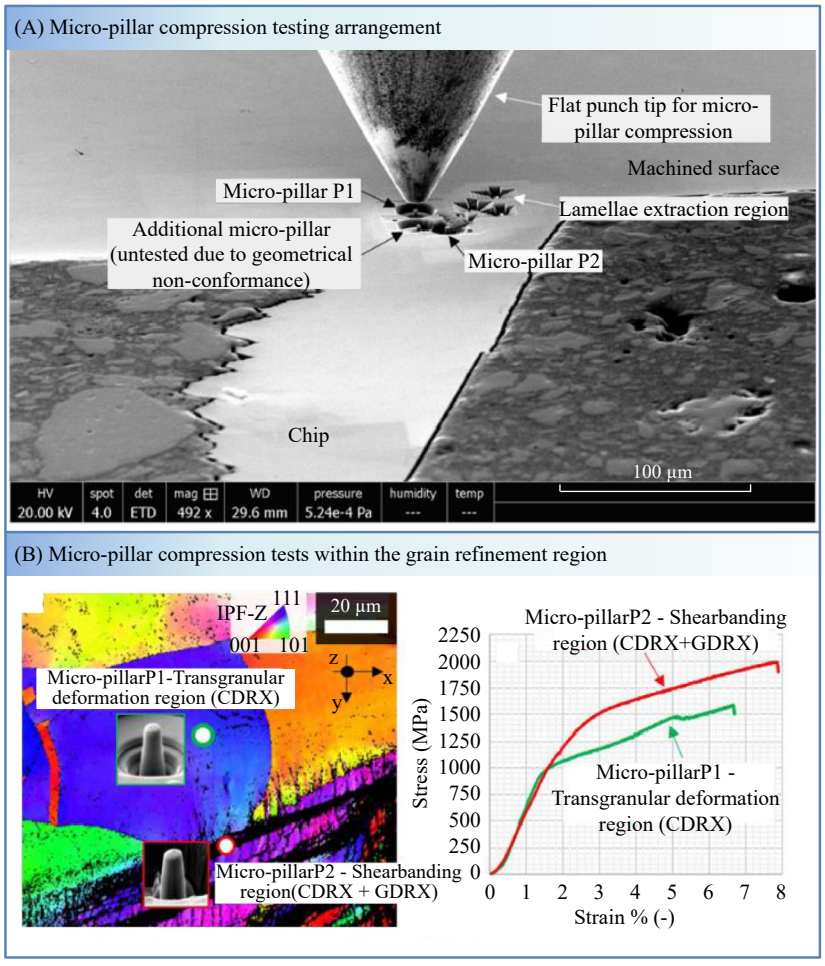


Fig. 31 Micro-pillar compression analysis of grain-refined zones [325]. (A) Test configuration. (B) Site-specific stress-strain responses.

effectively predicted, with simulation results showing agreement with experimental measurements. However, hardness prediction based on multi-scale and multi-mechanism approaches (including grain boundary strengthening, dislocation strengthening, solid solution strengthening, precipitation strengthening, etc.) still requires further in-depth investigation.

4.2.3.2 Residual stress

Residual stress refers to the stress that remains in a solid part after external loads, including the mechanical and thermal load, have been released [326]. Residual stress is one of the most important factors affecting surface integrity, due to its direct influence on fatigue life, wear and corrosion resistance [40,326–328]. In the machining of thin-walled components made of titanium alloys and superalloys which are widely used in aerospace applications, residual stress is a primary factor contributing to deformation and failure [329]. Machining-induced residual stresses originate from the complex thermomechanical loading history inherent to cutting processes, which includes mechanical loading/unloading cycles as well as rapid heating and cooling phenomena [330]. The distribution and magnitude of these stresses are influenced by the interactive effects of multiple factors, such as cutting parameters, tool geometry (e.g., rake angle and edge radius), tool wear state, and cooling conditions [331,332]. Consequently, accurate prediction and control of machining-induced residual stresses are of paramount importance [329,330].

Current research on residual stress primarily combines experimental measurement techniques with numerical prediction methodologies. Experimental approaches, including X-ray diffraction [333] and the focused ion beam–digital image correlation (FIB-DIC) ring-core method [334], can provide direct measurements. However, they suffer from high costs, low efficiency, and limited capability for capturing residual stress distributions in large-scale engineering components [335]. To overcome these limitations, the development of efficient and high-precision prediction models has

become a shared goal in both academia and industry. Since the early 2000s, the FEM has emerged as the predominant tool for residual stress prediction, owing to its ability to comprehensively account for material nonlinearity, thermomechanical coupling, and complex boundary conditions [336].

In the cutting process, residual stress in the machined surface is highly related to the thermal and mechanical effects including the elastic strain, plastic strain and thermal strain near the surface and subsurface after cutting [332,337], as indicated in Fig. 24. During the orthogonal and oblique cutting process, it was reported that the cutting-induced principal directions of residual stress are oriented along and normal to the cutting edge [337]. Several studies have attempted to analyze the mechanisms of residual stress formation through numerical simulation during machining. Research indicates that cutting parameters, such as feed rate and cutting speed, significantly influence the depth of the residual stress layer and the distribution of tensile/compressive stress by altering heat input and plastic strain depth [50]. Tool geometry and wear are other crucial factors that affect the residual stress of machined surface. An increased edge radius or flank wear will intensify the plastic extrusion and thermal load on the workpiece surface layer, often resulting in a deeper tensile stress layer. Geometric parameters like the rake angle, on the other hand, affect the direction and magnitude of the cutting force, thereby changing the stress distribution pattern [332,338,339]. The tool wear process alters tool geometry, thereby influencing thermomechanical loads and residual stress distribution in manufactured parts. Liang et al. [338] proposed a multi-physical-field model that accounts for tool geometry changes (flank wear, cutting edge radius, and rake angle) to predict residual stress distribution in orthogonal turning of Ti–6Al–4V. They established a response relationship between residual stress and tool wear conditions and proposed a novel method to control residual stress distribution by monitoring tool wear morphology.

Existing residual stress prediction models for machining processes are characterized by complexity, time-consuming computation, and low efficiency. To address these challenges, Zhou et al. [333] proposed a hybrid residual stress prediction model based on a FE–analytical–neural network approach. They investigated the prediction accuracy of three network architectures for residual stress, finding that the Sparrow Search Algorithm-Back Propagation (SSA-BP) network outperforms conventional BP and Genetic Algorithm-BP networks in predicting maximum tensile residual stress. The effects of tool geometry parameters and cutting parameters on residual stress distribution and maximum tensile/compressive stresses in H13 steel were systematically analyzed. Meanwhile, an enhanced two-scale global hybrid numerical method which integrates a 3D hybrid modeling framework with local 2D orthogonal cutting simulations was proposed for predicting turning-induced residual stresses, enabling more accurate characterization of thermomechanical loading fields [340]. Notably, the method simplifies calibration by relying solely on measured cutting forces while inherently accounting for realistic machined surface topography. As summarized in Fig. 32B, the 3D numerical modeling of turning-induced residual stress and its corresponding simulation outputs were systematically validated against experimental data. Quantitative comparison with X-ray diffraction measurements on 15-5PH martensitic stainless steel revealed excellent agreement between predicted and measured residual stress states. Besides, multi-physics model that considered tool geometry changes caused by wear was established by Liang et al. [338] in orthogonal turning simulation. As shown in Fig. 32C(1), at a cutting speed of 200 m/min, the predicted residual stresses were in good agreement with experimental results, both exhibiting a spoon-shaped distribution from surface tension to subsurface compression. As illustrated in Fig. 32C(2), verification results demonstrated that increased tool wear and cutting speed turned surface residual stress from compressive to tensile and significantly enhanced the peak compressive stress below the machined surface. These studies demonstrate that incorporating hybrid computational strategies, metallurgical phase transformations, and tool-wear-induced geometry changes into residual stress prediction models significantly improves both accuracy and efficiency, offering reliable tools for optimizing machining processes.

Many researchers have also attempted to analyze the relationship between the mechanical behavior of hardness and residual stress on machined surfaces. It has been reported that the hardness distribution is influenced by both microstructure evolution and residual stress [334,341,342]. However, due to the complex formation mechanisms of hardness and residual stress, the specific influence of residual stress on hardness remains difficult to determine [334]. For instance, Pan et al. [342] produced a gradient dislocation structure in AISI 304 stainless steel via cyclic torsion treatment. Although very low residual stress (~70 MPa) was obtained—attributed to pure shear plastic strain without tool contact—the microhardness at the topmost surface significantly increased from 2.0 to 3.2 GPa [342]. This suggests that the improvement in hardness may be achieved through

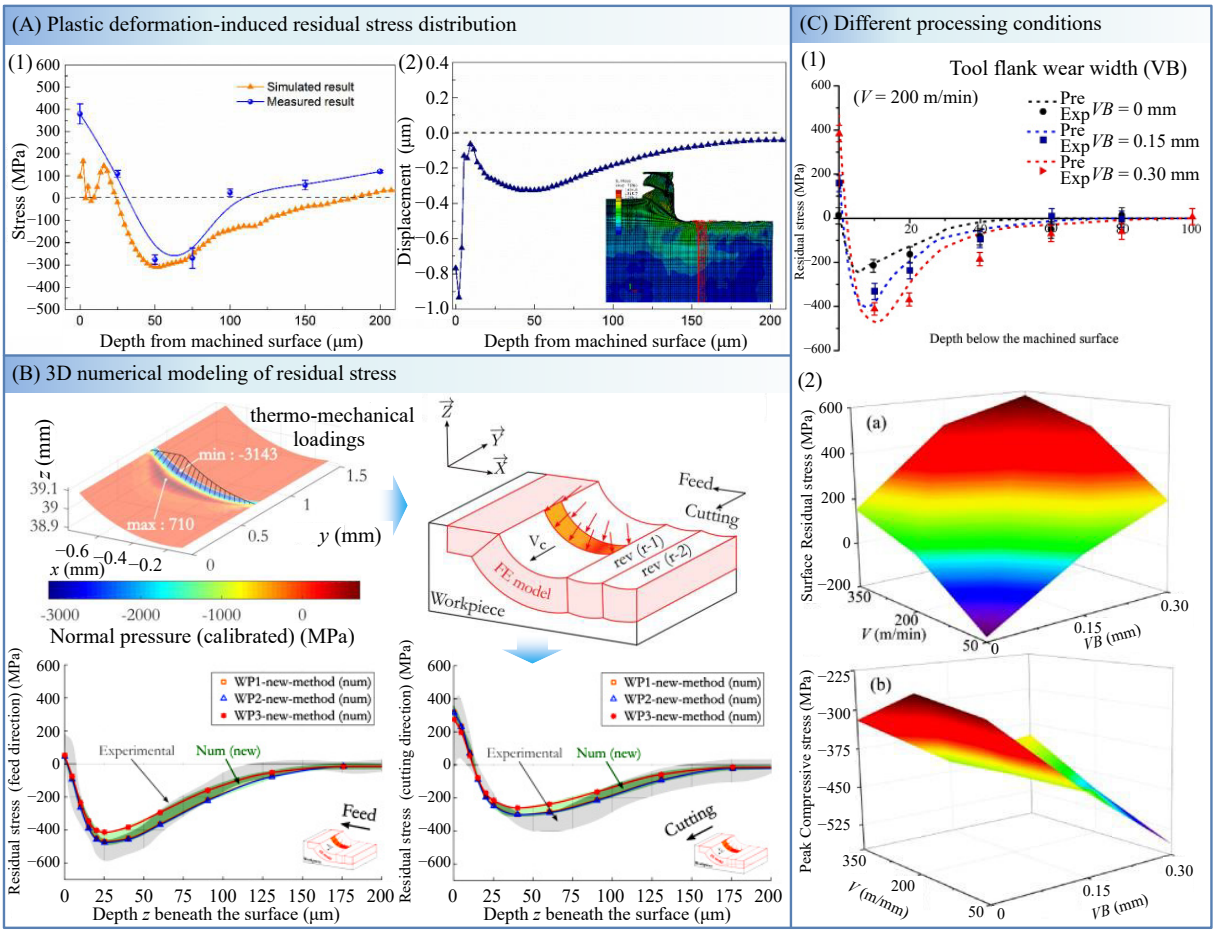


Fig. 32 Residual stress prediction on machined surface. (A) Residual stress distribution with plastic deformation along the normal direction of the machined surface [59]. (B) 3D numerical modeling of residual stress induced by turning process [340]. (C) Simulated residual stress under different tool flank wear widths and cutting speeds [338].

microstructure evolution induced by high dislocation density, accompanied by low residual stress. In a related numerical study [59], a validated numerical model was used to investigate the factors that influence residual stress in machined Ti–6Al–4V. The simulation results showed that the distribution of residual stress beneath the machined surface is primarily controlled by the displacement component perpendicular to the surface, as illustrated in Fig. 32A. Furthermore, the analysis revealed a proportional relationship between the height of the stagnation zone in front of the cutting tool and the resulting peak compressive stresses. These compressive stresses arise from the interaction between material flow and the cutting edge, thereby linking the location of the stagnation point directly to the residual stress state in the finished component.

In summary, the main breakthrough direction for future research lies in accurately predicting and revealing the residual stress distribution under thermo-mechanical deformation conditions during cutting processes through a combination of numerical simulation and experiments, as well as in elucidating the interaction mechanisms between microstructure evolution and mechanical properties, including hardness, residual stress, and fatigue resistance.

4.3 Summary

Over the past several decades, predictive modeling for machined surface integrity has evolved from early analytical shear plane theories to fully coupled thermomechanical finite element simulations. Today, numerical models can reasonably estimate a broad set of process responses, including cutting forces, temperature fields, chip morphology, tool wear progression and machined surface integrity, such as hardness, residual stress distributions, and microstructural transformations such as DRX, grain refinement, dislocation density evolution, and phase changes. These capabilities have made simulation an indispensable complement to

experimental characterization, particularly in scenarios where direct measurement of transient microscale phenomena is impractical.

Nevertheless, substantial challenges remain for numerical modeling of cutting mechanics and surface integrity. High-fidelity predictions remain computationally intensive, and numerous critical issues remain unresolved. These include accurate decomposition of individual cutting force components, reliable temperature field prediction, mechanistic modeling of white layer formation, and accurate characterization of subsurface microstructure and mechanical property gradients. The selection of material constitutive models, friction models, damage initiation criteria, and boundary conditions exerts a significant impact on simulation results, which are often poorly guided by first-principles theories.

Key challenges include developing multi-scale, multi-physics models that couple crystal plasticity (e.g., dislocation slip, DRX, phase transformation, and twinning) within a unified theoretical framework. High-resolution characterization techniques (e.g., TKD) should be integrated with CPFE simulations to predict grain evolution and deformation mechanisms more comprehensively. Real-time process–morphology mapping enabled by online monitoring and machine learning will allow active control of chip morphology and surface integrity. For tool wear, future models must incorporate synergistic effects of coatings, surface textures, and lubrication under extreme conditions, while combining high-precision experimental calibration with ma-chine learning optimization for intelligent tool life prediction. Meanwhile, future breakthroughs should focus on accurately predicting residual stress distribution under thermo-mechanical deformation through integrated numerical simulation and experiment, and on elucidating the interaction mechanisms between microstructure evolution and mechanical properties (hardness, residual stress, fatigue resistance). Ultimately, the goal is to achieve green, efficient, and intelligent manufacturing through data-driven, physics-informed simulations that link in-process states to ex-service performance. Collectively, these efforts are expected to move the field toward predictive, adaptive, and ultimately intelligent frameworks for controlling machined surface integrity.

5 Conclusions and Prospects

5.1 Conclusions

Over the past few decades, numerical modeling for metal machining has evolved from early analytical shear slip theory to finite element simulations that incorporate material microstructural evolution and macro–micro thermomechanical coupling effects. Today, these models accurately predict machining performances (cutting forces, temperature, chip morphology, tool wear) and surface integrity indicators (hardness, residual stress, and microstructural evolution including dislocation density, dynamic recrystallization, and phase transformation). As a result, numerical modeling provides an essential approach that can be used to investigate the in-process states and underlying mechanisms of the instantaneous machining process. In light of these advances, this work presents a comprehensive review of the fundamental theories, key methods, and application progress in machining simulation modeling, focusing on three core aspects: material constitutive modeling (including plastic and damage modeling approaches), numerical modeling approaches for chip formation, and modeling applications for cutting mechanics and surface integrity. The main conclusions are drawn as follows:

- Material constitutive models are the core factor ensuring the accuracy and reliability of metal cutting simulations. Plastic constitutive models which characterize the work hardening behavior in machining normally fall into three categories: phenomenological, physics-based, and semi-physical. Phenomenological models (e.g., JC, modified JC, KHL, and TANH) are capable of modeling stress–strain relationships under various loading conditions due to their simple mathematical formulations and convenient parameter calibration via macroscopic tests.
- Physics-based models (e.g., ZA and MTS) focus on material-related microstructural evolution mechanisms to characterize the evolution of dislocation density, grain size, and phase transformation during machining. However, their parameter identification is challenging due to reliance on microstructural characterization. Semi-physical models strike a balance between engineering practicality and physical interpretability—either by coupling microscale models (e.g., JMAK) to output microstructural parameters or by incorporating physical variables into phenomenological frameworks to enhance prediction accuracy. Overall, the primary goal of plastic constitutive modeling is to accurately capture plastic flow behavior under various loading conditions, enable the prediction of microstructure evolution and microstructure dependent mechanical behaviors based on material and physical fundamentals.
- Plastic instability and damage-mediated mechanical

behavior readily emerge under machining conditions, where failure/damage constitutive descriptions serve as critical modeling inputs governing chip formation, material separation behavior and post-machining surface integrity. Ductile fracture susceptibility is strongly governed by local stress states, which are conventionally quantified via stress triaxiality and the normalized Lode-angle parameter. Empirical damage models, such as the JC damage model and Bao–Wierzbicki criterion, which use cumulative strain damage considering stress state, or the Cockcroft–Latham criterion, which employs a mixed stress-strain damage law, are widely adopted due to their high computational efficiency and ease of calibration. Energy-based fracture models, which take fracture work or failure energy density as the critical threshold, provide an effective way to characterize fracture resistance or toughness, to preserve the stress-strain behavior during the damage evolution stage, and to alleviate mesh dependence in cutting simulations. Data-driven calibration methods show great potential; however, current models still exhibit notable limitations in coupling physical mechanisms, calibration convenience, and computational stability.

- Numerical modeling methods for chip formation are systematically summarized into continuum methods, particle methods, and multiscale modeling methods, with distinct features and applicable scales. Continuum methods dominated by FEM are mature in predicting macroscopic field variables and thermomechanical responses. In terms of material-mesh coupling strategies, the LAG method enables the prediction of plastic flow orientations on machined surfaces by virtue of mesh deformation. Both ALE and CEL methods have a better ability to avoid element distortion, and CEL delivers robust large-deformation handling together with stable time integration. Even so, neither method can well reproduce plastic flow driven by microstructural evolution. Particle-based techniques (SPH, MD, DEM) excel at simulating large deformation, crack propagation and nanoscale behaviors, yet their application is limited by high computational costs and oversimplified constitutive models. Multiscale approaches including PFEM, CPFE and FEM-CA coupling represent advanced tools to link macro-scale cutting responses with meso-scale microstructural evolution. Multiscale simulation has become a mainstream route to interpret microstructural gradient distribution and dynamic recrystallization, supporting grain refinement control and surface integrity optimization. However, existing multiscale models still confront bottlenecks, such as discontinuous microstructure output from CA models and insufficient stability of CPFE under high-strain-rate thermo-microstructural coupling, which gives rise to inherent contradictions among the simulation accuracy of micro- and macro-mechanical behaviors, computational efficiency, and physical completeness.
- Modeling of cutting mechanics and microstructure dependent surface integrity has developed from early analytical shear plane models to fully coupled thermomechanical finite element simulations. Modern numerical models can effectively predict a series of process responses including cutting force, temperature field, chip morphology, tool wear evolution, and microstructure evolution induced surface integrity (hardness, residual stress, dynamic recrystallization, grain refinement, dislocation evolution, and phase transformation). Simulation has become an indispensable supplement to experimental characterization, especially for revealing the machining mechanism concerning the physical transient microscale phenomena which are hard to measure directly. Nevertheless, high-accuracy simulation still consumes enormous computational resources, and numerous key scientific challenges remain unresolved. These include the accurate decomposition of cutting force components, reliable acquisition of the temperature field, physical modeling of white layer formation, and precise characterization of subsurface microstructure and mechanical property gradients. The selection of mechanical and microstructure constitutive models, friction models, and boundary conditions exerts a significant influence on simulation results, and relevant research still lacks systematic theoretical guidance.

5.2 Prospects

In view of the current research status and existing challenges of machining simulation modeling, the future development trends and key research directions (Fig. 33) are prospected as follows:

- Future research on machining constitutive models should focus on improving the prediction accuracy of flow stress, microstructure evolution and damage behavior under complex thermomechanical loading conditions during machining, including large strain, high strain rate, elevated temperature

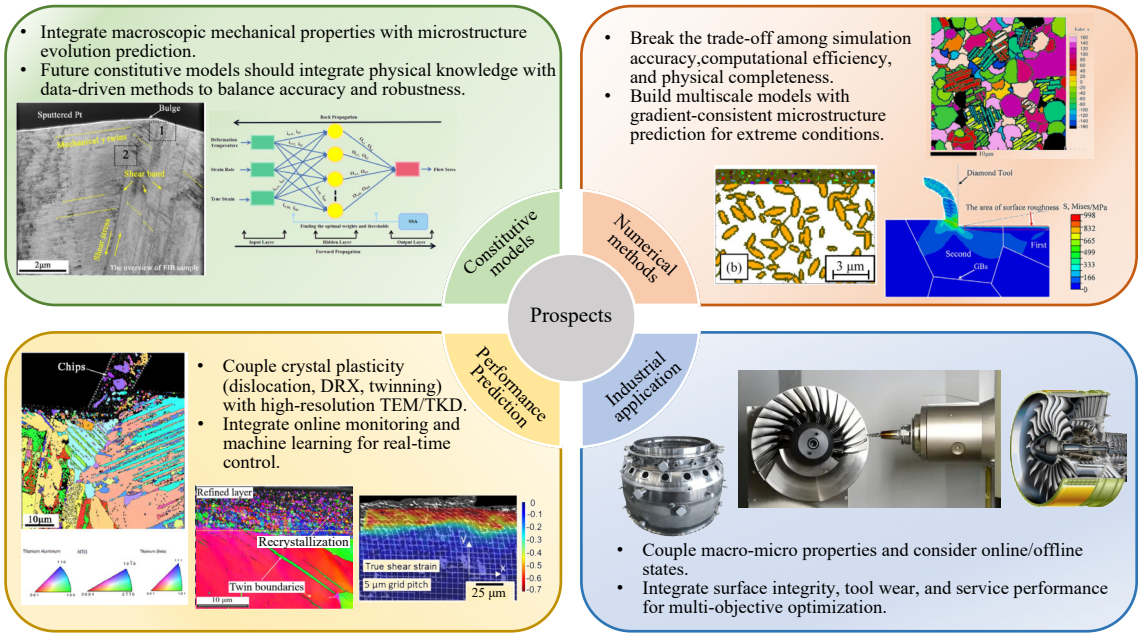


Fig. 33 Key scientific issues and future prospects in metal cutting modeling. Reprinted from Ref. [42,264,318,343–346].

and complex stress states. It is imperative to further develop mechanical experimental methods for the characterization of such extreme loading conditions. A core challenge lies in establishing reliable stress–strain relationships to enable accurate cutting force prediction, while preserving the fidelity of microstructure prediction under variable strain, strain rate and temperature conditions. The organic integration of macroscopic and microscopic mechanical properties with material microstructure prediction will serve as a vital direction for the future advancement of machining numerical simulation technology.

- In terms of damage and failure models, it is necessary to construct systematic and comprehensive theoretical frameworks that balance physical accuracy, calibration feasibility and computational robustness, so as to facilitate the industrial application of machining simulation technology. Future studies should further deepen the understanding of intrinsic physical damage mechanisms under extreme cutting conditions and remedy the inherent limitations of existing data-driven approaches via the embedding of physical prior knowledge. The in-depth fusion of physical mechanisms into data-driven calibration frameworks is expected to improve the convenience of parameter identification and enhance overall computational robustness.
- For the numerical modeling of chip formation, future research will focus on developing integrated multiscale models that feature gradient-consistent microstructure prediction capability and high-fidelity constitutive descriptions applicable to extreme cutting conditions. It is essential to break the inherent trade-off among simulation accuracy, computational efficiency and physical completeness, so as to achieve the synchronous characterization of macroscopic cutting behavior and microscopic microstructure evolution. Although considerable progress has been made in existing studies, the upcoming CPFE models still face prominent challenges in the coupled regime of high strain rate, thermal effect and microstructural evolution, where the intrinsic conflict among accuracy, efficiency and physical completeness remains unresolved. Accordingly, subsequent investigations should prioritize the establishment of integrated multiscale models equipped with gradient-consistent microstructure prediction and highly accurate mechanical behaviors tailored to complex machining environments.
- For modeling cutting mechanics and surface integrity, future efforts will focus on developing multi-scale, multi-physics models that couple crystal plasticity (dislocation slip, dynamic recrystallization, phase transformation, and twinning) with high-resolution characterization (e.g., TKD, TEM) and CPFE simulations to predict grain evolution and deformation mechanisms. Online monitoring and machine learning will enable real-time process-morphology mapping and

active control of chip shape and surface integrity. For tool wear, the synergistic effects of coating, surface texture, and lubrication under extreme conditions should be incorporated, with intelligent tool life prediction achieved via high-precision experimental calibration and machine learning optimization. Key breakthroughs include accurately predicting micro-hardness and residual stress under thermomechanical coupling through combined numerical and experimental verification, and clarifying the interactive mechanisms between microstructure evolution and mechanical properties (hardness, residual stress, fatigue).

- To meet the rising demand for performance-centric manufacturing, future simulation systems must transcend single-physics prediction by establishing a full-link model that synchronously couples macro-micro physical and mechanical properties while considering both online and offline spatiotemporal states. Numerical modeling should comprehensively integrate surface integrity (residual stress, microstructure, white layer), machining stability (chatter), tool wear, and final service performance (strength, toughness, fatigue, corrosion resistance). This will enable performance-driven, multi-scale, multi-objective collaborative prediction and process optimization, bridging the gap between in-process states and in-service performance, and elevating machining simulation from a post-processing tool to a core element for process design and decision-making in high-performance manufacturing.

Data availability No datasets were generated or analyzed for this work.

Acknowledgments This work was supported by the National Natural Science Foundation of China (Grant Nos. 52475208, 51575384 and 51205284), National Key Research and Development Program of China (Grant No. 2024YFB3410203) and Natural Science Foundation of Tianjin (Grant No. 16JCQNJC04600). The authors used DeepSeek (online version) as a language-editing tool to improve grammar, clarity, and readability. The AI tool was not used for data analysis, data generation, image processing, or scientific content creation. All outputs were carefully reviewed and verified by the authors, who take full responsibility for the final content.

Competing interests The authors declare no conflicts of interest.

References

1. Guo D M. High performance manufacturing. Journal of Mechanical Engineering, 2022, 58(1): 225–242
2. Rodríguez J M, Carbonell J M, Jonsén P. Numerical methods for the modelling of chip formation. Archives of Computational Methods in Engineering, 2020, 27(2): 387–412
3. Arrazola P J, Özel T, Umbrello D, et al. Recent advances in modelling of metal machining processes. CIRP Annals, 2013, 62(2): 695–718
4. Astakhov V P, Davim J P. Tools (geometry and material) and tool wear. In: Davim J P, ed. Machining: Fundamentals and Recent Advances. London: Springer, 2008
5. Korkmaz M E, Gupta M K. A State of the Art on simulation and modelling methods in machining: future prospects and challenges. Archives of Computational Methods in Engineering, 2023, 30(1): 161–189
6. Jawahir I S, Schoop J, Kaynak Y, et al. Progress toward modeling and optimization of sustainable machining processes. Journal of Manufacturing Science and Engineering, 2020, 142(11): 110811
7. Hardy M C, Detrois M, McDevitt E T, et al. Solving recent challenges for wrought Ni-base superalloys. Metallurgical and Materials Transactions A, 2020, 51(6): 2626–2650
8. Ulutan D, Ozel T. Machining induced surface integrity in titanium and nickel alloys: a review. International Journal of Machine Tools and Manufacture, 2011, 51(3): 250–280
9. Merchant M E. Basic mechanics of the metal-cutting process. Journal of Applied Mechanics, 1944, 11(3): A168–A175
10. Palmer W B, Oxley P L B. Mechanics of orthogonal machining. Proceedings of the Institution of Mechanical Engineers, 1959, 173(1): 623–654
11. Sridhar P, Rodríguez Prieto J M, de Payrebrune K M. Discretization approaches to model orthogonal cutting with Lagrangian, Arbitrary Lagrangian Eulerian, Particle Finite Element method and Smooth Particle Hydrodynamics formulations. Procedia CIRP, 2020, 93: 1496–1501
12. Xu X, Zhang J, Liu H G, et al. Grain refinement mechanism under high strain-rate deformation in machined surface during high speed machining Ti6Al4V. Materials Science and Engineering: A, 2019, 752: 167–179
13. Xu X, Zhang J, Outeiro J, et al. Multiscale simulation of grain refinement induced by dynamic recrystallization of Ti6Al4V alloy during high speed machining. Journal of Materials Processing Technology, 2020, 286: 116834
14. Wang B, Liu Z Q. Evaluation on fracture locus of serrated chip generation with stress triaxiality in high speed machining of Ti6Al4V. Materials & Design, 2016, 98: 68–78
15. Ullah I, Akinlabi E T, Songmene V. Thermo-metallo-mechanical based phase transformation modeling for high-speed milling of Ti–6Al–4V through stress-strain and temperature effects. Journal of Materials Research and Technology, 2024, 30: 894–909
16. Xu X, Outeiro J, Zhang J, et al. Machining simulation of Ti6Al4V using coupled Eulerian-Lagrangian approach and a constitutive model considering the state of stress. Simulation Modelling Practice and Theory, 2021, 110: 102312
17. Chen G, Ge J Y, Lu L P, et al. Mechanism of ultra-high-speed cutting of Ti–6Al–4V alloy considering time-dependent microstructure and mechanical behaviors. The International Journal of Advanced Manufacturing Technology, 2021, 113(1): 193–213

18. Ullah I, Akinlabi E T, Songmene V, et al. A multiscale finite element modeling for predicting the surface integrity induced by thermo-mechanical loads during high-speed milling of Ti–6Al–4V. CIRP Journal of Manufacturing Science and Technology, 2024, 52: 246–263
19. Lin Y C, Chen X M. A critical review of experimental results and constitutive descriptions for metals and alloys in hot working. Materials & Design, 2011, 32(4): 1733–1759
20. Johnson G R, Cook W H. A constitutive model and data for metals subjected to large strains, high strain rates and high temperatures. In: Proceedings of the 7th International Symposium on Ballistics. The Hague, Netherlands, 1983
21. Khan A S, Huang S J. Experimental and theoretical study of mechanical behavior of 1100 aluminum in the strain rate range 10^{-5}–$10^{4}s^{-1}$. International Journal of Plasticity, 1992, 8(4): 397–424
22. Khan A S, Baig M, Choi S H, et al. Quasi-static and dynamic responses of advanced high strength steels: experiments and modeling. International Journal of Plasticity, 2012, 30−31: 1–17.
23. Zerilli F J. Dislocation mechanics-based constitutive equations. Metallurgical and Materials Transactions A, 2004, 35(9): 2547–2555
24. Zerilli F J, Armstrong R W. Dislocation-mechanics-based constitutive relations for material dynamics calculations. Journal of Applied Physics, 1987, 61(5): 1816–1825
25. Khan A S, Kazmi R, Farrokh B. Multiaxial and non-proportional loading responses, anisotropy and modeling of Ti–6Al–4V titanium alloy over wide ranges of strain rates and temperatures. International Journal of Plasticity, 2007, 23(6): 931–950
26. Bakhshan H, Oñate E, Carbonell I Puigbó J M. A review of the constitutive modelling of metals and alloys in machining process. Archives of Computational Methods in Engineering, 2024, 31(3): 1611–1658
27. Liu G X, Zhang D H, Yao C F. A modified constitutive model coupled with microstructure evolution incremental model for machining of titanium alloy Ti–6Al–4V. Journal of Materials Processing Technology, 2021, 297: 117262
28. Wang Q Q, Niu C Y, Liu Z Q, et al. The hardening effect of deformation twinning based on visco-plastic self consistent model and a multi-scale grain refinement prediction model during machining of titanium alloy. Journal of Materials Research and Technology, 2023, 26: 1922–1937
29. Rinaldi S, Umbrello D, Melkote S N. Modelling the effects of twinning and dislocation induced strengthening in orthogonal micro and macro cutting of commercially pure titanium. International Journal of Mechanical Sciences, 2021, 190: 106045
30. Chen G, Ren C Z, Yang X Y, et al. Finite element simulation of high-speed machining of titanium alloy (Ti–6Al–4V) based on ductile failure model. The International Journal of Advanced Manufacturing Technology, 2011, 56(9): 1027–1038
31. Umbrello D, Bordin A, Imbrogno S, et al. 3D finite element modelling of surface modification in dry and cryogenic machining of EBM Ti6Al4V alloy. CIRP Journal of Manufacturing Science and Technology, 2017, 18: 92–100
32. Imbrogno S, Rinaldi S, Umbrello D, et al. A physically based constitutive model for predicting the surface integrity in machining of Waspaloy. Materials & Design, 2018, 152: 140–155
33. Zhong B F, Dang J Q, Xue S Z, et al. Surface integrity of carbon steel under three heat treatment states subjected to orthogonal turning process. Journal of Manufacturing Processes, 2024, 119: 699–714
34. Wang Q Q, Liu Z Q, Wang B, et al. Evolutions of grain size and micro-hardness during chip formation and machined surface generation for Ti–6Al–4V in high-speed machining. The International Journal of Advanced Manufacturing Technology, 2016, 82(9): 1725–1736
35. Zhang J, Xu X, Outeiro J, et al. Simulation of grain refinement induced by high-speed machining of OFHC copper using cellular automata method. Journal of Manufacturing Science and Engineering, 2020, 142(9): 091006
36. Liu H G, Xu X, Zhang J, et al. The state of the art for numerical simulations of the effect of the microstructure and its evolution in the metal-cutting processes. International Journal of Machine Tools and Manufacture, 2022, 177: 103890
37. Umbrello D, Filice L. Improving surface integrity in orthogonal machining of hardened AISI 52100 steel by modeling white and dark layers formation. CIRP Annals, 2009, 58(1): 73–76
38. Ramesh A, Melkote S N. Modeling of white layer formation under thermally dominant conditions in orthogonal machining of hardened AISI 52100 steel. International Journal of Machine Tools and Manufacture, 2008, 48(3−4): 402–414
39. Guo Y B, Warren A W, Hashimoto F. The basic relationships between residual stress, white layer, and fatigue life of hard turned and ground surfaces in rolling contact. CIRP Journal of Manufacturing Science and Technology, 2010, 2(2): 129–134
40. Jawahir I S, Brinksmeier E, M'Saoubi R, et al. Surface integrity in material removal processes: recent advances. CIRP Annals, 2011, 60: 603–626
41. Afrasiabi M, Klippel H, Roethlin M, et al. Smoothed particle hydrodynamics simulation of orthogonal cutting with enhanced thermal modeling. Applied Sciences, 2021, 11(3): 1020
42. Wang Z F, Zhang J J, Xu Z W, et al. Crystal plasticity finite element modeling and simulation of diamond cutting of polycrystalline copper. Journal of Manufacturing Processes, 2019, 38: 187–195
43. Zhang W X, Wang Z F, Zhang J J. Coupling CPFE-CA simulation for grain refinement in ultrasonic elliptical vibration diamond cutting of polycrystalline Cu. Journal of Materials Processing Technology, 2024, 334: 118638
44. M'Saoubi R, Larsson T, Outeiro J, et al. Surface integrity analysis of machined Inconel 718 over multiple length scales. CIRP Annals, 2012, 61(1): 99–102
45. Liu H G, Zhang J, Xu B B, et al. Whole process analysis of microstructure evolution during chip formation of high-speed machining OFHC copper. Journal of Manufacturing Processes, 2021, 66: 470–482

46. Umbrello D, Caruso S, Imbrogno S. Finite element modelling of microstructural changes in dry and cryogenic machining AISI 52100 steel. Materials Science and Technology, 2016, 32(11): 1062–1070
47. Chen G, Chen S, Schoop J, et al. The influence of sustainable cooling strategies and uncut chip thickness on surface integrity in finish machining of Ti–6Al–4V alloy. In: ASME 2021 International Mechanical Engineering Congress and Exposition. 2021: V02BT02A067
48. Zan S S, Liao Z R, Robles Linares J A, et al. Micrometric orthogonal cutting can lead to sideway chip flow: uncovering crystallographic orientation and grain boundary effects. International Journal of Machine Tools and Manufacture, 2026, 215: 104363
49. Rotella G, Imbrogno S, Candamano S, et al. Surface integrity of machined additively manufactured Ti alloys. Journal of Materials Processing Technology, 2018, 259: 180–185
50. Sadeghifar M, Sedaghati R, Jomaa W, et al. A comprehensive review of finite element modeling of orthogonal machining process: chip formation and surface integrity predictions. The International Journal of Advanced Manufacturing Technology, 2018, 96(9): 3747–3791
51. Wang L, Yue C X, Liu X L, et al. Conventional and micro scale finite element modeling for metal cutting process: a review. Chinese Journal of Aeronautics, 2024, 37(2): 199–232
52. Bai Y L, Wierzbicki T. A new model of metal plasticity and fracture with pressure and Lode dependence. International Journal of Plasticity, 2008, 24(6): 1071–1096
53. Afrasiabi M, Roethlin M, Klippel H, et al. Meshfree simulation of metal cutting: an updated Lagrangian approach with dynamic refinement. International Journal of Mechanical Sciences, 2019, 160: 451–466
54. Samanta A, Shen N G, Ji H P, et al. Cellular automaton simulation of microstructure evolution for friction stir blind riveting. Journal of Manufacturing Science and Engineering, 2018, 140(3): 031016
55. Xu B B, Zhang J, Liu H G, et al. Serrated chip formation induced periodic distribution of morphological and physical characteristics in machined surface during high-speed machining of Ti6Al4V. Journal of Manufacturing Science and Engineering, 2021, 143(10): 101006
56. Bai W, Sun R L, Leopold J, et al. Microstructural evolution of Ti6Al4V in ultrasonically assisted cutting: numerical modelling and experimental analysis. Ultrasonics, 2017, 78: 70–82
57. Denkena B, Krödel A, Heckemeyer A. Numerical and experimental analysis of thermal and mechanical tool load when turning AISI 52100 with ground cutting edge microgeometries. CIRP Journal of Manufacturing Science and Technology, 2021, 35: 494–501
58. Sima M, Özel T. Modified material constitutive models for serrated chip formation simulations and experimental validation in machining of titanium alloy Ti–6Al–4V. International Journal of Machine Tools and Manufacture, 2010, 50(11): 943–960
59. Chen G, Caudill J, Ren C Z, et al. Numerical modeling of Ti–6Al–4V alloy orthogonal cutting considering microstructure dependent work hardening and energy density-based failure behaviors. Journal of Manufacturing Processes, 2022, 82: 750–764
60. Sung J H, Kim J H, Wagoner R H. A plastic constitutive equation incorporating strain, strain-rate, and temperature. International Journal of Plasticity, 2010, 26(12): 1746–1771
61. Wedberg D, Svoboda A, Lindgren L E. Modelling high strain rate phenomena in metal cutting simulation. Modelling and Simulation in Materials Science and Engineering, 2012, 20(8): 085006
62. Liang X L, Liu Z Q, Wang B, et al. Friction behaviors in the metal cutting process: state of the art and future perspectives. International Journal of Extreme Manufacturing, 2023, 5(1): 012002.
63. Hao G C, Liu Z Q. The heat partition into cutting tool at tool-chip contact interface during cutting process: a review. The International Journal of Advanced Manufacturing Technology, 2020, 108(1): 393–411
64. Shu A L, Ren J X, Zhou J H, et al. Grain refinement mechanism in chip and the machined subsurface during high-speed machining of Inconel 718 alloy. Materials Characterization, 2024, 207: 113559
65. Wang B, Liu Z Q, Su G S, et al. Investigations of critical cutting speed and ductile-to-brittle transition mechanism for workpiece material in ultra-high speed machining. International Journal of Mechanical Sciences, 2015, 104: 44–59
66. Zhu B Y, Xiong L S, Xu M X. Double-edged cutting simulation with a new combined constitutive model for AISI 1045 steel. Journal of Materials Processing Technology, 2022, 302: 117496
67. Zhu Y T, Wu X L. Heterostructured materials. Progress in Materials Science, 2023, 131: 101019
68. Mabrouki T, Courbon C, Zhang Y C, et al. Some insights on the modelling of chip formation and its morphology during metal cutting operations. Comptes Rendus. Mécanique, 2016, 344(4-5): 335–354
69. Peng S Y, Gong W, Tian Y Z, et al. Strengthening characteristics of CoCrNi alloys with different stacking fault energies. International Journal of Plasticity, 2025, 191: 104401
70. Zhao J F, Pan X L, Li J, et al. Laser shock peened Ti-6Al-4 V alloy: experiments and modeling. International Journal of Mechanical Sciences, 2022, 213: 106874
71. Zhao Z J, Dai C W, Weng Z M, et al. Cutting forces and microstructures evolution in ultraprecision machining SLM Ti6Al4V. International Journal of Mechanical Sciences, 2025, 302: 110549
72. Khan A S, Yu S J. Deformation induced anisotropic responses of Ti–6Al–4V alloy. Part I: experiments. International Journal of Plasticity, 2012, 38: 1–13
73. Khan A S, Liu H W. Variable strain rate sensitivity in an aluminum alloy: response and constitutive modeling. International Journal of Plasticity, 2012, 36: 1–14
74. Lin Y C, Chen X M, Liu G. A modified Johnson–Cook model for tensile behaviors of typical high-strength alloy steel.

Materials Science and Engineering: A, 2010, 527(26): 6980–6986
75. Chen G, Ren C Z, Qin X D, et al. Temperature dependent work hardening in Ti–6Al–4V alloy over large temperature and strain rate ranges: experiments and constitutive modeling. Materials & Design, 2015, 83: 598–610
76. Field J E, Walley S M, Proud W G, et al. Review of experimental techniques for high rate deformation and shock studies. International Journal of Impact Engineering, 2004, 30(7): 725–775
77. Kajberg J, Sundin K G. Material characterisation using high-temperature Split Hopkinson pressure bar. Journal of Materials Processing Technology, 2013, 213(4): 522–531
78. Farrokh B, Khan A S. Grain size, strain rate, and temperature dependence of flow stress in ultra-fine grained and nanocrystalline Cu and Al: synthesis, experiment, and constitutive modeling. International Journal of Plasticity, 2009, 25(5): 715–732
79. Melkote S N, Liu R, Fernandez-Zelaia P, et al. A physically based constitutive model for simulation of segmented chip formation in orthogonal cutting of commercially pure titanium. CIRP Annals, 2015, 64(1): 65–68
80. Liu R, Melkote S, Pucha R, et al. An enhanced constitutive material model for machining of Ti–6Al–4V alloy. Journal of Materials Processing Technology, 2013, 213(12): 2238–2246
81. Rotella G, Dillon O W Jr, Umbrello D, et al. Finite element modeling of microstructural changes in turning of AA7075-T651 Alloy. Journal of Manufacturing Processes, 2013, 15(1): 87–95
82. Nemat-Nasser S, Guo W G, Nesterenko V F, et al. Dynamic response of conventional and hot isostatically pressed Ti–6Al–4V alloys: experiments and modeling. Mechanics of Materials, 2001, 33(8): 425–439
83. Yaich M, Gavrus A. New phenomenological material constitutive models for the description of the Ti6Al4V titanium alloy behavior under static and dynamic loadings. Procedia Manufacturing, 2020, 47: 1496–1503
84. Zhu S S, Liu J, Deng X. Modification of strain rate strengthening coefficient for Johnson-Cook constitutive model of Ti6Al4V alloy. Materials Today Communications, 2021, 26: 102016
85. Yue C X, Li M, Zhang M, et al. The modified constitutive model considering strain-temperature coupling and dynamic recrystallization effective for FEM simulation of milling process. The International Journal of Advanced Manufacturing Technology, 2022, 119(1): 1217–1232
86. Hou Q S, Chen N C, Luo Z Q, et al. Stress-state-dependent constitutive model and fracture criterion of annealed 6056 aluminum alloy. AIP Advances, 2025, 15(6): 065124
87. Wang X Y, Huang C Z, Zou B, et al. Dynamic behavior and a modified Johnson–Cook constitutive model of Inconel 718 at high strain rate and elevated temperature. Materials Science and Engineering: A, 2013, 580: 385–390
88. Hou X, Liu Z Q, Wang B, et al. Stress-strain curves and modified material constitutive model for Ti–6Al–4V over the wide ranges of strain rate and temperature. Materials, 2018, 11(6): 938
89. Khan A S, Liang R Q. Behaviors of three BCC metal over a wide range of strain rates and temperatures: experiments and modeling. International Journal of Plasticity, 1999, 15(10): 1089–1109
90. Chen Z, Huang C Z, Shi Z Y, et al. A modified Johnson-Cook constitutive model of Inconel 690 weld overlay taking into account the strain rate softening effect. Materials Today Communications, 2024, 41: 110551
91. Fan F, Xu T L, Zhi X D, et al. Research on dynamic constitutive model and fracture criterion of 6082-T6 aluminium alloy. Structures, 2022, 38: 14–27
92. Bian Y P, Jin G, Wang L H, et al. Mechanical properties and JC constitutive modification of tungsten alloys under high strain rates and high/low temperatures. Materials Today Communications, 2024, 41: 110542
93. Zeng S Q, Hu S B, Peng B, et al. The constitutive relations and thermal deformation mechanism of nickel aluminum bronze. Materials & Design, 2022, 220: 110853
94. Hu C, Outeiro J, Zhuang K J, et al. Selection of the numerical formulation for modeling the effect of tool cutting edge microgeometries in machining of Ti6Al4V titanium alloy. Simulation Modelling Practice and Theory, 2023, 129: 102816
95. Cheng W Y, Outeiro J C. Modelling orthogonal cutting of Ti-6Al-4 V titanium alloy using a constitutive model considering the state of stress. The International Journal of Advanced Manufacturing Technology, 2022, 119(7): 4329–4347
96. Khan A S, Liu H W. A new approach for ductile fracture prediction on Al 2024-T351 alloy. International Journal of Plasticity, 2012, 35: 1–12
97. Liu J, Khan A S, Takacs L, et al. Mechanical behavior of ultrafine-grained/nanocrystalline titanium synthesized by mechanical milling plus consolidation: experiments, modeling and simulation. International Journal of Plasticity, 2015, 64: 151–163
98. Kabirian F, Khan A S, Pandey A. Negative to positive strain rate sensitivity in 5xxx series aluminum alloys: experiment and constitutive modeling. International Journal of Plasticity, 2014, 55: 232–246
99. Khan A S, Sung Suh Y, Kazmi R. Quasi-static and dynamic loading responses and constitutive modeling of titanium alloys. International Journal of Plasticity, 2004, 20(12): 2233–2248
100. Calamaz M, Coupard D, Girot F. A new material model for 2D numerical simulation of serrated chip formation when machining titanium alloy Ti–6Al–4V. International Journal of Machine Tools and Manufacture, 2008, 48(3−4): 275–288
101. Özel T, Sima M, Srivastava A K, et al. Investigations on the effects of multi-layered coated inserts in machining Ti–6Al–4V alloy with experiments and finite element simulations. CIRP Annals, 2010, 59(1): 77–82.
102. Bakhshan H, Oñate E, Carbonell J M. Microstructure evolution modeling of Ti6Al4V alloy during cutting using the Particle

Finite Element Method and homogeneous field distributions. Journal of Manufacturing Processes, 2024, 131: 73–92

103. Niu W L, Mo R, Sun H B, et al. A smooth particle hydrodynamic model for two-dimensional numerical simulation of Ti–6Al–4V serrated chip deformation based on TANH constitutive law. Proceedings of the Institution of Mechanical Engineers, Part C: Journal of Mechanical Engineering Science, 2019, 233(9): 3004–3017
104. Zhou Z Y, Wang Y, Xia Z J. A thermo-mechanical fully coupled model for high-speed machining of Ti6Al4V. Industrial Lubrication and Tribology, 2024, 76(7−8): 906–914
105. Chen S Y, Li Y, Chen Y, et al. Comparison of Johnson–Cook and TANH plastic models for 3D numerical modeling of turning titanium alloy Ti5553. Journal of Materials Engineering and Performance, 2024, 33(17): 9126–9144
106. Xu B B, Liu X, Liu H G, et al. Development of a novel constitutive model incorporating phase transformation and dynamic recrystallization effects for laser-assisted machining of Ti6Al4V alloy. Journal of Materials Research and Technology, 2025, 36: 9994–10024
107. Zhang J Y, Ding S R, Du S Y. A damage-effect-involved phenomenological crystal plasticity model and computational methods for mechanical responses of FeCrAl alloys. Materials Today Communications, 2021, 28: 102595
108. Man X L, Ren D Y, Usui S, et al. Validation of finite element cutting force prediction for end milling. Procedia CIRP, 2012, 1: 663–668
109. Maekawa K, Shirakashi T, Usui E. Flow stress of low carbon steel at high temperature and strain rate (part 2)—flow stress under variable temperature and variable strain rate. Bulletin of the Japan Society of Precision Engineering, 1983, 17(3): 167–172
110. Fields D S, Backofen W A. Determination of strain hardening characteristics by torsion testing. Proceeding of American Society for Testing and Materials, 1957, 57: 1259–1272
111. Molinari A, Ravichandran G. Constitutive modeling of high-strain-rate deformation in metals based on the evolution of an effective microstructural length. Mechanics of Materials, 2005, 37(7): 737–752
112. Voce E. The relationship between stress and strain for homogeneous deformation. Journal of the Institute of Metals, 1948, 74: 537–562
113. Chaboche J L. A review of some plasticity and viscoplasticity constitutive theories. International Journal of Plasticity, 2008, 24(10): 1642–1693
114. Liang R Q, Khan A S. A critical review of experimental results and constitutive models for BCC and FCC metals over a wide range of strain rates and temperatures. International Journal of Plasticity, 1999, 15(9): 963–980
115. Sadeghifar M, Javidikia M, Songmene V, et al. Finite element simulation-based predictive regression modeling and optimum solution for grain size in machining of Ti6Al4V alloy: influence of tool geometry and cutting conditions. Simulation Modelling Practice and Theory, 2020, 104: 102141
116. Fernandez-Zelaia P, Melkote S, Marusich T, et al. A microstructure sensitive grain boundary sliding and slip based constitutive model for machining of Ti–6Al–4V. Mechanics of Materials, 2017, 109: 67–81
117. Chen G, Wu Z Y, Caudill J, et al. Finite element simulation of Ti–6Al–4V alloy machining with a grain-size-dependent constitutive model considering the ploughing effect under MQL and cryogenic conditions. Journal of Manufacturing and Materials Processing, 2024, 8(6): 239
118. Li B X, Zhang S, Zhang Q, et al. Modelling of phase transformations induced by thermo-mechanical loads considering stress-strain effects in hard milling of AISI H13 steel. International Journal of Mechanical Sciences, 2018, 149: 241–253
119. Zhang X P, Shivpuri R, Srivastava A K. Role of phase transformation in chip segmentation during high speed machining of dual phase titanium alloys. Journal of Materials Processing Technology, 2014, 214(12): 3048–3066
120. Pan Z P, Liang S Y, Garmestani H, et al. Prediction of machining-induced phase transformation and grain growth of Ti–6Al–4V alloy. The International Journal of Advanced Manufacturing Technology, 2016, 87(1): 859–866
121. Rodríguez J M, Larsson S, Carbonell J M, et al. Dislocation density based flow stress model applied to the PFEM simulation of orthogonal cutting processes of Ti–6Al–4V. Materials, 2020, 13(8): 1979
122. Estrin Y, Tóth L S, Molinari A, et al. A dislocation-based model for all hardening stages in large strain deformation. Acta Materialia, 1998, 46(15): 5509–5522
123. Attia H, Sadek A, Altintas Y, et al. Physics based models for characterization of machining performance – A critical review. CIRP Journal of Manufacturing Science and Technology, 2024, 51: 161–189
124. Shu A L, Zhou J H, Ren J X, et al. A modified constitutive model considering dynamic recrystallization behavior for cutting Inconel 718. Journal of Manufacturing Processes, 2023, 104: 189–204
125. Zhang C L, Li X Z, Zheng Q, et al. Hierarchically O-enriched nanostructures deliver titanium alloys with unprecedented combination of yield strength and ductility. International Journal of Plasticity, 2026, 200: 104655
126. Liu R, Salahshoor M, Melkote S N, et al. A unified internal state variable material model for inelastic deformation and microstructure evolution in SS304. Materials Science and Engineering: A, 2014, 594: 352–363
127. Liu R, Salahshoor M, Melkote S N, et al. A unified material model including dislocation drag and its application to simulation of orthogonal cutting of OFHC Copper. Journal of Materials Processing Technology, 2015, 216: 328–338
128. Wang Q Q, Liu Z Q. Microhardness prediction based on a microstructure-sensitive flow stress model during high speed machining Ti–6Al–4V. Journal of Manufacturing Science and Engineering, 2018, 140(9): 091003
129. Follansbee P S, Kocks U F. A constitutive description of the

deformation of copper based on the use of the mechanical threshold stress as an internal state variable. Acta Metallurgica, 1988, 36(1): 81–93

130. Anurag S, Guo Y B. A modified micromechanical approach to determine flow stress of work materials experiencing complex deformation histories in manufacturing processes. International Journal of Mechanical Sciences, 2007, 49(7): 909–918
131. Jaspers S P F C, Dautzenberg J H. Material behaviour in conditions similar to metal cutting: flow stress in the primary shear zone. Journal of Materials Processing Technology, 2002, 122(2–3): 322–330
132. Childs T H C. Modelling orthogonal machining of carbon steels. Part I: strain hardening and yield delay effects. International Journal of Mechanical Sciences, 2009, 51(5): 402–411
133. Childs T H C, Rahmad R. Modelling orthogonal machining of carbon steels. Part II: comparisons with experiments. International Journal of Mechanical Sciences, 2009, 51(6): 465–472
134. Kocks U F. Laws for work-hardening and low-temperature creep. Journal of Engineering Materials and Technology, 1976, 98(1): 76–85
135. Estrin Y, Mecking H. A unified phenomenological description of work hardening and creep based on one-parameter models. Acta Metallurgica, 1984, 32(1): 57–70
136. Mecking H, Kocks U F. Kinetics of flow and strain-hardening. Acta Metallurgica, 1981, 29(11): 1865–1875
137. Nemat-Nasser S, Isaacs J B. Direct measurement of isothermal flow stress of metals at elevated temperatures and high strain rates with application to Ta and TaW alloys. Acta Materialia, 1997, 45(3): 907–919
138. Svoboda A, Wedberg D, Lindgren L E. Simulation of metal cutting using a physically based plasticity model. Modelling and Simulation in Materials Science and Engineering, 2010, 18(7): 075005
139. Malakizadi A, Saelzer J, Berger S, et al. A physics-based constitutive model for machining simulation of Ti–6Al–4V titanium alloy. Procedia CIRP, 2023, 117: 335–340
140. Atmani Z, Haddag B, Nouari M, et al. Combined microstructure-based flow stress and grain size evolution models for multi-physics modelling of metal machining. International Journal of Mechanical Sciences, 2016, 118: 77–90
141. To'th L S, Molinari A, Estrin Y. Strain hardening at large strains as predicted by dislocation based polycrystal plasticity model. Journal of Engineering Materials and Technology, 2002, 124(1): 71–77
142. Baik S C, Estrin Y, Kim H S, et al. Dislocation density-based modeling of deformation behavior of aluminium under equal channel angular pressing. Materials Science and Engineering: A, 2003, 351(1-2): 86–97
143. Ding H T, Shen N G, Shin Y C. Modeling of grain refinement in aluminum and copper subjected to cutting. Computational Materials Science, 2011, 50(10): 3016–3025
144. Ding H T, Shin Y C. Dislocation density-based grain refinement modeling of orthogonal cutting of titanium. Journal of Manufacturing Science and Engineering, 2014, 136(4): 041003
145. Tong Z P, Zhang Y Z, Wang Y C, et al. Achieving strength-ductility synergy of an additively manufactured metastable high-entropy alloy via deep cryogenic treatment followed by laser shock peening. International Journal of Extreme Manufacturing, 2026, 8(1): 015006
146. Lin T Y, Zhou L, Guo Y F, et al. Synergic strength-ductility enhancement in bimodal titanium alloy via a heterogeneous structure induced by the $\langle c + a \rangle$ slip. Journal of Materials Science & Technology, 2025, 204: 255–267
147. Rinaldi S, Rotella G, Del Prete A. A physically based constitutive model of microstructural evolution of *Ti6Al4V* hard machining under different lubri-cooling conditions. The International Journal of Advanced Manufacturing Technology, 2021, 112(5): 1641–1659
148. Li D, Huang H L, Chen C, et al. Additive manufacturing of high strength near β titanium alloy Ti-55511 by engineering nanoscale secondary α laths via in-situ heat treatment. Materials Science and Engineering: A, 2021, 814: 141245
149. Zhang C L, Liu S Y, Zhang J Y, et al. Trifunctional nanoprecipitates ductilize and toughen a strong laminated metastable titanium alloy. Nature Communications, 2023, 14(1): 1397
150. Yanagimoto J, Karhausen K, Brand A J, et al. Incremental formulation for the prediction of flow stress and microstructural change in hot forming. Journal of Manufacturing Science and Engineering, 1998, 120(2): 316–322
151. Bakhshan H, Oñate E, Carbonell J M, et al. A microstructure-integrated acoustoplastic constitutive model for ultrasonic-assisted machining of Ti6Al4V alloy. CIRP Journal of Manufacturing Science and Technology, 2025, 57: 14–31
152. Khan A S, Zhang H Y, Takacs L, et al. Mechanical response and modeling of fully compacted nanocrystalline iron and copper. International Journal of Plasticity, 2000, 16(12): 1459–1476
153. Yameogo D, Haddag B, Makich H, et al. A physical behavior model including dynamic recrystallization and damage mechanisms for cutting process simulation of the titanium alloy Ti–6Al–4V. The International Journal of Advanced Manufacturing Technology, 2019, 100(1): 333–347
154. Denguir L A, Outeiro J C, Fromentin G, et al. A physical-based constitutive model for surface integrity prediction in machining of OFHC copper. Journal of Materials Processing Technology, 2017, 248: 143–160
155. Babu B, Lindgren L E. Dislocation density based model for plastic deformation and globularization of Ti–6Al–4V. International Journal of Plasticity, 2013, 50: 94–108
156. Zener C, Hollomon J H. Effect of strain rate upon plastic flow of steel. Journal of Applied Physics, 1944, 15(1): 22–32
157. Sheppard T, Tunnicliffe P J, Patterson S J. Direct and indirect extrusion of a high strength aerospace alloy (AA 7075). Journal of Mechanical Working Technology, 1982, 6(4): 313–331
158. Yu W W, Wang T, Yang L, et al. Finite element and experimental analysis of grain refinement caused by dynamic recrystallization during high-speed cutting of nickel-based

superalloys. Simulation Modelling Practice and Theory, 2023, 128: 102807
159. Bai Y L, Teng X Q, Wierzbicki T. On the application of stress triaxiality formula for plane strain fracture testing. Journal of Engineering Materials and Technology, 2009, 131(2): 021002
160. Gangireddy S, Mates S P. High temperature dynamic response of a Ti–6Al–4V alloy: a modified constitutive model for gradual phase transformation. Journal of Dynamic Behavior of Materials, 2017, 3(4): 557–574
161. Wang Q Q, Liu Z Q, Yang D, et al. Metallurgical-based prediction of stress-temperature induced rapid heating and cooling phase transformations for high speed machining Ti–6Al–4V alloy. Materials & Design, 2017, 119: 208–218
162. Frydrych K, Maj M, Urbański L, et al. Twinning-induced anisotropy of mechanical response of AZ31B extruded rods. Materials Science and Engineering: A, 2020, 771: 138610
163. Coghe F, Tirry W, Rabet L, et al. Importance of twinning in static and dynamic compression of a Ti–6Al–4V titanium alloy with an equiaxed microstructure. Materials Science and Engineering: A, 2012, 537: 1–10
164. Salem A A, Kalidindi S R, Semiatin S L. Strain hardening due to deformation twinning in α-titanium: constitutive relations and crystal-plasticity modeling. Acta Materialia, 2005, 53(12): 3495–3502
165. Wang Q Q, Shankar R M, Liu Z Q. Visco-plastic self-consistent modeling of crystallographic texture evolution related to slip systems activated during machining Ti–6Al–4V. Journal of Alloys and Compounds, 2021, 853: 157336
166. Jin L, Chen G, Wang J L, et al. Microstructure-mechanical properties modeling for a novel surface milling-burnishing process. International Journal of Mechanical Sciences, 2025, 306: 110839
167. Khan A S, Baig M. Anisotropic responses, constitutive modeling and the effects of strain-rate and temperature on the formability of an aluminum alloy. International Journal of Plasticity, 2011, 27(4): 522–538
168. Cheng H, Li X T, Sun L X, et al. Improving ductility of high strength nanotwinned steel with reverse transformation of epsilon martensite inside nanotwin lamellae. Materials Science and Engineering: A, 2024, 900: 146402
169. Zhang Y Q, Ngan A H W. Extracting dislocation microstructures by deep learning. International Journal of Plasticity, 2019, 115: 18–28
170. Yadav R, Chakladar N D, Paul S. A dynamic recrystallization based constitutive flow model for micro-machining of Ti–6Al–4V. Journal of Manufacturing Processes, 2022, 77: 463–484
171. Pujana J, Arrazola P J, M'Saoubi R, et al. Analysis of the inverse identification of constitutive equations applied in orthogonal cutting process. International Journal of Machine Tools and Manufacture, 2007, 47(14): 2153–2161
172. Tounsi N, Vincenti J, Otho A, et al. From the basic mechanics of orthogonal metal cutting toward the identification of the constitutive equation. International Journal of Machine Tools and Manufacture, 2002, 42(12): 1373–1383
173. Liu Y P, He J H, Cao Y, et al. Revisiting parametric identification in Johnson–Cook constitutive equation based on multi-objective optimization and 3D metal cutting process simulation. Journal of Materials Engineering and Performance, 2026, 35(1): 878–898
174. Settgast C, Abendroth M, Kuna M. Constitutive modeling of plastic deformation behavior of open-cell foam structures using neural networks. Mechanics of Materials, 2019, 131: 1–10
175. Li X Y, Roth C C, Mohr D. Machine-learning based temperature- and rate-dependent plasticity model: application to analysis of fracture experiments on DP steel. International Journal of Plasticity, 2019, 118: 320–344
176. Mangal A, Holm E A. Applied machine learning to predict stress hotspots I: face centered cubic materials. International Journal of Plasticity, 2018, 111: 122–134
177. Melkote S N, Grzesik W, Outeiro J, et al. Advances in material and friction data for modelling of metal machining. CIRP Annals, 2017, 66(2): 731–754
178. Saelzer J, Thimm B, Zabel A. Systematic in-depth study on material constitutive parameter identification for numerical cutting simulation on 16MnCr5 comparing temperature-coupled and uncoupled Split Hopkinson pressure bars. Journal of Materials Processing Technology, 2022, 302: 117478
179. Kolsky H. An investigation of the mechanical properties of materials at very high rates of loading. Proceedings of the Physical Society. Section B, 1949, 62(11): 676–700
180. Lee W S, Lin C F. Plastic deformation and fracture behaviour of Ti–6Al–4V alloy loaded with high strain rate under various temperatures. Materials Science and Engineering: A, 1998, 241(1-2): 48–59
181. Wang B, Liu Z Q, Su G S, et al. Brittle removal mechanism of ductile materials with ultrahigh-speed machining. Journal of Manufacturing Science and Engineering, 2015, 137(6): 061002
182. Bariani P F, Dal Negro T, Bruschi S. Testing and modelling of material response to deformation in bulk metal forming. CIRP Annals, 2004, 53(2): 573–595
183. Özel T, Zeren E. Determination of work material flow stress and friction for FEA of machining using orthogonal cutting tests. Journal of Materials Processing Technology, 2004, 153−154: 1019–1025
184. Chen G, Ren C Z, Yu W, et al. Application of genetic algorithms for optimizing the Johnson–Cook constitutive model parameters when simulating the titanium alloy Ti–6Al–4V machining process. Proceedings of the Institution of Mechanical Engineers, Part B: Journal of Engineering Manufacture, 2012, 226(8): 1287–1297
185. Vaz M, Cardoso E L, Muñoz-Rojas P A, et al. Identification of constitutive parameters–optimization strategies and applications. Materials Science & Engineering Technology, 2015, 46(4-5): 477–491
186. Zheng X Y, Zhang X B, Chen T T, etal. Deep Learning in Mechanical Metamaterials: From Prediction and Generation to Inverse Design. Advanced Materials, 2023, 35: 2302530.

187. Fernandez-Zelaia P, Melkote S N. Statistical calibration and uncertainty quantification of complex machining computer models. International Journal of Machine Tools and Manufacture, 2019, 136: 45–61
188. Chokshi P, Dashwood R, Hughes D J. Artificial Neural Network (ANN) based microstructural prediction model for 22MnB5 boron steel during tailored hot stamping. Computers & Structures, 2017, 190: 162–172
189. Ali U, Muhammad W, Brahme A, et al. Application of artificial neural networks in micromechanics for polycrystalline metals. International Journal of Plasticity, 2019, 120: 205–219
190. Gorji M B, Mozaffar M, Heidenreich J N, et al. On the potential of recurrent neural networks for modeling path dependent plasticity. Journal of the Mechanics and Physics of Solids, 2020, 143: 103972
191. Wierzbicki T, Bao Y B, Lee Y W, et al. Calibration and evaluation of seven fracture models. International Journal of Mechanical Sciences, 2005, 47(4-5): 719–743
192. Bao Y B, Wierzbicki T. On fracture locus in the equivalent strain and stress triaxiality space. International Journal of Mechanical Sciences, 2004, 46(1): 81–98
193. Zou Z C, He L, Zhang T, et al. Research on serrated chip morphology for turning Ti6Al4V titanium alloy by considering damage evolution. Journal of Manufacturing Processes, 2024, 118: 283–301
194. Shi H Y, Zhao X F, Wang Z Q, et al. Research of fracture mechanics applied in the cutting process of plastic metals. Journal of Northwestern Polytechnical University, 2019, 37(6): 1209–1222
195. Mabrouki T, Girardin F, Asad M, et al. Numerical and experimental study of dry cutting for an aeronautic aluminium alloy (A2024-T351). International Journal of Machine Tools and Manufacture, 2008, 48(11): 1187–1197
196. Wang B, Xiao X R, Astakhov V P, et al. A quantitative analysis of the transition of fracture mechanisms of Ti6Al4V over a wide range of stress triaxiality and strain rate. Engineering Fracture Mechanics, 2020, 231: 107020
197. Bai Y L, Wierzbicki T. Application of extended Mohr–Coulomb criterion to ductile fracture. International Journal of Fracture, 2010, 161(1): 1–20
198. Roth C C, Mohr D. Effect of strain rate on ductile fracture initiation in advanced high strength steel sheets: experiments and modeling. International Journal of Plasticity, 2014, 56: 19–44
199. Teng B G, Wang W N, Xu Y C. Ductile fracture prediction in aluminium alloy 5A06 sheet forming based on GTN damage model. Engineering Fracture Mechanics, 2017, 186: 242–254
200. Wang B, Xiao X R, Astakhov V P, et al. The effects of stress triaxiality and strain rate on the fracture strain of Ti6Al4V. Engineering Fracture Mechanics, 2019, 219: 106627
201. Chen G, Ren C Z, Lu L P, et al. Determination of ductile damage behaviors of high strain rate compression deformation for Ti–6Al–4V alloy using experimental-numerical combined approach. Engineering Fracture Mechanics, 2018, 200: 499–520
202. Merchant M E. Mechanics of the metal cutting process. I. Orthogonal cutting and a type 2 chip. Journal of Applied Physics, 1945, 16(5): 267–275
203. Hancock J W, Mackenzie A C. On the mechanisms of ductile failure in high-strength steels subjected to multi-axial stress-states. Journal of the Mechanics and Physics of Solids, 1976, 24(2-3): 147–160
204. Zhang X P, Shivpuri R, Srivastava A K. Chip fracture behavior in the high speed machining of titanium alloys. Journal of Manufacturing Science and Engineering, 2016, 138(8): 081001
205. Giglio M, Manes A, Viganò F. Ductile fracture locus of Ti–6Al–4V titanium alloy. International Journal of Mechanical Sciences, 2012, 54(1): 121–135
206. Taylor G I. The use of flat-ended projectiles for determining dynamic yield stress I. Theoretical considerations. Proceedings of the Royal Society A: Mathematical, Physical and Engineering Sciences, 1948, 194(1038): 289–299
207. Johnson G R, Cook W H. Fracture characteristics of three metals subjected to various strains, strain rates, temperatures and pressures. Engineering Fracture Mechanics, 1985, 21(1): 31–48
208. Rice J R, Tracey D M. On the ductile enlargement of voids in triaxial stress fields. Journal of the Mechanics and Physics of Solids, 1969, 17(3): 201–217
209. Teng X, Wierzbicki T. Evaluation of six fracture models in high velocity perforation. Engineering Fracture Mechanics, 2006, 73(12): 1653–1678
210. Teng X, Wierzbicki T, Hiermaier S, et al. Numerical prediction of fracture in the Taylor test. International Journal of Solids and Structures, 2005, 42(9-10): 2929–2948
211. Oh S I, Chen C C, Kobayashi S. Ductile fracture in axisymmetric extrusion and drawing—part 2: workability in extrusion and drawing. Journal of Manufacturing Science and Engineering, 1979, 101(1): 36–44
212. Zhang C L, Zhang J Y, Bao X Y, et al. Hierarchically ordered coherent interfaces-driven ultrahigh specific-strength and toughness in a nano-martensite titanium alloy. Acta Materialia, 2024, 263: 119540
213. Dolinski M, Rittel D, Dorogoy A. Modeling adiabatic shear failure from energy considerations. Journal of the Mechanics and Physics of Solids, 2010, 58(11): 1759–1775
214. Hillerborg A, Modéer M, Petersson P E. Analysis of crack formation and crack growth in concrete by means of fracture mechanics and finite elements. Cement and Concrete Research, 1976, 6(6): 773–781
215. Zhang Y C, Mabrouki T, Nelias D, et al. FE-model for Titanium alloy (Ti–6Al–4V) cutting based on the identification of limiting shear stress at tool-chip interface. International Journal of Material Forming, 2011, 4(1): 11–23
216. Zhang Y C, Mabrouki T, Nelias D, et al. Chip formation in orthogonal cutting considering interface limiting shear stress and damage evolution based on fracture energy approach. Finite Elements in Analysis and Design, 2011, 47(7): 850–863
217. Chen G, Ren C Z, Zhang P, et al. Measurement and finite element simulation of micro-cutting temperatures of tool tip and workpiece. International Journal of Machine Tools and

Manufacture, 2013, 75: 16–26
218. Cockcroft M G, Latham D J. Ductility and the workability of metals. Journal Institute of Metals, 1968, 96: 33–39
219. Courant R. Variational methods for the solution of problems of equilibrium and vibrations. Bulletin of the American Mathematical Society, 1943, 49(1): 1–23
220. Zienkiewicz O C. *The finite element method in structural and continuum mechanics*. New York: McGraw-Hill, 1967
221. List G, Sutter G, Bouthiche A. Cutting temperature prediction in high speed machining by numerical modelling of chip formation and its dependence with crater wear. International Journal of Machine Tools and Manufacture, 2012, 54–55: 1–9.
222. Hu C, Zhuang K J, Birembaux H, et al. An improved Lagrange-based numerical model for machining Ti–6Al–4V alloy concerning tool cutting edge microgeometry. Procedia CIRP, 2024, 126: 469–474
223. Duan C Z, Zhang F Y, Qin S W, et al. Modeling of dynamic recrystallization in white layer in dry hard cutting by finite element—cellular automaton method. Journal of Mechanical Science and Technology, 2018, 32(9): 4299–4312
224. Jin X L, Altintas Y. Prediction of micro-milling forces with finite element method. Journal of Materials Processing Technology, 2012, 212(3): 542–552
225. Sabkhi N, Moufki A, Nouari M, et al. Prediction of the hobbing cutting forces from a thermomechanical modeling of orthogonal cutting operation. Journal of Manufacturing Processes, 2016, 23: 1–12
226. Zhang C, Choi H. Study of segmented chip formation in cutting of high-strength lightweight alloys. The International Journal of Advanced Manufacturing Technology, 2021, 112(9): 2683–2703
227. Movahhedy M R, Gadala M S, Altintas Y. Simulation of chip formation in orthogonal metal cutting process: an ale finite element approach. Machining Science and Technology, 2000, 4(1): 15–42
228. Klocke F, Döbbeler B, Peng B, et al. FE-simulation of the cutting process under consideration of cutting fluid. Procedia CIRP, 2017, 58: 341–346
229. Ambrosio D, Tongne A, Wagner V, et al. A new damage evolution criterion for the coupled Eulerian-Lagrangian approach: application to three-dimensional numerical simulation of segmented chip formation mechanisms in orthogonal cutting. Journal of Manufacturing Processes, 2022, 73: 149–163
230. Ayed Y, Robert C, Germain G, et al. Development of a numerical model for the understanding of the chip formation in high-pressure water-jet assisted machining. Finite Elements in Analysis and Design, 2016, 108: 1–8
231. Vovk A, Sölter J, Karpuschewski B. Finite element simulations of the material loads and residual stresses in milling utilizing the CEL method. Procedia CIRP, 2020, 87: 539–544
232. Shuang F, Chen X Y, Ma W. Numerical analysis of chip formation mechanisms in orthogonal cutting of Ti6Al4V alloy based on a CEL model. International Journal of Material Forming, 2018, 11(2): 185–198
233. Zhang Y C, Outeiro J C, Mabrouki T. On the selection of Johnson-cook constitutive model parameters for Ti–6Al–4V using three types of numerical models of orthogonal cutting. Procedia CIRP, 2015, 31: 112–117
234. Gingold R A, Monaghan J J. Smoothed particle hydrodynamics: theory and application to non-spherical stars. Monthly Notices of the Royal Astronomical Society, 1977, 181(3): 375–389
235. Limido J, Espinosa C, Salaün M, et al. SPH method applied to high speed cutting modelling. International Journal of Mechanical Sciences, 2007, 49(7): 898–908
236. Ruettimann N, Buhl S, Wegener K. Simulation of single grain cutting using SPH method. Journal of Machine Engineering, 2011, 10(3): 17–29
237. Zhang N Y, Klippel H, Afrasiabi M, et al. Hybrid SPH-FEM solver for metal cutting simulations on the GPU including thermal contact modeling. CIRP Journal of Manufacturing Science and Technology, 2023, 41: 311–327
238. Zahedi S A, Demiral M, Roy A, et al. FE/SPH modelling of orthogonal micro-machining of f. c. c. single crystal. Computational Materials Science, 2013, 78: 104–109
239. Gao S, Wang H X, Huang H, et al. Molecular simulation of the plastic deformation and crack formation in single grit grinding of 4H-SiC single crystal. International Journal of Mechanical Sciences, 2023, 247: 108147
240. Ren Z H, Feng R C, Zhou B C, et al. Molecular dynamics simulation for temperature assisted machining of a polycrystalline γ-TiAl alloy. Journal of Manufacturing Processes, 2024, 132: 615–628
241. He Y, Zhang J, Andriollo T, et al. Investigation of the elastoplastic and fracture behavior of solid materials considering microstructural anisotropy: a discrete element modeling study. Computational Materials Science, 2019, 170: 109164
242. Liu Z C, Zhang J, He Y, et al. A Godunov-type discrete element model for elastic-viscoplastic continuum impact problems. International Journal for Numerical Methods in Engineering, 2021, 122(21): 6384–6404
243. Goel S, Luo X C, Agrawal A, et al. Diamond machining of silicon: a review of advances in molecular dynamics simulation. International Journal of Machine Tools and Manufacture, 2015, 88: 131–164
244. Cremonesi M, Franci A, Idelsohn S, et al. A state of the art review of the particle finite element method (PFEM). Archives of Computational Methods in Engineering, 2020, 27(5): 1709–1735
245. Oñate E, Idelsohn S R, Del Pin F, et al. The particle finite element method-an overview. International Journal of Computational Methods, 2004, 1(2): 267–307
246. Idelsohn S R, Oñate E, Pin F D. The particle finite element method: a powerful tool to solve incompressible flows with free-surfaces and breaking waves. International Journal for Numerical Methods in Engineering, 2004, 61(7): 964–989
247. Bakhshan H, Oñate E, Carbonell J M. Modeling of ultrasonic vibration-assisted micromachining using the particle finite element method. Computational Particle Mechanics, 2024, 11(5): 2267–2290

248. Zhang S, Liu F, Zou D L, et al. Review of plastic deformation mechanisms and crystal plasticity modelling of uranium. Materials Science and Engineering: A, 2025, 934: 148324
249. Roters F, Eisenlohr P, Hantcherli L, et al. Overview of constitutive laws, kinematics, homogenization and multiscale methods in crystal plasticity finite-element modeling: theory, experiments, applications. Acta Materialia, 2010, 58(4): 1152–1211
250. Yaghoobi M, Voyiadjis G, Sundararaghavan V. Crystal plasticity simulation of magnesium and its alloys: a review of recent advances. Crystals, 2021, 11(4): 435
251. Peirce D, Asaro R J, Needleman A. An analysis of nonuniform and localized deformation in ductile single crystals. Acta Metallurgica, 1982, 30(6): 1087–1119
252. Tong X, Li Y, Fu M W. Modelling of grain size effects in progressive microforming using CPFEM. International Journal of Mechanical Sciences, 2024, 267: 108971
253. Zan X D, Guo X, Weng G J. Hydride-enhanced strain localization in zirconium alloy: a study by crystal plasticity finite element method. International Journal of Plasticity, 2024, 174: 103911
254. Liu Q, Roy A, Tamura S, et al. Micro-cutting of single-crystal metal: finite-element analysis of deformation and material removal. International Journal of Mechanical Sciences, 2016, 118: 135–143
255. Lee W B, Wang H, Chan C Y, et al. Finite element modelling of shear angle and cutting force variation induced by material anisotropy in ultra-precision diamond turning. International Journal of Machine Tools and Manufacture, 2013, 75: 82–86
256. Wang Z F, Zhang J J, Zhang J G, et al. Towards an understanding of grain boundary step in diamond cutting of polycrystalline copper. Journal of Materials Processing Technology, 2020, 276: 116400
257. Zambaldi C, Roters F, Raabe D, et al. Modeling and experiments on the indentation deformation and recrystallization of a single-crystal nickel-base superalloy. Materials Science and Engineering: A, 2007, 454–455: 433–440
258. von Neumann J. The general and logical theory of automata. In: Jeffress L A, ed. Cerebral Mechanisms in Behavior: The Hixon Symposium. New York: John Wiley & Sons, 1951
259. Stahl W R. Algorithmically unsolvable problems for a cell automaton. Journal of Theoretical Biology, 1965, 8(3): 371–394
260. Zhu H J, Chen F, Zhang H M, et al. Review on modeling and simulation of microstructure evolution during dynamic recrystallization using cellular automaton method. Science China Technological Sciences, 2020, 63(3): 357–396
261. Shen N G, Samanta A, Ding H T. Microstructure simulations for orthogonal cutting via a cellular automaton model. Procedia CIRP, 2017, 58: 543–548
262. Zhou X R, He L, Zhou T, et al. Multiscale research of microstructure evolution during turning Ti–6Al–4V alloy based on FE and CA. Journal of Alloys and Compounds, 2022, 922: 166202
263. Liu G X, Zhang D H, Yao C F. Investigation of the grain refinement mechanism in machining Ti–6Al–4V: experiments and simulations. Journal of Manufacturing Processes, 2023, 94: 479–496
264. Chen S Y, Hou L, Li H Z, et al. Multiscale modelling with data-calibrated material parameters for microstructure evolution in Ti5553 machining. Journal of Manufacturing Processes, 2026, 162: 21–42
265. Lee E H, Shaffer B W. The theory of plasticity applied to a problem of machining. Journal of Applied Mechanics, 1951, 18(4): 405–413
266. Oxley P L B, Hatton A P. Shear angle solution based on experimental shear zone and tool-chip interface stress distributions. International Journal of Mechanical Sciences, 1963, 5(1): 41–55
267. Jawahir I S, Dillon Jr O W, Balajj A K, et al. Predictive modeling of machining performance in turning operations. Machining Science and Technology, 1998, 2(2): 253–276
268. Armarego E J A. A generic mechanics of cutting approach to predictive technological performance modeling of the wide spectrum of machining operations. Machining Science and Technology, 1998, 2(2): 191–211
269. van Luttervelt C A, Childs T H C, Jawahir I S, et al. Present situation and future trends in modelling of machining operations progress report of the CIRP working group ‘modelling of machining operations’. CIRP Annals, 1998, 47(2): 587–626
270. Sun S J. Observation and quantitative characterization of geometric and cyclical features associated with chip segmentation during machining of Ti6Al4V alloy. Journal of Materials Processing Technology, 2025, 338: 118794
271. Theraroz J, Tuysuz O, Schoop J. An improved machining temperature prediction model for aerospace alloys: effect of cutting edge radius and tool wear. Journal of Manufacturing Processes, 2025, 133: 1100–1110
272. Hou Z B, Komanduri R. Modeling of thermomechanical shear instability in machining. International Journal of Mechanical Sciences, 1997, 39(11): 1273–1275, 1277–1281, 1283, 1285–1314.
273. Chen G, Ren C, Yang X, et al. Evidence of thermoplastic instability about segmented chip formation process for Ti–6Al–4V alloy based on the finite-element method. Proceedings of the Institution of Mechanical Engineers, Part C: Journal of Mechanical Engineering Science, 2011, 225(6): 1407–1417
274. Zhong B F, Dang J Q, Wang D F, et al. Experimental microstructure evolution and cutting simulation for dynamic mechanical behaviors of 18CrNiMo7–6 steel considering heat treatment conditions. Journal of Manufacturing Processes, 2024, 119: 888–901
275. Ullah I, Zhang S, Zhang Q, et al. Numerical investigation on serrated chip formation during high-speed milling of Ti–6Al–4V alloy. Journal of Manufacturing Processes, 2021, 71: 589–603
276. Arısoy Y M, Özel T. Prediction of machining induced microstructure in Ti–6Al–4V alloy using 3-D FE-based simulations: effects of tool micro-geometry, coating and cutting

conditions. Journal of Materials Processing Technology, 2015, 220: 1–26
277. Rodríguez J M, Jonsén P, Svoboda A. Dislocation density based material model applied in PFEM-simulation of metal cutting. Procedia CIRP, 2017, 58: 193–197
278. Merchant M E. Mechanics of the Metal Cutting Process. I. Orthogonal Cutting and a Type 2 Chip, Journal of Applied Physics, 1945, 16: 267–275.
279. Umbrello D. Finite element simulation of conventional and high speed machining of Ti6Al4V alloy. Journal of Materials Processing Technology, 2008, 196(1−3): 79–87
280. Liang X L, Zhang C B, Wang C J, et al. Microstructural characteristics with process-microstructure-property relations during high-frequency ultrasonic vibration-assisted cutting of metallic material. Materials & Design, 2024, 245: 113254
281. Zhang P, Chen Z M, Guo L W, et al. Machining of Invar 36 alloy: chip-flow behaviors and formation mechanisms. Journal of Manufacturing Processes, 2024, 132: 477–493
282. Zan S S, Liu G Y, Liao Z R, et al. Inverse size effect and deformation mechanism in Ti–6Al–4V cutting process–investigation on effect of bimodal microstructure on machining. CIRP Annals, 2023, 72(1): 41–44
283. Castejón M, Alegre E, Barreiro J, et al. On-line tool wear monitoring using geometric descriptors from digital images. International Journal of Machine Tools and Manufacture, 2007, 47(12-13): 1847–1853
284. Yang S M, Kim D Y, Park H W. Investigation of wear behavior for large pulsed electron beam irradiated cutting tools under the turning process of Ti–6Al–4V. Journal of Manufacturing Processes, 2025, 139: 133–143
285. Akhavan Niaki F, Mears L. A comprehensive study on the effects of tool wear on surface roughness, dimensional integrity and residual stress in turning IN718 hard-to-machine alloy. Journal of Manufacturing Processes, 2017, 30: 268–280
286. Jaffery S H I, Mativenga P T. Wear mechanisms analysis for turning Ti–6Al–4V—towards the development of suitable tool coatings. The International Journal of Advanced Manufacturing Technology, 2012, 58(5): 479–493
287. Liang X L, Liu Z Q, Wang B. Multi-pattern failure modes and wear mechanisms of WC-Co tools in dry turning Ti–6Al–4V. Ceramics International, 2020, 46(15): 24512–24525
288. Zhuang K J, Zhu K, Wei X Y, et al. A dual-stage wear rate model based on wear mechanisms analysis during cutting Inconel 718 with TiAlN coated tools. Journal of Manufacturing Processes, 2024, 126: 24–34
289. Cantero J L, Díaz-Álvarez J, Miguélez M H, et al. Analysis of tool wear patterns in finishing turning of Inconel 718. Wear, 2013, 297(1-2): 885–894
290. Wang Y, Su H H, Dai J B, et al. A novel finite element method for the wear analysis of cemented carbide tool during high speed cutting Ti6Al4V process. The International Journal of Advanced Manufacturing Technology, 2019, 103(5): 2795–2807
291. Yen Y C, Jain A, Altan T. A finite element analysis of orthogonal machining using different tool edge geometries. Journal of Materials Processing Technology, 2004, 146(1): 72–81
292. Özel T. Computational modelling of 3D turning: Influence of edge micro-geometry on forces, stresses, friction and tool wear in PcBN tooling. Journal of Materials Processing Technology, 2009, 209(11): 5167–5177
293. Jacobson M, Dahlman P, Gunnberg F. Cutting speed influence on surface integrity of hard turned bainite steel. Journal of Materials Processing Technology, 2002, 128: 318–323.
294. Field M, Kahles J F. Review of surface integrity of machined components. Annals of the CIRP, 1971, 20(2): 153–163
295. Zhao B, Wang Y F, Peng J H, et al. Overcoming challenges: advancements in cutting techniques for high strength-toughness alloys in aero-engines. International Journal of Extreme Manufacturing, 2024, 6(6): 062012
296. Rotella G, Saffioti M R, Sanguedolce M, et al. Finite element modelling of combined turning/burnishing effects on surface integrity of Ti6Al4V alloy. The International Journal of Advanced Manufacturing Technology, 2022, 119(1): 177–187
297. Xu X, Outeiro J, Zhang J, et al. A framework to efficiently simulate the cyclic variation of the residual stresses induced by chip formation in machining of Ti–6Al–4V alloy. CIRP Journal of Manufacturing Science and Technology, 2024, 51: 57–72
298. Liao Z R, La Monaca A, Murray J, et al. Surface integrity in metal machining—Part I: fundamentals of surface characteristics and formation mechanisms. International Journal of Machine Tools and Manufacture, 2021, 162: 103687
299. Ginting A, Nouari M. Surface integrity of dry machined titanium alloys. International Journal of Machine Tools and Manufacture, 2009, 49(3-4): 325–332
300. Chen Z, Peng R L, Zhou J M, et al. Effect of machining parameters on cutting force and surface integrity when high-speed turning AD 730^{TM} with PCBN tools. The International Journal of Advanced Manufacturing Technology, 2019, 100(9): 2601–2615
301. Zhou J M, Bushlya V, Avdovic P, et al. Study of surface quality in high speed turning of Inconel 718 with uncoated and coated CBN tools. The International Journal of Advanced Manufacturing Technology, 2012, 58(1): 141–151
302. Soo S L, Hood R, Aspinwall D K, et al. Machinability and surface integrity of RR1000 nickel based superalloy. CIRP Annals, 2011, 60(1): 89–92
303. Simoneau A, Ng E, Elbestawi M A. Grain size and orientation effects when microcutting AISI 1045 Steel. CIRP Annals, 2007, 56(1): 57–60
304. Simoneau A, Ng E, Elbestawi M A. Surface defects during microcutting. International Journal of Machine Tools and Manufacture, 2006, 46(12-13): 1378–1387
305. Fernández-Abia A I, Barreiro J, de Lacalle L N L, et al. Effect of very high cutting speeds on shearing, cutting forces and roughness in dry turning of austenitic stainless steels. The International Journal of Advanced Manufacturing Technology, 2011, 57(1): 61–71
306. Wang B, Liu Z Q, Cai Y K, et al. Advancements in material

removal mechanism and surface integrity of high speed metal cutting: a review. International Journal of Machine Tools and Manufacture, 2021, 166: 103744
307. Tekkaya B, Meurer M, Münstermann S. Modelling of grain size evolution with different approaches via FEM when hard machining of AISI 4140. Metals, 2020, 10(10): 1296
308. Herbert C R J, Kwong J, Kong M C, et al. An evaluation of the evolution of workpiece surface integrity in hole making operations for a nickel-based superalloy. Journal of Materials Processing Technology, 2012, 212(8): 1723–1730
309. Yang P Q, Li X, Zhang X P, et al. Improved dynamic recrystallization modeling in the high-speed machining of titanium alloy. The International Journal of Advanced Manufacturing Technology, 2024, 130(5): 2563–2586
310. Tang Z Y, Huang C Z, Shi Z Y, et al. A new characterisation method for stress, hardness, microstructure, and slip lines using the stored energy field in the cutting deformation zones of workpiece. International Journal of Machine Tools and Manufacture, 2022, 178: 103891
311. Ranganath S, Guo C, Hegde P. A finite element modeling approach to predicting white layer formation in nickel superalloys. CIRP Annals, 2009, 58(1): 77–80
312. Lv M H, Li A H, Ge D J, et al. Step-dependent grain refinement and micro-hardness evolution during chip formation process in orthogonal cutting of titanium alloy Ti–6Al–4V. The International Journal of Advanced Manufacturing Technology, 2022, 119(7): 4219–4236
313. Brinksmeier E, Gläbe R, Klocke F, et al. Process signatures – an alternative approach to predicting functional workpiece properties. Procedia Engineering, 2011, 19: 44–52
314. Imbrogno S, Rotella G, Del Prete A. Advanced finite element model for predicting surface integrity in high-speed turning of AA7075-T6 under dry and cryogenic conditions. The International Journal of Advanced Manufacturing Technology, 2023, 124(5): 1735–1749
315. Wang Z Y, Chen G, Wang J L, et al. Variable direction shear deformation induced strengthening mechanism of Ti–6Al–4V alloy treated by a novel ultrasonic milling-burnishing process. Journal of Manufacturing Processes, 2025, 144: 294–310
316. Yan X C, Yin S, Chen C Y, et al. Effect of heat treatment on the phase transformation and mechanical properties of Ti6Al4V fabricated by selective laser melting. Journal of Alloys and Compounds, 2018, 764: 1056–1071
317. Kaynak Y, Manchiraju S, Jawahir I S, et al. Chip formation and phase transformation in orthogonal machining of NiTi shape memory alloy: microstructure-based modelling and experimental validation. CIRP Annals, 2020, 69(1): 85–88
318. Sun Y H, Liu H G, Liao C G, et al. A novel approach for modelling the coupled effects of phase transformation and dynamic recrystallization in high-temperature deformation of dual-phase Ti6Al4V. Journal of Alloys and Compounds, 2026, 1054: 186337
319. Brinell J A. Sätt att bestämma kroppars hårdhet jämte några tillämpningar af detsamma. Teknisk Tidskrift, 1900, 30: 69–87.
320. Zhang P, Li S X, Zhang Z F. General relationship between strength and hardness. Materials Science and Engineering: A, 2011, 529: 62–73
321. Cordero Z C, Knight B E, Schuh C A. Six decades of the Hall–Petch effect – a survey of grain-size strengthening studies on pure metals. International Materials Reviews, 2016, 61(8): 495–512
322. Chen Y, Gao N, Sha G, et al. Microstructural evolution, strengthening and thermal stability of an ultrafine-grained Al–Cu–Mg alloy. Acta Materialia, 2016, 109: 202–212
323. Mustafa G, Baghel M, Wang T X, et al. Multiscale simulation for predicting grain size and microhardness in high-speed milling of Inconel 718. Metals and Materials International, 2026, 32(6): 1891–1915
324. Jafarian F, Masoudi S, Umbrello D, et al. New strategies for improvement of numerical model accuracy in machining of nickel-based alloy. Simulation Modelling Practice and Theory, 2019, 94: 134–148
325. la Monaca A, Axinte D, Liao Z R, et al. Interaction and competition between continuous and geometric dynamic recrystallization in high-strain-rate deformation of nickel-based superalloys. Acta Materialia, 2025, 297: 121377
326. Guo Y B, Li W, Jawahir I S. Surface integrity characterization and prediction in machining of hardened and difficult-to-machine alloys: a state-of-art research review and analysis. Machining Science and Technology, 2009, 13(4): 437–470
327. Liang X L, Liu Z Q, Wang B. State-of-the-art of surface integrity induced by tool wear effects in machining process of titanium and nickel alloys: a review. Measurement, 2019, 132: 150–181
328. Rahul Y, Vipindas K, Jose M. Methodology for prediction of sub-surface residual stress in micro end milling of Ti–6Al–4V alloy. Journal of Manufacturing Processes, 2021, 62: 600–612
329. Huang X M, Sun J, Li J F. Effect of initial residual stress and machining-induced residual stress on the deformation of aluminium alloy plate. Strojniški vestnik – Journal of Mechanical Engineering, 2015, 61(2): 131–137
330. Wan M, Ye X Y, Wen D Y, et al. Modeling of machining-induced residual stresses. Journal of Materials Science, 2019, 54(1): 1–35
331. Dahlman P, Gunnberg F, Jacobson M. The influence of rake angle, cutting feed and cutting depth on residual stresses in hard turning. Journal of Materials Processing Technology, 2004, 147(2): 181–184
332. Liu Y, Xu D D, Agmell M, et al. Numerical and experimental investigation of tool geometry effect on residual stresses in orthogonal machining of Inconel 718. Simulation Modelling Practice and Theory, 2021, 106: 102187
333. Zhou T, Zhou T, Zhang C, et al. Hybrid modeling with finite element—analysis—neural network for predicting residual stress in orthogonal cutting of H13. Journal of Materials Research and Technology, 2024, 29: 4954–4977
334. He Y, Yue Q B, Li Y F, et al. Multiscale residual stress and mechanical behavior analysis in machining of Ti–6Al–4V alloy

with advanced microscopic characterization. Journal of Manufacturing Processes, 2024, 120: 568–578

335. Guo J, Fu H Y, Pan B, et al. Recent progress of residual stress measurement methods: a review. Chinese Journal of Aeronautics, 2021, 34(2): 54–78
336. El-Axir M H. A method of modeling residual stress distribution in turning for different materials. International Journal of Machine Tools and Manufacture, 2002, 42(9): 1055–1063
337. Jacobus K, DeVor R E, Kapoor S G. Machining-induced residual stress: experimentation and modeling. Journal of Manufacturing Science and Engineering, 2000, 122(1): 20–31
338. Liang X L, Liu Z Q, Wang B, et al. Prediction of residual stress with multi-physics model for orthogonal cutting Ti–6Al–4V under various tool wear morphologies. Journal of Materials Processing Technology, 2021, 288: 116908
339. Clavier F, Valiorgue F, Courbon C, et al. Impact of cutting tool wear on residual stresses induced during turning of a 15–5 PH stainless steel. Procedia CIRP, 2020, 87: 107–112
340. Dumas M, Fabre D, Valiorgue F, et al. 3D numerical modelling of turning-induced residual stresses–a two-scale approach based on equivalent thermo-mechanical loadings. Journal of Materials Processing Technology, 2021, 297: 117274
341. Yue Q B, Li Y F, Liang C, et al. Quantitative evaluation of residual stress and microstructural effects on the surface hardness of machined Ti-6Al-4 V alloy with microscopic characterization techniques. Journal of Materials Processing Technology, 2024, 327: 118382
342. Pan Q S, Ding K Q, Guo S, et al. Superior resistance to cyclic creep in a gradient structured steel. Science, 2025, 388(6742): 82–88
343. Zhang Y, Lee Y J, Chang S, et al. Microstructural modulation of TiAl alloys for controlling ultra-precision machinability. International Journal of Machine Tools and Manufacture, 2022, 174: 103851
344. Zhang S, Zhang H Y, Liu X J, et al. Thermal deformation behavior investigation of Ti–10V–5Al-2. 5fe-0. 1B titanium alloy based on phenomenological constitutive models and a machine learning method. Journal of Materials Research and Technology, 2024, 29: 589–608.
345. Li J N, Gao D, Lu Y, et al. Temperature-dependent microstructural evolution and surface integrity in machining of directed energy deposition-316L. Journal of Materials Processing Technology, 2025, 344: 119044
346. Brown M, M'Saoubi R, Crawforth P, et al. On deformation characterisation of machined surfaces and machining-induced white layers in a milled titanium alloy. Journal of Materials Processing Technology, 2022, 299: 117378